THESIS FOR THE DEGREE OF LICENTIATE OF ENGINEERING

Optimal Energy Scheduling of Grid-connected Microgrids with Battery Energy Storage

KYRIAKI ANTONIADOU-PLYTARIA

CHALMERS
UNIVERSITY OF TECHNOLOGY

Department of Electrical Engineering
Chalmers University of Technology
Gothenburg, Sweden 2020

Optimal Energy Scheduling of Grid-connected Microgrids with Battery Energy Storage
KYRIAKI ANTONIADOU-PLYTARIA

Thesis for Licentiate of Engineering 2020
ISSN No.: 1403-266X

Division of Electric Power Engineering
Department of Electrical Engineering
Chalmers University of Technology
SE-412 96 Gothenburg
Telephone +46 (0)31 772 1000

Printed by Chalmers Reproservice
Gothenburg, Sweden 2020

To my family

Optimal Energy Scheduling of Grid-connected Microgrids with Battery Energy Storage

KYRIAKI ANTONIADOU-PLYTARIA
Division of Electric Power Engineering
Department of Electrical Engineering
Chalmers University of Technology

Abstract

The coupling of small-scale renewable-based energy sources, such as photovoltaic systems, with residential battery energy storages forms clusters of local energy resources and customers, which can be represented as controllable entities to the main distribution grid. The operation of these clusters is similar to that of grid-connected microgrids. The future distribution grid of multiple grid-connected microgrids will require proper coordination to ensure that the energy management of the microgrid resources satisfies the targets and constraints of both the microgrids' and the main grid's operation. The link between the battery dispatch and the induced battery degradation also needs to be better understood to implement energy management with long-term economic benefits.

This thesis contributes to the solution of the above-mentioned issues with an energy management model developed for a grid-connected microgrid that uses battery energy storage as a flexible energy resource. The performance of the model was evaluated in different test cases (simulations and demonstrations) in which the model optimized the schedule of the microgrid resources and the energy exchange with the connected main grid, while satisfying the constraints and operational objectives of the microgrid. Coordination with the distribution system operator was proposed to ensure that the microgrid energy scheduling solution would not violate the constraints of the main grid.

Two radial distribution grids were used in simulation studies: the 12-kV electrical distribution grid of the Chalmers University of Technology campus and a 12.6-kV 33-bus test system. Results of the Chalmers' test case assuming the operation of two grid-connected microgrids with battery energy storage of 100-200 kWh showed that the microgrids' economic optimization could reduce the cost for the distribution system operator by up to 2%. Coordination with the distribution system operator could achieve an even higher reduction, although it would lead to sub-optimal solutions for the microgrids. Application of decentralized coordination showed the effectiveness of utilizing microgrids as flexible entities, while preserving the privacy of the microgrid data, in the simulations performed with the 33-bus test system.

The developed microgrid energy management model was also applied for a building microgrid, where the battery energy storage was modeled considering both degradation and real-life operation characteristics derived from measurements conducted at real residential buildings equipped with stationary battery energy storages. Simulation results of a building microgrid with a 7.2 kWh battery energy storage showed that the annual building energy and battery degradation cost could be reduced by up to 3% compared to when the impact of battery degradation was neglected in the

energy scheduling. To demonstrate the model's practical use, it was integrated in an energy management system of the real buildings, where the buildings' battery energy storages and, by extent, their energy exchange with the main grid, were dispatched based on the model's decisions in several test cases.

The test cases' results showed that the model can reduce the energy cost of the microgrid both in short-term and in long-term. Moreover, with the help of this model, the microgrid can be employed as a flexible resource and reduce the operation cost of the main distribution grid.

Keywords: Battery energy storage, energy management, energy scheduling, distribution network, microgrids, optimization.

Acknowledgements

First, I would like to thank my supervisors Dr. Anh Tuan Le and Dr. David Steen as well as my examiner Prof. Ola Carlson for their consistent support and guidance throughout this period. I would also like to thank Dr. Ali Fotouhi and Dr. Ioannis Bouloumpasis for dedicating so much of their time to help me and for always being there, whenever I wanted to think aloud.

The work of this thesis has been carried out within the 2017-2020 project "From micro to Mega-GRID: Interactions of micro-grids in active distribution networks". The project has received funding from the Swedish Energy Agency in the framework of the joint programming initiative ERA-Net Smart Energy Systems' focus initiative Smart Grids Plus, with support from the European Union's Horizon 2020 research and innovation programme under grant agreements No 646039 and No 775970. The financial support is gratefully acknowledged. I would also like to thank my project partners for their help and the interesting discussions that contributed to my work.

Although I wrote this thesis while working from home, before the corona pandemic started, I had the pleasure to share the office with many fantastic colleagues over the years: Selam, Ehsan, Christos, Anant, Ioannis and Hannes. It has been a privilege to get to know all of you! My warmest gratitude also goes to all colleagues at the division of Electric Power Engineering who have been there to answer my questions, teach me, and share their knowledge and experience. A very special thanks to Ankur Srivastava, the best friend and colleague one could possibly have.

Eleni and Apostolis, ξενιτεμένοι μου, our ways might have parted but I have always felt you by my side. Last but not least, my family, where life begun and love will never end. Thank you for supporting me in any possible way.

Κέλλυ Αντωνιάδου/Kelly Antoniadou
Gothenburg, July 2020

List of Acronyms

Below is the list of acronyms that have been used throughout this thesis listed in alphabetical order:

BES	Battery Energy Storage
BMG	Building Microgrid
BMG-EMS	Building Microgrid Energy Management System
BRP	Balance Responsible Party
CHP	Combined Heat and Power
DER	Distributed Energy Resource
DMS	Distribution Management System
DoD	Depth-of-discharge
DR	Demand Response
DRR	Demand Response Resource
DSO	Distribution System Operator
EMS	Energy Management System
EV	Electric Vehicle
OPF	Optimal Power Flow
LP	Linear Programming
MILP	Mixed-Integer Linear Programming
MIQCP	Mixed-Integer Quadratically Constrained Programming
MG	Microgrid
MG-EMS	Microgrid Energy Management System
QCP	Quadratically Constrained Programming
PCC	Point of Common Coupling
PV	Photovoltaic
RES	Renewable-based Energy Sources
RH	Rolling Horizon
SoC	State-of-charge
SoE	State-of-energy
TSO	Transmission System Operator

Nomenclature

Below is the nomenclature of indices, sets, parameters, and variables that have been used throughout this thesis. The symbols are listed in alphabetical order in each category. The sets, parameters, and variables are also defined in the text, where they first appear.

Indices

i,j	Indices for distribution network buses
k,m	Index for charging/discharging sample data
n	Index for iteration loop
p	Index for lifecycle loss function sample point
t	Index for time step

Sets

$\mathcal{D}$	Set of distribution network buses
$\mathcal{D}_s$	Set of substation buses
$\mathcal{H}$	Set of time steps (simulation/scheduling horizon)
$\mathcal{M}$	Set of discharging data
$\mathcal{MG}$	Set of the MGs' PCC with the distribution network
$\mathcal{K}$	Set of charging data
$\mathcal{N}$	Set of MG buses
$\mathcal{P}$	Set of sample points of the lifecycle loss function

Parameters

γ	Penalty coefficient
B_1	Pre-exponential factor used in empirical cycle aging model

B_2	Exponential factor used in empirical cycle aging model
Δt	Time discretization step (time interval)
η	Percentage of end-of-life retained capacity of a BES
η_j^{ch}	Charging efficiency of BES
η_j^{dis}	Discharging efficiency of BES
κ_j	Power to energy ratio related to the technology of BES
κ_j^{DR}	Power to energy ratio related to the technology of DRR
$\widehat{\rho}_{j,p}$	Sample point of lifecycle loss percentage
a_j	Calendar aging coefficient
B_i	Shunt susceptance from bus i to ground
$C_j^{B,0}$	Replacement cost of the BES
C_j^{CHP}	Operation cost of the CHP plant (related to the scheduling period)
C_j^f	Fuel cost of the CHP plant
$C^{SS,p}$	Power-based grid tariff paid by the DSO
C^p	Power-based grid tariff paid by the MG customers
$C^{SS,tr}$	Energy transmission charge paid by the DSO
C^{tr}	Grid charge for energy transmission paid by the MG customers
C^r	Reimbursement fee paid to producers of small-scale generation
$DoD_{j,p}$	Sample point of DoD
E_j^{max}	Installed capacity of BES
G_i	Shunt conductance from bus i to ground
$\boldsymbol{H}$	Adjacency matrix
I_c	Average C-rate of a BES over the scheduling period
M	A very large number (used with the linearization technique called big-M approach)
N	Number of iterations
$P_{j,m}^-$	Sample measurement of output power from the battery cells
$P_{j,k}^+$	Sample measurement of input power to the battery cells
$P_{j,k}^{ch}$	Sample measurement of charging power absorbed from the grid
$P_{j,m}^{dis}$	Sample measurement of discharging power injected to the grid
$P_{j,t}^H$	Heating output from the CHP plant
$P_j^{G,min}$	Minimum electrical power output from the CHP plant
$P_{j,t}^L$	Active power of load demand
P_{max}^-	Maximum discharging power of BES
P_{max}^+	Maximum charging power of BES

P_i^{MG}	Active power exchange at PCC at bus i according to MG's schedule
$P_{j,t}^{PV}$	Active power from solar generation
P_{req}	Balancing power request
P^{spot}	Spot price [$/kWh]
$Q_{j,t}^{L}$	Reactive power of load demand
$Q_{j,t}^{MG}$	Reactive power exchange at PCC at bus i according to MG's schedule
R_{ij}	Resistance of line $i-j$
r_j^{CHP}	Ratio of electrical power to heating power output
S_{ij}^{max}	Rated apparent capacity of line $i-j$
SoE_j^{min}	Lower state-of-energy limit
SoE_j^{max}	Upper state-of-energy limit
$SoE_{j,k}^{ch}$	Sample measurement of BES state-of-energy during charging
$SoE_{j,m}^{dis}$	Sample measurement of BES state-of-energy during discharging
T	Temperature
V_{max}	Upper voltage limit
V_{min}	Lower voltage limit
X_{ij}	Reactance of line $i-j$

Variables

Δp_i	Optimal flexibility amount that the DSO asks from the MGs
$\xi_{j,p,t}$	Positive variable indicating choice of lifecycle loss function sample point p
$\rho_{j,t}$	Percentage of lifecycle loss for one cycle at a specific DoD
$\phi(DoD)$	Lifecycle as a function of DoD
$b_{j,p,t}$	Binary variable used with adjacency constraints
c_j^B	Cycle aging cost (calculated over the scheduling period)
c_i^{DER}	Operation cost (calculated over the scheduling period) associated with the DER owned by the MG
$c_{j,t}^{DoD}$	Cycle aging cost per time step t
$dod_{j,t}$	Depth-of-discharge (DoD)
$e_{j,t}^{DR}$	The part of energy available from DRRs that has already been curtailed at time t
p_j	Active power injection at bus j
p_{ji}	Active power flow from bus j to bus i

$p^{-}_{j,t}$	Power output from the battery cells (before battery losses have been taken into account)
$p^{+}_{j,t}$	Power input to the battery cells (after battery losses have been taken into account)
$p^{ex}_{i,t}$	Exported power to the main grid
$p^{im}_{i,t}$	Imported power from the main grid
$p^{ch}_{j,t}$	Charging power of BESs (power absorbed from the grid)
$p^{dis}_{j,t}$	Discharging power from BESs (power injected to the grid)
$p^{DR}_{j,t}$	Curtailed (or increased) power from DRRs
$p^{G}_{j,t}$	Electrical power output from the CHP plant
$P^{L,r}_{j,t}$	Available responsive load
p^{PCC}_{n}	Average active power exchange at PCC
$p^{SS}_{i,t}$	Active power at the substation
q_j	Reactive power injection at bus j
q_{ji}	Reactive power flow from bus j to bus i
$q^{DR}_{j,t}$	Reactive power of DRRs
q^{idx}	Percentage of the difference between the estimated SoE and the measured SoC at one time step
$q^{G}_{j,t}$	Reactive power from the CHP plant
Q^{l}_{j}	Percentage of cycle-based capacity loss a BES
Q^{r}_{j}	Percentage of retained BES capacity after a rest period
$Q^{r,0}_{j}$	BES capacity percentage at the beginning of a rest period
$r^{SS,p}$	Cost of the distribution network's peak power measured at the substation
r^{p}_{i}	Cost of the MG's peak power drawn from the main grid
$q^{SS}_{i,t}$	Reactive power at the substation
soc	State-of-charge (SoC)
$soe_{j,t}$	State-of-energy (SoE)
V_i	Voltage at bus i
v_i	Square of voltage magnitude at bus i
$x_{j,m,t}$	Positive variable indicating choice of discharging sample measurement m
$y_{j,k,t}$	Positive variable indicating choice of charging sample measurement k
$z_{j,t}$	Binary variable that indicates if the BES is charging or discharging

Contents

Chapter 1

Introduction

This chapter presents the problem overview and the main research questions that are being addressed in this thesis. It describes the objectives and the main contributions of the thesis and it also includes the publications that resulted from the thesis work.

1.1 Background and main research questions

Under the Paris agreement signed in 2016, the European Union (EU) countries have committed to significant reductions of CO_2 emissions by 2050 to achieve carbon neutrality. A carbon-neutral scenario requires an 85% reduction of energy and process related CO_2 emissions by 2050 in comparison to the amount of CO_2 emissions [1] in 1990. To fight climate change and balance the amounts of carbon emitted to the atmosphere and absorbed by the atmosphere the generation of electrical energy is undergoing a transition from fossil-based energy sources to renewable-based energy sources (RES) such as solar energy, wind power and others. Sweden, in particular, has set ambitious energy goals of 100 % renewable energy production by 2040 and zero net emissions of greenhouse gases by 2045 [2].

Despite the fact that the EU has so far focused on large-scale deployment of RES, small-scale integration of renewables has also been achieved with residential photovoltaics (PVs) thanks to the feed-in tariffs. The solar panel subsidy makes own production from PVs worthwhile and appealing to the consumers leading to a "solar energy revolution" in Sweden [3]. This marks the transition of the former passive consumers to active prosumers, i.e., electrical energy consumers that also have the capability of producing their own electrical energy, which can be used either for self-consumption or exported to the main grid.

Following a decrease in the cost of batteries (e.g., the price of Li-ion batteries has dropped by 73% between 2010 and 2016 [4]) the installation of residential, stationary battery energy storages (BESs) has increased [5], signifying their value in reducing the electricity cost of the prosumers. Behind-the-meter BESs can be combined with residential PVs to increase the self-supply level of end-users during the day and, in fact, such a market has already been developed in Germany [6], where almost 100

000 households have installed BESs. BESs can help small-scale RES owners increase their revenue by maximizing self-consumption of PV generation [7] and by engaging in energy arbitrage (load-shifting). Besides this, residential, stationary BESs are a promising application for recycling of electric vehicle (EV) BESs. Retired EV BESs can be re-used as second-life BESs in load-shifting and peak-shaving. These functions, which aim to reduce the electricity cost, are less demanding than powering EVs or offering balancing services to the grid.

The coupling of small-scale generation with residential BESs could promote the integration of microgrids (MGs), i.e., clusters of local energy sources, energy storages, and customers which are represented as a single controllable entity [8]. The term "microgrid" has been subjected to many definitions. The U.S. Department of Energy has defined the MG as [9]: "a group of interconnected loads and distributed energy resources within clearly defined electrical boundaries that acts as a single controllable entity with respect to the grid. A microgrid can connect and disconnect from the grid to enable it to operate in both grid-connected or island mode." The Conseil International des Grandes Réseaux Électriques (CIGRÉ) Working Group C6.22 Microgrid Evolution Roadmap (WG6.22) emphasized on two fundamental requirements that characterize every MG system, which are [10]: 1) that the MG "contains sources and sinks under local control" and 2) that the MG can "operate either grid-connected or islanded". The WG6.22 provided the following definition of the MG: "Microgrids are electricity distribution systems containing loads and distributed energy resources, (such as distributed generators, storage devices, or controllable loads) that can be operated in a controlled, coordinated way either while connected to the main power network or while islanded."

MGs can be employed at various locations including both rural and urban areas. Off-grid solutions are usually ideal for remote rural areas. In cities, on the other hand, grid-connected MGs can be formed by clusters of distributed energy resources that are integrated in commercial or residential buildings. These type of MGs, where the management of the DERs is in tight relation with the electricity load consumption of a building or clusters of buildings have also been defined as building MGs (BMGs) [11, 12].

Up until now, the driving force for the deployment of MGs [8] around the globe has been the need to have uninterrupted and reliable power supply in remote locations or areas. Therefore, the main focus of their application has been islanding capability, black-start capability, and grid-forming control. In the case of grid-connected MGs, the focus in the literature has shifted from the grid-forming control to the optimal energy management of the resources, which is performed by the energy management system (EMS).

Energy storage emerges as a critical resource in MG energy management [13] offering services such as increased self-consumption of RES-based generation and energy arbitrage [5], which benefit the MG owners. Microgrid energy management systems (MG-EMSs) can apply the proposed energy scheduling solutions that enable the end-users to fully utilize the BES potential in reducing the energy cost. Ref. [13–33]

have published results of studies on MG energy management considering energy storage. A comprehensive literature review on optimal energy scheduling of MGs can be found in Section 2.2.

Many of the above studies (e.g., [13–15, 17, 18]) assumed MG-EMSs that operate in uncoordinated schemes, i.e., without coordinating with the distribution system operator (DSO) to solve the MG energy scheduling problem. Others have applied coordinated energy management of grid-connected MGs considering interaction with the DSO, e.g., [19–22]. It is unspecified, however, in these studies, how the MG integration can affect the cost of the DSO, if unbundling of network operation is considered.

Furthermore, it is a challenge to introduce a linear mathematical model that can realistically represent the non-linear BES behavior and the induced BES degradation. The studies that have presented results on optimal MG energy management considering BES dispatch often oversimplify the BES scheduling model to reduce complexity of the optimal MG energy scheduling problem, as is discussed in the literature review in Section 2.3. For the same reason, the impact of degradation is often ignored. However, the link between BES dispatch and BES degradation is essential, as it can be exploited to further reduce the operation cost of the MG [11].

Within the scope of this thesis the following research questions have been identified:

- **Research question 1:** How can MG energy scheduling strategies affect the cost for the DSO in the unbundled framework of operation? How to define the cost of MG re-scheduling in order to assist the operation of the main distribution grid in this case?
- **Research question 2:** How can the mathematical model of the BES be improved to capture both real-life performance characteristics and the impact of degradation, while having a formulation that does not add complexity to the optimal energy scheduling problem?
- **Research question 3:** How much does BES degradation impact the cost of the MG energy scheduling solution?

The thesis examines these questions and presents findings that can provide answers or further knowledge and insight on the studied subject.

1.2 Objectives and main contributions

The aim of this thesis was to develop and validate an energy management model for a grid-connected MG, which uses BES as the main flexible resource. The model can be integrated to a MG-EMS, which schedules the BES and potentially other MG resources considering objectives that are either related with economic operation or with the level of interaction with the main grid.

The problem of the MG energy scheduling has been solved using both uncoordinated

and coordinated schemes. In the uncoordinated schemes, the aim was to obtain the solution that best satisfied the operational objectives of the MG operator and evaluate the impact on the cost and operation of the distribution network. In coordinated schemes, the aim was to find the solution that best satisfied the operational targets of the DSO considering the unbundled framework of network operation.

In addition, the energy management model was applied for a BMG, where a market-based approach was used for the BES dispatch. The aim was to more accurately characterize the building operational costs considering both the profit from load shifting and the cost of BES degradation, which has often been neglected in the literature on MG energy management. Moreover, the purpose of this work was to incorporate an improved BES scheduling model into the mathematical model of MG energy management, which can capture a more realistic BES operation performance.

The main contributions of this thesis include the following:

- Development of MG energy management models for multi-period energy scheduling of the MG resources, where AC power flow was used for the distribution network modeling. The models can be employed by the MG operator or by the DSO depending on the implemented coordination scheme.
- A long-term case study using the real distribution network of a university campus and different energy scheduling strategies of grid-connected MGs. Unlike existing studies, the cost and performance were assessed considering the unbundling of network operation. The link between expected BES lifetime and applied energy scheduling strategy was also investigated.
- Development of a BMG energy management model with a market-based approach for BES dispatch. The model can be utilized by building owners for close to real-time (5-15 min) energy management and monthly or annual assessment of the building energy cost. A measurement-based BES model and the impact of degradation were considered in the BES dispatch, while the effect of DoD was assessed both in cycle and in calendar aging.
- Comprehensive evaluation of the BES dispatch under the proposed BMG energy management model with a long-term study using a real energy-flexible residential building. The evaluation was performed under different technical and degradation BES models revealing which modeling approach could yield the maximum reduction to the electricity cost of the residents.
- Validation of the BMG energy management model integrating on-site BESs at two demonstration sites. The validation proved the effectiveness of integrating a measurement-based model in a MG-EMS and confirmed its advantage against the conventional BES scheduling model.

1.3 Structure of the thesis

The thesis is organized in seven chapters:

- **Chapter 1** presents the background and research questions, the objectives, and the main contributions of the thesis.
- **Chapter 2** describes the task of the energy management system and presents a state-of-the-art survey on MG energy management as well as BES scheduling and BES degradation models that have been used with energy management. Industrial perspectives of grid-connected MGs are also discussed.
- **Chapter 3** presents the basic structure of the energy scheduling problem and the methodology that was used in the thesis for the solution of the MG energy scheduling problem.
- **Chapter 4** presents the optimization models that were developed to formulate the optimal energy scheduling problem for grid-connected MGs.
- **Chapter 5** describes the test cases that have been studied in simulations and demonstrations. This chapter also describes the demo sites and the communication and control set-up of the designed testbed.
- **Chapter 6** presents and discusses simulation and demonstration results.
- **Chapter 7** concludes the thesis and provides suggestions for future work.

1.4 List of publications

The following is the list of publications resulting from the thesis work.

Published

(I) **K.E. Antoniadou–Plytaria**, D. Steen, L.A. Tuan, and O. Carlson, "Energy scheduling strategies for grid-connected microgrids: A case study on Chalmers campus," in *Proc. Innovative Smart Grid Technologies Conference (ISGT-Europe)*, Bucharest, Romania, Sep. 29–Oct. 2, 2019.

(II) **K.E. Antoniadou–Plytaria**, A. Srivastava, M. A. F. Ghazvini, D. Steen, L.A. Tuan, and O. Carlson, "Chalmers campus as a testbed for intelligent grids and local energy systems," in *Proc. 2nd International Conference on Smart Grid Energy Syst. and Technologies (SEST) Europe*, Porto, Portugal, Sep. 9–11, 2019.

Submitted–Under review

(I) **K.E. Antoniadou–Plytaria**, D. Steen, L.A. Tuan, O. Carlson, and M. A. F. Ghazvini, "Market-based energy management model of a building microgrid considering battery degradation," submitted for second-round review on *Transactions on Smart Grid*, Aug. 2020.

Chapter 2

Microgrid Energy Management

The following section is an overview of the state-of-the-art on MG energy management. Special focus is given in the use of BES as a flexible resource in MG energy management. Industrial perspectives on MG energy management and integration of MGs into existing distribution grids are also discussed.

2.1 Energy management system

MGs are defined as clusters of distributed energy sources (generation, storage, flexible loads, etc.) and energy consumers (non-flexible load). The MGs can operate either in grid-connected or in island mode and many MGs can support seamless transition between the two modes to increase supply reliability for the customers. In grid-connected mode, the difference between the MG generation and consumption can be imported or exported to the main grid. In island mode, the MG is completely autonomous meaning that energy is supplied exclusively from the MG resources and any excess in generation must be stored or curtailed, if self-consumption is not an option.

Regardless of the mode of operation, a MG can be considered as a controllable entity, which is represented as a single entity to the distribution grid. This can be achieved with the help of the MG controller, which is the key component of the MG in control of the producing and consuming units (distributed generation, flexible loads, storage) that are clustered together to form the MG. The MG controller ensures that the operation of the MG is both secure and reliable as well as efficient and economical.

The MG-EMS is employed by the MG controller and its main task is to optimally balance load and supply both in the planning phase and in the delivery phase (either by MG resources or through interconnections). The MG-EMS belongs to the tertiary level of hierarchical MG control [34]. The IEC 61970 standard [35] on EMS application program interface has defined EMS as "a computer system comprising a software platform providing basic support services and a set of applications providing the functionality needed for the effective operation of electrical generation and

transmission facilities so as to assure adequate security of energy supply at minimum cost".

The use of the MG-EMS is essential in dispatching the MG resources in an intelligent, secure, and reliable manner and in achieving coordination both among the MG components as well as with other grids. The objectives and strategies that determine the decisions of MG-EMS are defined by the MG operator. If the MG operator is different from the DSO and the MG operates in grid-connected mode, then these objectives might not be co-aligned with the operational objectives that optimize the operation of the main distribution network.

The MG-EMS also determines the power exchange between the MG and the main grid at the point of common coupling (PCC), which is the physical interface of the MG with the distribution network. Thus, it becomes clear that the scheduling of the MG resources affects the operation of the interconnected system (e.g., voltage profile, utilization of feeders). Although the MG resources are managed by the MG-EMS, they could also be scheduled either directly or indirectly by the distribution management system (DMS), which is a part of the utility control centre.

The operation between multiple grid-connected MGs and the distribution network can be coordinated by controlling the active (and/or reactive) power exchange at the PCCs. This can ensure the satisfaction of grid technical constraints, contribute to an economical operation of the interconnected systems and assist in ancillary services. To achieve this level of coordination, a control and communication MG interface should be developed as an add-on DMS functionality to integrate the MG energy scheduling with the network optimal power flow (a functionality already available at the DMS). Such an interface would allow MGs and DSO to exchange information including desired MG schedule, the voltage at PCC and flexibility requests among others.

2.2 Optimal energy scheduling of MGs

Recent research has studied the optimal energy scheduling of MGs with their MG-EMS operating in uncoordinated schemes, i.e., without considering interaction with the DSO, even when the MG is connected to the main grid (e.g., [13–18]). Apart from control of conventional generators, control of energy storage and demand response (DR) are usually employed to minimize the operation cost of the MG. An exhaustive review on optimization methods that have been proposed for MG energy management can be found in [36].

The future distribution grid of multiple, grid-connected MGs could create new challenges for the DSOs and requires proper control and coordination of different network entities. Therefore, a lot of studies (e.g., [19–22, 37–42]) have also been applying coordinated energy management of grid-connected MGs considering interaction between the MG-EMSs and the DSO. The MG energy scheduling is the result of a decision-making process, where the MGs and the DSO (or a MG aggregator) need to exchange information to determine the interactions between the MGs and the

main grid (e.g., power exchange, energy prices). In this decision making process, there is often a hierarchy with the DSO usually acting as the leader (upper level) and the MG operators are the followers (lower level). When this type of hierarchy is applied in the coordinated MG energy scheduling problem, then this problem can be formulated as a bilevel optimization problem.

Applications of both stochastic [37–39] and deterministic [19, 20, 40–42] bilevel optimization can be found in the recent literature on coordinated energy management of grid-connected MGs. In most works, the DSO is viewed as a supervisor and central coordinator for the energy exchange among all interconnected network entities. Therefore, these studies usually assume that the DSO has full knowledge of MG information, which extends beyond the PCC data such as the MGs' objectives, MG grid constraints as well as DER and customer data in order to solve the bilevel optimization problem (e.g., [21, 22, 37, 41]). Full knowledge helps to simplify the bilevel optimization problem, as it can then be transformed into an equivalent single-level mathematical problem with complementarity constraints (MPCC), as in, e.g., [37,40]. Full MG information, however, comes into conflict with the requirement of preserving the privacy of the MG data.

According to the guidelines provided in [43], the DMS should not require any information of the MG network and capacity configuration (except perhaps of the status of some tie-line switches) in order to be functional. In this regard, some decentralized and privacy-preserving methods have been developed. Authors in [38] propose a decentralized solution for the same problem, which was solved in a centralized manner in [37]. Specifically, the MGs share information only about the power exchange at the PCC and iteratively increasing penalties are introduced to incorporate the coupling of the different entities and ensure convergence of the solution. Multi-period energy scheduling with inter-temporal constraints for generators and energy storage is considered in [19], where the MGs can also exchange energy with each other. In this case, the DSO first sends the energy exchange schedule to the MGs and then receives information from them to update it iteratively until the optimal decision is reached. The DMS does not require any MG values as input except from PCC measurements and the MG information related to the worst-case operating cost, therefore MG privacy is preserved. The multi-microgrid concept in [20] also utilizes decentralized coordination as the aggregator only requires the scheduled energy exchange of each MG at PCC and the corresponding MG profits in order to generate a congestion price signal and avoid violation of PCC capacity.

Studies on coordinated MG energy management often ignore the distribution network modeling or simplify it using DC power flow equations. If the grid constraints are considered, then this applies to the main grid, while the MG grid constraints are neglected. The network power flow within the MGs was only considered in [41], where an equivalent single-level problem was solved. As it was mentioned, this approach requires that the DSO has data/measurements of the MG network and/or resources. In this case, full information of the MG configuration was shared with the DSO to ensure that the global grid constraints would be satisfied with the application of the individual optimal solution.

What is missing from recent publications is a study of the MG integration considering the unbundled framework of operation. All of the previously mentioned studies assume that both the DSO and the MGs can own and schedule DERs and they trade energy with each other. Thus, the proposed methodologies and the published results are not particularly relevant to the European DSOs, where unbundling rules usually apply to their operation.

2.3 BES scheduling

The need for dispatchable RES has increased the focus on connecting storage units to energy systems. Energy storages support the penetration of RES by reducing the grid power fluctuations they cause and can offer many other services that benefit the grid operators (e.g., peak shaving, load leveling, frequency regulation [44]). So far, BESs have mostly been used in frequency regulation, which accounts for about half of their applications, while energy arbitrage accounts for about 10% according to [5]. However, as recent research has been investigating the potential contribution of energy arbitrage in reducing the energy cost, BES has started to emerge as a critical resource for energy management. This is evident by many research publications on MGs [13, 17–33] and BMGs [11, 12] that have especially focused on BES scheduling. Many of the above-mentioned studies (e.g., [18–22, 31–33]), however, do not consider BES degradation.

Publications that do consider the effect of battery degradation on energy management usually neglect the impact of calendar aging [17, 24–28, 30], which reduces the BES capacity during open-circuit periods. Instead, they focus on cycle aging, often disregarding the effect of the depth-of-discharge (DoD) as a stress factor [24, 25, 30]. In addition, most works use simplified BES scheduling models, which could reduce the reliability of the scheduling solution.

As was observed from the literature review, the mathematical models employed in energy scheduling of MGs with BESs had at least one of the following shortcomings: 1) simplified BES scheduling model assuming constant BES charging/discharging efficiencies and/or maximum power rates and 2) no implementation of a degradation model to consider the impact of BES degradation. Below is a detailed review of state-of-the-art on optimal BES dispatch focusing on BES degradation and BES scheduling models to present the modeling approaches that have been used in recent publications.

2.3.1 BES degradation

Some of the most recent studies that have published results on optimal BES dispatch (not necessarily using the MG concept) and consider BES degradation cost are [17, 24–30, 45–48]. A penalty is often used in the objective function in order to reduce BES stress, usually by avoiding deep cycle depths and/or high power rates [25, 46, 47]. Other works consider the impact of low state-of-charge (SoC) [26–28, 45], while the simplest approach is to limit the number of cycles [24].

In [25], a mixed-integer non-linear programming model links the degradation cost to the cycle depth and updates the BES capacity per time-step. The battery degradation in [46] is a function of the power rates, while authors in [47] link degradation cost to both cycle depth and charge/discharge rates. However, neither of the studies [25, 46, 47], consider the DoD of each cycle.

In contrast, the degradation cost in [26] is calculated using an approximation that links BES loss with a weighted sum of SoC levels. Authors in [27] also consider SoC level and use Q-learning to approximate the non-convex cycle aging cost. The rainflow algorithm is employed in [45], where the authors prove convexity of the cycle-based degradation cost function provided that the DoD stress function is also convex. Then, they use a subgradient algorithm to approximate the solution of optimal BES dispatch. The loss of lifecycle as a function of DoD is also studied in [28], although the specific DoD related to each cycle is not considered. The authors propose a piecewise linearization of the lifecycle loss function, where the BES sizing of a MG is decided based on the expected degradation associated with the maximum DoD of all cycles. A sensitivity analysis is performed in [48] to define the impact of multiple stress factors on the BES degradation cost. For simplicity, the authors assume that the BES charging and discharging efficiencies are the same.

Unlike most studies, which neglect calendar aging, the authors in [29] incorporate both calendar and cycle aging into a mixed-integer linear programming (MILP) problem considering their dependencies on time elapsed and cumulative throughput, respectively. However, a predefined desired BES lifetime must be entered as a parameter to include calendar aging in the MILP problem, while the impact of SoC is not evaluated in either cycle or calendar aging.

The BES degradation can be expressed either as loss of available capacity or increase in the BES resistance. Most of the studies reviewed in this section link the degradation cost with a percentage of the estimated capacity loss. This percentage is multiplied with the initial investment cost of the BES to define a degradation cost term in the objective function. Thus, these studies determine the optimal BES dispatch considering the trade-off between degradation cost and revenue from load shifting (an interesting study on the trade-off between profit and BES degradation investigating the participation of the BES owner in different services can be found in [49]). For a more realistic representation of the BES degradation cost both the decreasing trends in BES replacement costs and the end-of-life retained capacity (the remaining capacity of the BES, when it is retired) for grid applications would have to be considered. These were not discussed in the previously mentioned works that linked the degradation cost with BES capacity reduction.

Practical approaches can also be found to calculate the degradation cost, as for example those proposed in [26, 28]. In these works, the BES depreciation was calculated using only data from the manufacturer's performance warranty without utilizing any modeling approach to account for the effect of aging mechanisms on the BES capacity or resistance. In [26], the BES degradation was calculated by estimating the effective cumulative throughput (depending on the SoC levels) of the

BES dispatch. Considering the cumulative throughput that the BES can deliver in its lifetime according to the manufacturer's warranty, the BES loss could then be calculated as a percentage of the cumulative throughput that was removed from the total throughput. Authors in [28] calculated degradation as a percentage of lifecycle loss, using manufacturer's data about the maximum number of cycles the BES could deliver at a specific DoD.

The manufacturers of residential, stationary BESs (e.g., Tesla's Powerwall [50], and Samsung's SDI [51]) give a performance warranty of 10 years considering, in addition, an operating limitation in terms of maximum throughput or number of cycles, especially if the end-user combines the BESs with products/applications provided from different vendors. The end-of-life retained BES capacity is 65%-80%, which can depend on the geographic location of the BES installation, if the BESs are coupled with PVs. These applications, however, are relatively new, as these BESs were introduced in the market in 2015, and the BES retirement age and end-of-life retained capacity is not as well determined as in EV applications. Further research is required to more accurately quantify the benefits of using residential, stationary BESs in load shifting applications considering the impact of degradation.

The challenge to accurately assess the impact of degradation on the operation cost of the MG is therefore twofold. First, the employed degradation model should be representative of the main aging factors associated with BES usage without adding unnecessary complexity to the optimal MG energy scheduling problem. Secondly, regardless of the followed modeling approach, the assessment should account for factors such as future BES replacement cost and expected BES retirement age.

2.3.2 BES scheduling models

Up until now, studies on optimal BES dispatch that consider degradation have been using technical BES models, which are built on some simplifying assumptions regarding the BES operation, e.g., the charging/discharging energy efficiency and the power limits are considered to be constant and independent of the BES's SoC. The BES scheduling in [30], which is formulated as a Markov decision process, considered both degradation and effective charging/discharging power dependent on the SoC resulting in an improved BES model compared to previously mentioned works. Still though, the round-trip efficiency was considered to be constant.

The simplifications of the BES scheduling models can lead to miscalculations and failure to implement the BES schedule, e.g., the scheduled BES energy might not be delivered or the BES might fail to reach the scheduled energy storage level. Neglecting the BES power dependency on SoC can actually be a valid assumption, if additional limits on stored energy are considered. Rated power can normally be delivered within the SoC region, which is available by the BES converter, i.e., where the storage voltage will not trigger the current limiter function. The benefit of additional SoC limits is twofold: 1) the power output becomes more predictable due to relatively stable voltage values and 2) the BES is protected from high stress. Thus, a BES model with this assumption is not expected to deviate much from the

behaviour of an actual BES. However, if the state-of-health (SoH) of the battery has deteriorated, the maximum power levels can be affected leading to decreased accuracy of this modeling approach.

As a way to deal with the issues that arise with the existing BES scheduling models, a few recent works proposed models that can integrate the actual, non-linear behavior of a real BES in linear programming (LP) optimization problems [52, 53]. The authors in [52] provide a piecewise linear approximation of the charging curve to account for the non-constant charging power limits, while simplifications are still applied on BES efficiency. Their BES model was tested for two C-rates, separately. In [53], each state of the BES operation is a linear combination of sampled points of operation taken from measurements. This approach considers dependency of both power and efficiency on SoC. Ref. [52, 53] did not consider BES degradation.

Promising results on the SoC estimation with the use of artificial neural networks (ANNs) have also been presented in [54, 55]. Boulmrharj et al. [54] showed that the use of ANN gave higher accuracy than model-based approaches for SoC estimation (the Coulomb counting method was used as a reference value). The long short-term memory (LSTM) method was deployed in [55] to forecast SoC estimation. Future research could integrate these methods in the optimal BES dispatch problem and investigate whether they could increase the reliability of the BES scheduling solution.

2.4 Industrial perspectives of MG integration

MG-EMSs are already offered by several manufacturers including ABB [56], Siemens [57], and General Electric [58] among others. Some of these platforms also provide integration with the supervisory control and data acquisition (SCADA) system of the utility through standard industrial protocols. Thus, the technology for both MG deployment and DSO integration is available. The adoption of MGs could benefit both end-users, which could reduce their energy cost, and the operation of the distribution system, which can exploit the energy flexibility offered by MGs. Despite the available technologies and the benefits to different stakeholders the MG integration raises questions from both sides.

In Europe, the development of MGs has not been significantly promoted yet, which is evident by the lack of regulations and policies on this concept [59]. In fact, only 11% of the total MG capacity can be found in Europe [60]. The low implementation can be attributed to the unbundled framework of operation. As the DSOs have generally not been able to own or operate DERs so far, it has been difficult to directly affect the MG integration. Besides, the DSOs deem flexibility services as less reliable compared to grid reinforcement, which reduces their incentive to implement MGs. Therefore, it seems that the general preference from the DSOs' side, especially in high-density urban areas, is a bottom-up integration initiated by the end-users. The investment on small-scale RESs and BESs is financially supported, however, there are no incentives for the end-users to invest on advanced control functions offered by the MG-EMSs. Apart from investments on advanced control systems, there are other

unresolved issues for the interested parties including communication infrastructure, standardization, grid ownership, cyber security, and data protection.

Interoperability and integration can also be challenging both for MGs and for MG components and heterogeneous devices, especially if these are provided by different vendors or manufacturers. Although Internet interface facilitates an easier integration of the control devices, each controllable device or converter-embedded controller might use a different communication protocol on top of the Transmission Control Protocol/Internet Protocol (TCP/IP) protocol. Moreover, not all control functions are available through Internet interface and, therefore, additional interfacing devices might be required, which adds to the complexity of the control system. Unless integration of end-user devices becomes a more standardized procedure, the prosumers will be discouraged to invest on smart devices, which could offer energy flexibility to the grid, or might not be interested on taking full advantage of their capabilities, unless there are very strong incentives from the utility company.

The future interest of DSOs in grid-connected MGs and their contribution in the distribution system operation could, however, rise considering the relaxation of the rules about energy storage ownership. Up until now, distribution utilities were not allowed to own and operate energy storages due to the unbundling of network operation and energy supply, as already explained. In the latest report of the Swedish Energy Markets Inspectorate [61], which was published in February 2020, it is clearly stated that DSOs can, as an exception, own and operate energy storage, if it is used to handle unexpected events and as long as the DSOs do not buy or sell energy to the energy or the balance market. With creating MGs in form of clusters of energy storage systems in certain strategic areas the DSO could alleviate congestion or regulate voltage, when needed in a network area. With a large number of energy storage based MGs, the distribution network could even become dispatchable and reduce the effect of uncertainties of RES generation and EV integration. However, excluding the participation to energy and balancing markets reduces the revenue streams from BESs, such as, for example, revenues associated with frequency response services and energy arbitrage. Thus, despite the change in the regulation and despite the services that BESs can offer to the operation of the distribution network, the DSOs' investment in BESs might not be efficiently rewarded.

Demonstrators of MGs

There are many laboratory-scaled MGs that are used for research on MG control, e.g., at the Electric Energy Systems laboratory in National Technical University of Athens [62], in Aalborg University [63] in Denmark, at the KIOS laboratory [64] in Cyprus, the Prince lab microgrid testbed [65] at Polytechnic University of Bari, in Italy and others. Jansen et al. [66] present a survey of smart grid labs, most of which can be found in Europe and many of these labs already implement MGs.

The need to bridge the gap between research and deployment motivated the development of field testbeds, e.g., in Kythnos island [67] of Greece, in Bornholm island [68, 69] of Denmark, at the University of California, San Diego [70] and others.

Among them, the Borrego Springs MG [71] in San Diego, California, is a characteristic example of an "unbundled utility MG", where the distribution assets of the MG are owned by the utility, while the DER of the MG are owned by independent producers and the MG customers.

In 2019, there were 4475 identified MG projects globally [60]. These MG projects are either in operation, under development, or under planning and the total MG capacity amounts to about 27 GW. Out of these about 11 GW (42.3%) belong to remote MGs, while the new MG projects that were recorded were mostly remote systems (93.4% of new entries). The projects that are taken into account include grid-connected systems that are capable of operating in island mode or remote systems that display at least one of the following characteristics: 1) RES-based generation, 2) combined heat and power (CHP) generation, 3) energy storage, and 4) control that enables optimal operation of the resources. The leader area in MG capacity is Asia Pacific with 37% of total MG capacity, followed by North America with 33%, Middle East and Africa with 14%, Europe with 11%, and finally Latin America with 5% [60].

In Sweden, there are no MGs, if the strict MG definition is considered, which requires islanding capability. There are, however, control systems, which cluster together the control of local energy sources. One example is Simris [72], a local energy system comprising a village of 140 households, a 500kW wind turbine, a 440kW solar power plant, and a 800 kWh battery. Other examples can found in local energy systems managed by the EnergyHub system provided by Ferroamp [73] such as e.g., the HSB Living Lab building [74, 75], the Brf Viva buildings [76], Fjärås [77], and others. The EnergyHub is a converter-embedded power management system, which integrates PV and BES DC/DC converters and can control the power exchange between the local energy system and the main grid by monitoring AC electricity load consumption and PV generation and controlling the BES power. These local energy systems resemble the operation of grid-connected MGs, which can also be viewed as platforms for small-scale integration of energy sources.

2.5 Summary of identified research gaps

From the literature review it was observed that studies on coordinated operation of the MGs and the DSO have exclusively focused on defining the amount of energy trade between the DSO and the MGs often without considering the underlying constraints of the distribution network operation. Thus, not all real-world examples of distribution network operation can be studied by these approaches. The first research question that was formulated in Section 1.1 indicates the attempt of this thesis work to assess the impact of MG integration and evaluate the cost of potential MG services considering unbundled network operation.

The role of BES as an energy-flexible resource was discussed in Section 2.3. For efficient BES dispatch and accurate evaluation of the BES utilization, it is important to consider both real-life performance and lifetime degradation of the BES, something which has not been investigated in published literature on optimal MG energy management, as was pointed out. This research gap is highlighted in the

second research question, which is addressed in the thesis. The literature survey also identified the drawbacks of the previous studies in realistically representing the BES degradation cost. Overcoming these issues is significant for answering the third research question in Section 1.1.

Chapter 3

Methodology

This chapter presents the methodology that was used to solve the MG energy scheduling problems, which are formulated in Section 4. First, the structure of the MG energy scheduling problem is described along with the coordination schemes that can be applied utilizing the DMS interface. Afterwards, the chapter presents the solution approaches that were followed in the simulation studies depending on the implemented coordination schemes and the studied problems. The final part of this chapter is dedicated to the study approach that was used with the simulations studies and the demonstrations of marked-based energy management designed for a BMG that uses BES as a flexible energy resource.

3.1 Structure of the energy scheduling problem

The fundamental structure of the MG energy scheduling problem is depicted in Fig. 3.1. An energy management scheme can have a scheduling horizon that depends on the accuracy of the forecasted values of load, non-dispatchable generation and electricity price. It can be applied hour-ahead, day-ahead, week-ahead or even month-ahead. The scheduling horizon is divided in time steps (time discretization steps), which usually (although not necessarily) correspond to the frequency update of the dispatched set-points and the resolution of the input data (resolution of forecast).

The profile of load and generation and the uncertainties of their fluctuation should be considered to choose an appropriate length for the time interval between two consecutive time steps. Typically, hourly or 15-minutes time intervals are used in energy management. Energy management schemes with time intervals which are shorter than 5 minutes can be classified as real-time energy management schemes [16, 36].

For implementation of real-time or close to real-time energy management, the rolling horizon (RH) approach (Fig. 3.2) must be adopted. When the MG energy scheduling follows a RH approach, the energy scheduling problem is solved before each time step. The set-points for the first time step are dispatched to the MG resources after

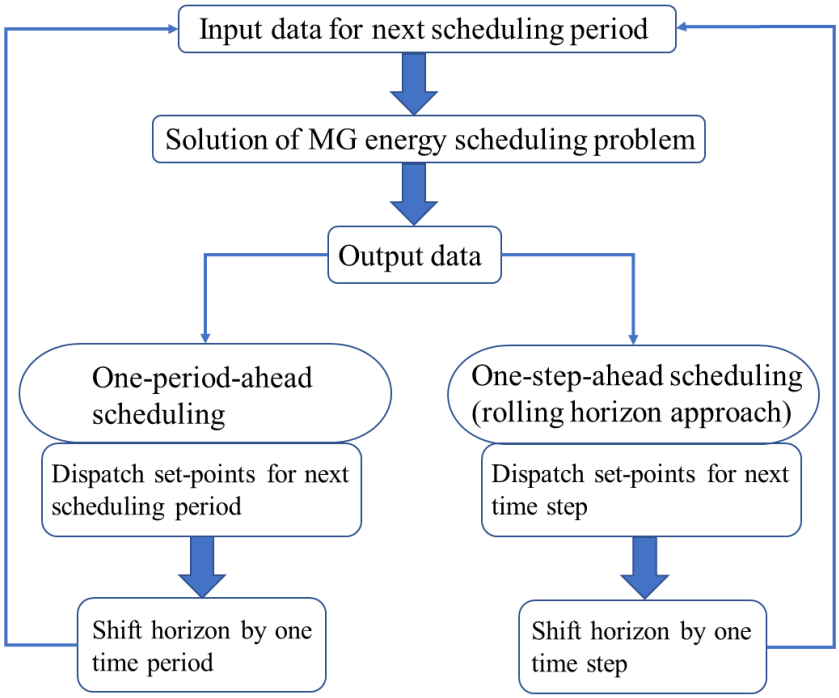

Figure 3.1: The structure of the energy scheduling problem.

each simulation that solves the energy scheduling problem, while the time horizon is shifted forward for the next simulation, as shown in the flow diagram (Fig. 3.1). The RH approach allows dynamic adjustment of the set-points and, therefore, the applied energy scheduling is less affected by errors in the forecast of the demand and the local generation (e.g., DERs) or errors in the state estimation of the network.

The MG-EMS retrieves the reference set-points, which are obtained from the solution of the MG energy scheduling problem, and transmits them to the MG resources (e.g., dispatchable generators, BESs, controllable loads) using the available communication links (see Fig. 3.3). The solution of the MG energy scheduling problem depends on the operational objectives of the MG operator. It is assumed that the MG operator is also the owner of the MG's DERs and is responsible for delivering power to the MG customers. The MG operator is a different entity from the DSO. As can be seen in Fig. 3.3, the MG-EMS has an interface with the DMS, which is used for the integration of the MG to the distribution system.

The proposed architecture for the integration of the MG to the distribution system can be seen in Fig. 3.4, which is a schematic representation of the interface between the MG-EMS and the DMS. Two-ways communication is always assumed between the MG-EMS and the DMS. No communication or interaction is considered between different MG-EMSs, i.e., the MG-EMSs can only interact with the DMS. Three different schemes of coordination between the MG-EMS and the DMS are depicted in Fig. 3.4. The grid-connected MGs might utilize the same coordination scheme for their interaction with the DSO or each MG might utilize a different scheme, depending on the agreement between the DSO and the MG operator. These coordination schemes, which affect the approach followed for the solution of the MG

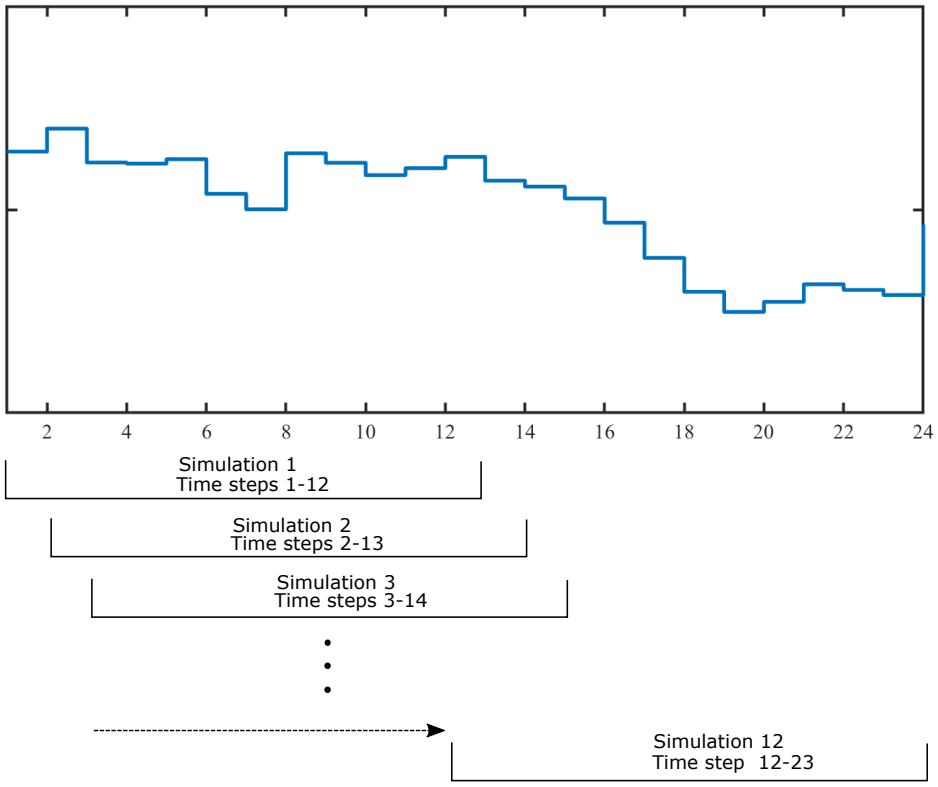

Figure 3.2: The rolling-horizon approach (each simulation shifts forward in time).

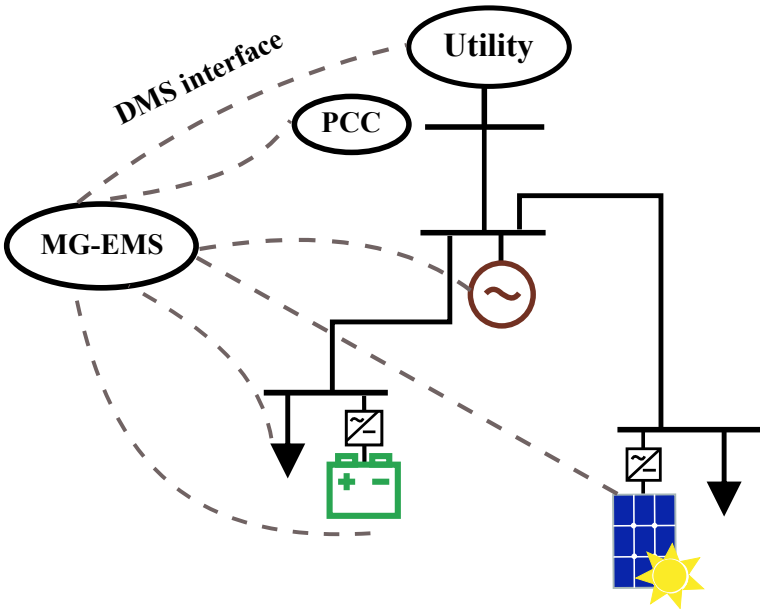

Figure 3.3: The communication infrastructure of the MG-EMS.

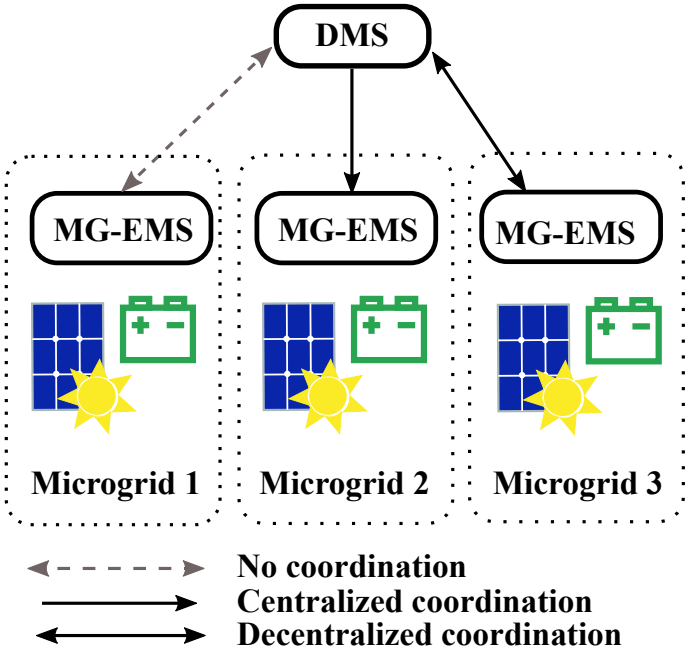

Figure 3.4: The integration of the MG-EMS to the DMS.

energy scheduling problem, can be described as follows:

- **No coordination:** The MG-EMS solves the energy scheduling problem and dispatches the MG resources according to this solution.
- **Centralized coordination:** It is assumed that the DMS is empowered to dispatch the MG resources. The MG-EMS receives the reference set-points from the DMS and then transmits them to the MG resources.
- **Decentralized coordination:** The DMS can only transmit the desired reference values for the PCC and is in no other way involved in the MG energy scheduling. Alternatively, the connected entities can negotiate the PCC reference set-points and the MG-EMS might solve the energy scheduling problem several times until the obtained solution satisfies both MG operator and DSO operator. Once the PCC set-points and the schedule of exchanged energy has been finalized, the MG-EMS transmits the set-points, which had been obtained from the solution of the energy scheduling problem, to the MG resources.

3.2 Uncoordinated and centralized energy scheduling strategies

This section presents MG energy scheduling strategies that can be used in uncoordinated and centrally coordinated schemes. The strategies solve the MG energy scheduling problem day-ahead and can be used to evaluate the performance of the MGs and the DSO under different operating scenarios. In the uncoordinated scheme, the MG operators seek to optimally schedule the available DERs, while satisfying

Table 3.1: Energy scheduling strategies

	MG-A	**MG-B**	**DSO**
Strategy 0 (BAU)	no optimization	no optimization	–
Strategy 1 (S1)	max. profit	min. cost	–
Strategy 2 (S2)	min. energy exchange	min. cost	–
Strategy 3 (S3)	min. import	min. import	–
Strategy 4 (S4)	–	–	min. cost

energy balance within the MG and the operational constraints of the resources. The MG resource mix can include BESs, demand response resources (DRRs), PV systems, which are non-dispatchable generation sources, and CHP plant, which is a dispatchable generation source. Each MG is assumed to have its individual operational targets and strategy. These determine the energy scheduling of the DERs, which is applied by the MG-EMS. In the centralized coordination scheme, the DSO directly dispatches the MG resources in order to satisfy an operational target that is applicable to the whole grid (including the MGs).

The energy scheduling strategies for a distribution network with two connected MGs are summarized in Table 3.1. Strategy 0 is the business as usual (BAU) scenario, where the dispatch of the BES follows a rule-based algorithm that triggers charging and discharging based on peak and low load thresholds. This algorithm is described in Section 5.6. No DR is considered in BAU. Strategies 1-3 (S1-S3) apply uncoordinated energy scheduling, and thus solve local optimization problems. As can be seen in Table 3.1, the MGs can have different objectives. Centrally coordinated energy scheduling (global optimization) is considered in Strategy 4 (S4). Depending on the strategy (operational objectives) and entity that dispatches the MG resources, a different day-ahead energy scheduling problem is formulated and solved. The optimization problems which are formulated for the strategies of uncoordinated and centrally coordinated energy scheduling can be found in Section 4.3.

The solution approach can be seen in Fig. 3.5. The results of day-ahead scheduling provide the hourly set-points of operation of the resources for the next day. The status of the resources (e.g., SoE level of BES) at the end of the day is given as input (initial operating status) for the next day-ahead simulation. The rest of the input data, which can be seen in Fig. 3.5, are the same across all studied strategies. Therefore, it is the different operation set-points that provide a different solution for each strategy.

3.3 Decentralized DMS and MG-EMS coordination

This section presents a decentralized coordination scheme for the optimal energy management of multiple grid-connected MGs. The MG-EMSs first coordinate their operation with the DMS before transmitting the reference set-points to the DERs.

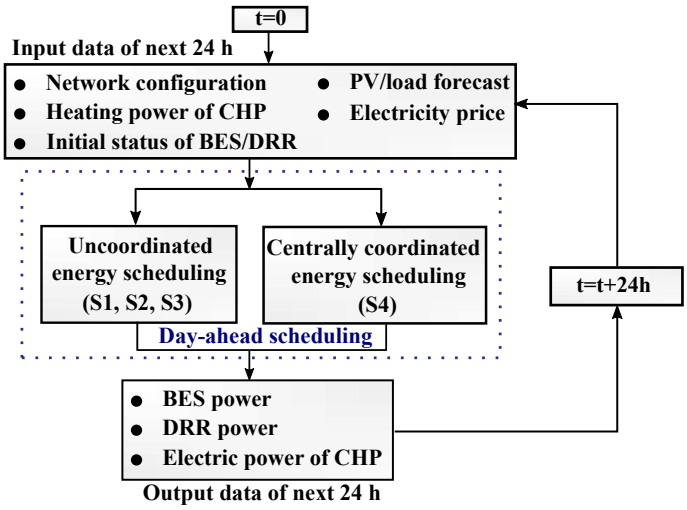

Figure 3.5: The flow diagram depicting the solution approach for energy scheduling strategies in an uncoordinated or centrally coordinated scheme.

The interaction with the DMS ensures that the scheduled exchange power at the PCC satisfies the solution of all connected entities. The interaction between the MG-EMS and the DMS ensures the technical feasibility of the scheduled PCC power exchange both on MG level and on distribution network level. If technical feasibility is at stake, the MGs are required to reschedule, i.e., solve the energy management problem again, considering the new information they have obtained from the communication with the DSO. The rescheduling seeks to solve the problems that the previous schedule was expected to cause. Thus, the DMS interface can be utilized by the DSO to indirectly dispatch the MGs, i.e., to modify the active power exchange between MGs and the connected network, and align the MG resource dispatch with the requirements of the distribution system.

This decentralized coordination scheme can also be used to dispatch MG flexibility, which can be used to offer balancing services to the transmission system. The MGs are considered as flexibility entities, which can provide energy flexibility by altering the injection or absorption of active or reactive power at the PCC. A balance responsible party (BRP) that operates within a distribution grid should coordinate with the DSO to ensure that the dispatched flexibility does not violate the distribution network's constraints. Therefore, even though it is the BRP that is financial representative and will be penalized in case of an imbalance to the transmission system, it is the DSO that interacts with the MGs to enable this flexibility provision and satisfy the balancing requests in order to ensure the safe network operation. In a future scenario, the economic responsibility for system balancing could be assigned to the DSO [78], especially if regulations promote energy storage investments by the DSOs, which could upgrade the distribution systems to dispatchable systems, as suggested by [79].

The proposed solution approach, which utilizes decentralized coordination for the energy scheduling of MGs, is privacy-preserving, as the DMS does not have any knowledge of the MG network and capacity configuration, which is aligned with

the guidelines provided in [43]. The MG-EMSs and the DMS do not exchange any additional information such as DER operating points, DER technical constraints, grid constraints or individual operational targets. The desired PCC values are the only data that need to be exchanged between the MG-EMSs and the DMS.

Three cases of energy scheduling with decentralized coordination have been examined. The optimization problems that have been formulated for the MG-EMSs and the DMS are defined in Section 4.3. Below is a description of the three cases.

Case-1

In this case, the MGs solve the MG energy scheduling hour-ahead. The interaction with the DMS ensures technical feasibility of the set-points in all inter-connected entities. After the MG-EMSs send the hour-ahead schedule of active and reactive power exchange to the DMS, the DMS calculates the voltage at MGs' PCCs and transmits it back to the MGs together with the confirmation that the MGs can proceed with their desired schedule. The MGs must then check again the validity of the previous solution utilizing the information they have received from the DMS, i.e., the expected hourly voltage profile at the PCC. If the previous solution is infeasible, the MGs must reschedule their resources. Therefore, the MG-EMSs solve the energy scheduling problem again and update the solution. The updated solution must satisfy the PCC values that have already been agreed with the DMS.

Case-2

The MG energy scheduling follows a RH approach, which means that the time horizon is shifted forward before each simulation by the time interval that corresponds to one time step. In addition, the hour-ahead load, PV, and electricity price forecast input is updated. Similar to Case-1, the obtained optimal set-points are dispatched by the MG-EMSs after coordination with the DMS to ensure that the set-points do not violate the network bus voltage and line current limits. As these set-points are dynamically adjusted within the hour, the information exchange and coordination that was described for Case-1, is more frequently performed in Case-2.

Case-3

In Case-3, the MG energy scheduling is formulated as a bilevel problem, where the upper level consists of the optimization problem solved by the DMS and the lower level consists of the optimization problems (optimal MG energy scheduling problems) solved by the MG-EMSs in a rolling-horizon approach. The solution methodology which is introduced decomposes the bilevel problem into two separate optimization problems that exchange information to update their parameters. Each network entity solves an AC optimal power flow problem considering individual operational objectives and technical constraints.

The DSO seeks to reschedule the MGs and dispatch MGs' flexibility in order to satisfy an intra-hour balancing power request to the extent that this does not violate the distribution network's constraints. With this flexibility, the DSO aims to reduce

the deviation between the aggregated power exchange at the MGs' PCCs and the active power amount, which is requested from the BRP operating within the utility's grid. It is assumed that the DMS receives a new imbalance signal before each time interval of the simulated period and that this signal is valid for the next time interval. The DMS also receives the MGs' desired schedule for the next time step, i.e., the active and reactive power exchange at the PCC, as the MGs apply energy scheduling with RH approach and thus adjust their scheduled power exchange before each time step. The DSO decides on the flexibility amount after having received the above-mentioned information from the BRP and the MG-EMSs.

The flexibility amounts are transmitted as flexibility requests to the MG-EMSs, which reply to the DMS to inform whether they can provide the requested power at PCC. If the MGs can satisfy the requests, then the coordination procedure terminates, and the interaction described in the previous cases finalizes the schedule, i.e., the DMS calculates and sends the voltages at the MGs' PCC and the MGs validate their energy scheduling solution. Otherwise, the DMS requests additional amounts from the MGs with higher dispatch flexibility. When a flexibility request is rejected, the DMS requests the maximum flexibility amount that can be provided. When no more flexibility is required or can be dispatched, the coordination procedure is terminated and the schedule is finalized. Fig. 3.6 depicts the solution methodology for Case-3.

3.4 Market-based energy management of a BMG

The proposed BMG energy management model is integrated in a BMG-EMS and is used to dispatch BES as a flexible resource considering the energy market-based participation of the buildings. The BMG-EMS controls the BES using the forecasted values of the electricity price, PV generation and building electricity consumption as inputs. It is assumed that the building owner is also the BES owner as well as the BMG operator, and employs the BMG-EMS for economic BES dispatch considering a business model, where the BMG can purchase and sell energy to a retail electricity provider at wholesale market price. The BMG-EMS solves the energy scheduling problem without coordination with the DSO.

A flow diagram of the approach adopted in the simulation studies and demonstrations of the BMG energy management model is depicted in Fig. 3.7. As can be seen in Fig. 3.7, four different energy management models have been defined depending on whether the mathematical model of the BES incorporates real-life performance characteristics (measurement-based model) and the impact of cycle-based degradation. Model-1 incorporates the simplified BES scheduling model typically used in MG energy management, while Model-2 makes use of a measurement-based BES scheduling model that can capture a more realistic BES operation performance. The impact of degradation is not considered in the BES scheduling decisions according to these two models. Instead, Model-3 and Model-4 consider the impact of cycle-based degradation and they incorporate both the measurement-based BES scheduling model and different cycle aging models to account for degradation cost.

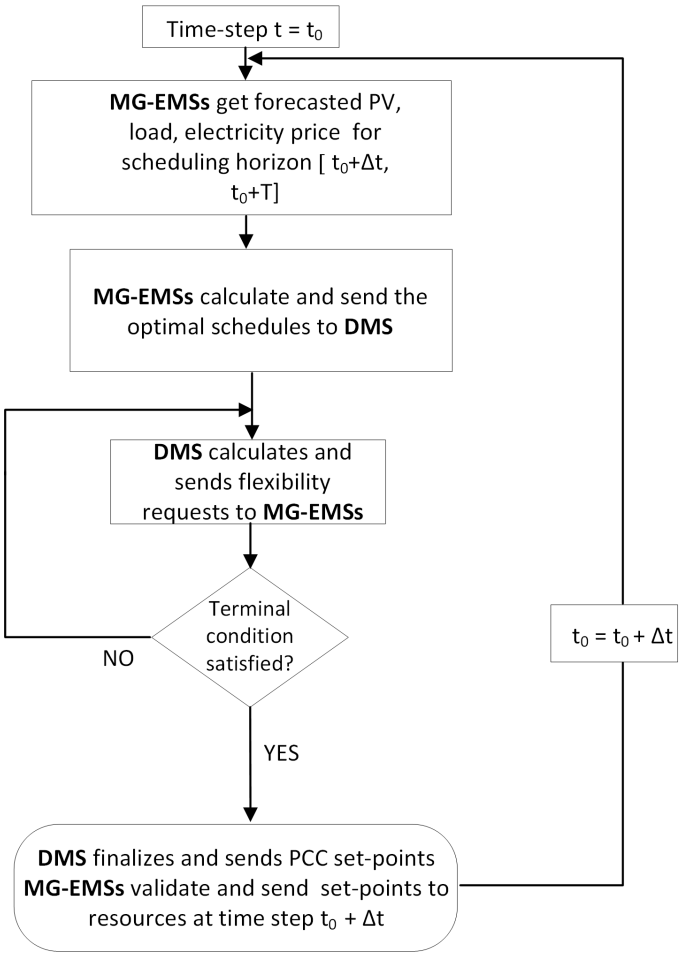

Figure 3.6: The flow diagram depicting the solution methodology for Case-3, where the DMS uses decentralized coordination to dispatch flexibility from grid-connected MGs.

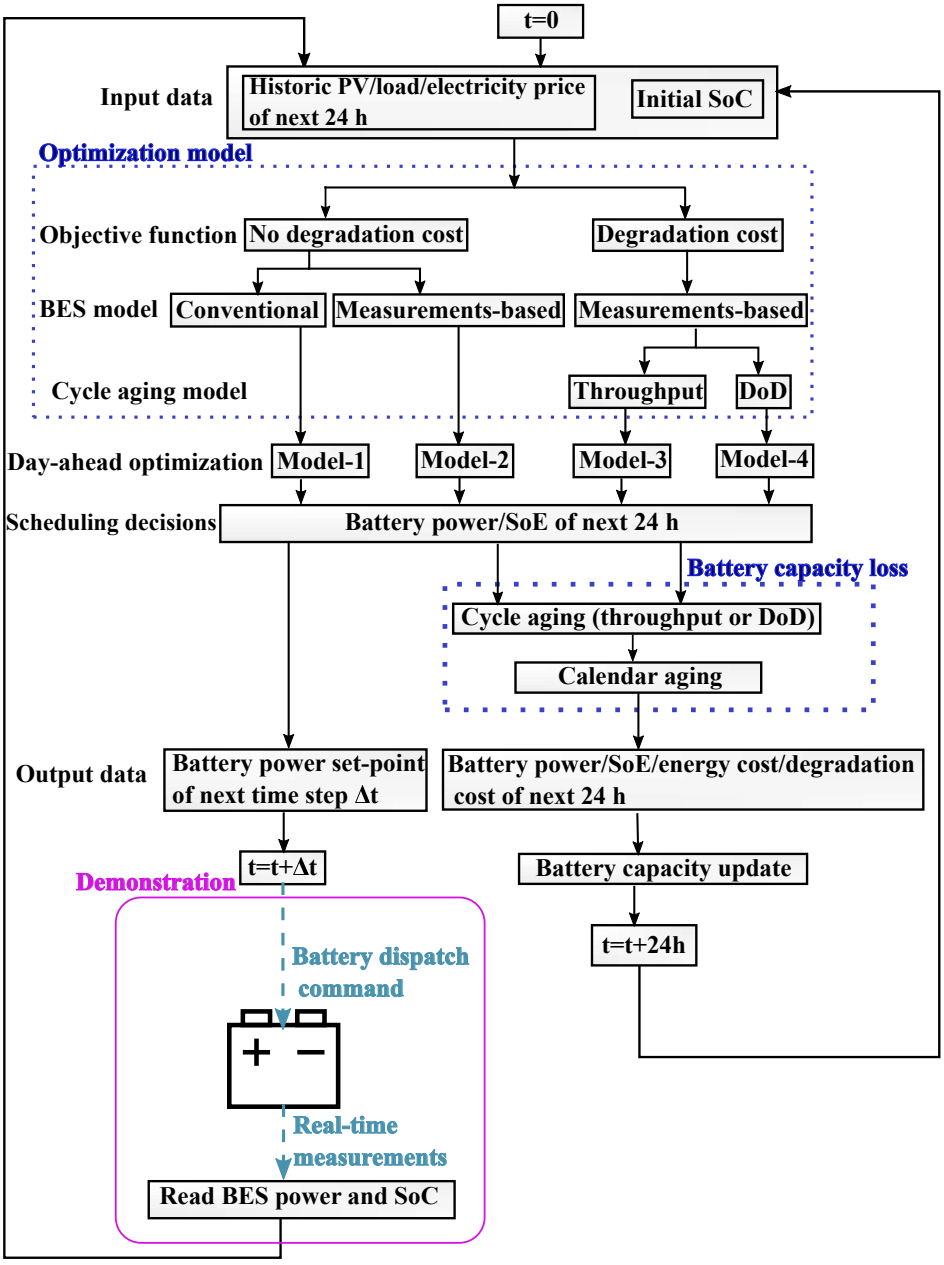

Figure 3.7: The flow diagram presenting the simulation studies and demonstration of the BMG energy management model.

The scheduling decisions resulting from the use of each of these four models can be used to assess the operation cost of the BMG and the BES utilization and degradation. Moreover, as Fig. 3.7 shows, the scheduling decisions can be used to control the BES (dispatch BES power). The formulated optimization problems according to these models are described in detail in Section 4.3.

Simulation studies

The BES capacity was updated after each day-ahead optimization, as shown in Fig. 3.7. First, the capacity loss due to cycle aging was calculated using one of the

models presented in Section 4.1.6 (dependency on throughput or DoD). Afterwards, this loss was subtracted from the capacity that the BES had at the beginning of the day. Finally, the loss due to calendar aging was calculated and subtracted from the remaining capacity for every time step of the scheduling period that was an open-circuit period for the BES.

Demonstrations

The purpose of the demonstrations was to validate the accuracy of the BES scheduling models, which are incorporated in the optimization models given in Section 4.3. A RH approach was used for the demonstrations. The optimization problem was solved before each time interval (Δt). The set-point for the first time step was dispatched after each simulation, while the time horizon was shifted forward by Δt for the next simulation, as shown in the flow diagram (Fig. 3.7).

Chapter 4

Optimal Energy Scheduling of Grid-connected Microgrids

This section presents the optimization models that were developed and used to formulate the optimal energy scheduling problem for grid-connected MGs. This problem is solved by the MG-EMS of each individual MG. However, the solution can also be affected (or even directly dispatched) by the DMS of the DSO depending on the level of interaction between the MGs and the DSO. Hence, the problem structure and optimization models will be presented separately for the MGs and the DSO. At the end of this section, the formulated optimization problems in relation with the followed solution approach will be described.

4.1 Optimization model for the grid-connected microgrids

The proposed MG-EMS is designed to control the electrical power supply of the MG loads and the electrical power exchange with the connected main distribution grid. The MG operators seek to optimally schedule the available DER, while satisfying power balance within the MG and the operational constraints of the resources. The DER considered in this work include: distributed generation provided by a biofuel based combined heat and power (CHP) plant, distributed generation of PVs, distributed BESs and demand response resources (DRRs).

4.1.1 Objective functions

In this section, two generic objective functions are formulated depending on the main operational target of the MG owner/operator. The first objective function is cost minimization, which can alternatively be formulated as profit maximization, and is related to economic operation targets. The other objective function is the energy exchange minimization and is related to the desired level of interaction between the microgrid and the main grid.

The objective function for *cost minimization* is:

$$\min \sum_{t\in\mathcal{H}}((P^{spot}+C^{tr})p^{im}_{i,t}\Delta t-(P^{spot}+C^{r})p^{ex}_{i,t}\Delta t)+c^{DER}_{i}+r^{p}_{i},\ \forall i\in\mathcal{MG}. \quad (4.1)$$

In (4.1), $\mathcal{MG}$ is the set of the MGs' PCC with the distribution network, $\mathcal{H}$ is the scheduling horizon, and Δt is the time discretization step. The positive variables $p^{im}_{i,t}/p^{ex}_{i,t}$ denote the MG imported/exported power from/to the upstream network through the PCC at bus i.

The first term in (4.1) is the cost of the imported energy, where P^{spot} is the spot price and C^{tr} is the grid charge for energy transmission (grid utilization). The second term is the revenue associated with the energy exported to the grid considering a business model, where the MG can purchase and sell energy to a retail electricity provider at wholesale market price. The reimbursement fee C^{r} is paid by the distribution system operator (DSO) as an incentive to reduce network losses.

The term c^{DER}_{i} refers to variable operation costs associated with the DER owned by the MG (e.g., fuel costs, degradation costs). Finally, r^{p}_{i} is the cost of the peak power drawn from the main grid, which satisfies:

$$r^{p}_{i}\geq C^{p}p^{im}_{i,t},\forall i\in\mathcal{MG},\ t\in\mathcal{H}. \quad (4.2)$$

In (4.2), C^{p} is the power-based grid tariff, which is linked to the maximum average power of the studied period (measured per Δt).

The objective function for *energy exchange minimization* is:

$$\min \sum_{t\in\mathcal{H}} p^{ex}_{i,t}\Delta t+p^{im}_{i,t}\Delta t,\forall i\in\mathcal{MG}. \quad (4.3)$$

A MG that minimizes the energy exchange with the distribution grid aims at increasing the level of autonomy and zero energy exchange indicates the possibility of off-grid operation provided that the MG has islanding operation and control capability. Besides the capacity and the technical constraints of the MG resources, the choice of scheduling horizon and solution methodology, i.e., if the scheduling problem is solved one-period ahead or in RH, can also affect the level of autonomy. If the first term is omitted from (4.3), then the MG operator aims to minimize imported energy, which is equivalent to maximizing the use of MG resources. If the second term is omitted instead i.e., the aim is to minimize exported energy, the objective function becomes equivalent to the *maximization of self-consumption.*

4.1.2 MG energy balance

The active and reactive power balance of the MG are given by

$$\sum_{j\in\mathcal{N}}(p^{G}_{j,t}+P^{PV}_{j,t}+p^{dis}_{j,t}+p^{DR}_{j,t}-P^{L}_{j,t}-p^{ch}_{j,t})+p^{im}_{i,t}-p^{ex}_{i,t}=0, \tag{4.4}$$

$$\sum_{j\in\mathcal{N}}(q^{G}_{j,t}+q^{DR}_{j,t}-Q^{L}_{j,t})+q^{im}_{i,t}=0, \tag{4.5}$$

for all $i \in \mathcal{MG},\ t \in \mathcal{H}$, where $\mathcal{N}$ denotes the set of MG buses (including the PCC bus). Constraint (4.4) defines the active power balance, where the variables $p^{G}_{j,t}$, $p^{dis}_{j,t}/p^{ch}_{j,t}$, and $p^{DR}_{j,t}$ refer to electrical power output from the CHP plant, charging/discharging power from distributed BESs and curtailed (or increased) power from DRRs, respectively, and the parameters $P^{PV}_{j,t}$ and $P^{L}_{j,t}$ refer to active power from PV generation and active power of load demand, respectively. The PV systems are non-dispatchable generation sources and can therefore be viewed as negative loads. They operate at fixed (unitary) power factor and they do not participate in Volt/Var control. Constraint (4.5) defines the reactive power balance, where constant power factor is considered for generation and load (flexible and inflexible). The variables $q^{G}_{j,t}$ and $q^{DR}_{j,t}$ refer to reactive power from the CHP plant and reactive power of DRRs, respectively, while parameter $Q^{L}_{j,t}$ refers to reactive power of load demand.

4.1.3 Combined heat and power plant

A CHP plant is a source of heat and electrical power. It is considered that the CHP is primarily scheduled for heating energy production. When there is generation of heat, the electrical power output of the CHP plant can be controlled and is constrained by

$$P^{G,min}_{j} \le p^{G}_{j,t} \le P^{H}_{j,t} r^{CHP}_{j},\ \forall j \in \mathcal{N},\ \forall\ t \in \mathcal{H}, \tag{4.6}$$

where $P^{G,min}_{j}$ is the minimum electrical power output and $P^{H}_{j,t}$ is the heating output, which is treated as a parameter. Constraint (4.6) is only effective, when there is generation of heating power. The parameter r^{CHP}_{j} is the ratio of electrical power to heating power output, which depends on the type of fuel and the operating point of the electric generator.

If the CHP plant is a part of the MG's resource mix, the term C^{CHP}_{j} is added as part of c^{DER}_{i} in (4.1), where

$$C^{CHP}_{j} = \sum_{t\in\mathcal{H}} C^{f}_{j} P^{H}_{j,t},\ \forall j \in \mathcal{N} \tag{4.7}$$

and C^{f}_{j} refers to the fuel cost of the CHP plant. Although C^{CHP}_{j} is not affected by the solution of the energy scheduling problem, the cost of the MG is affected by the electrical power output of the CHP, since the power exchange with the grid and potentially the peak imported power are also modified.

4.1.4 Demand response

The model for load flexibility is equivalent to a generic energy storage model and is described by the constraints on the energy that is available for demand response:

$$e_{j,t}^{DR} = e_{j,t-1}^{DR} + p_{j,t-1}^{DR}\Delta t,\ \forall j \in \mathcal{N},\ \forall t \in \mathcal{H}, \tag{4.8}$$

$$0 \leq e_{j,t}^{DR} \leq P_{j,t}^{L,r},\ \forall j \in \mathcal{N},\ \forall t \in \mathcal{H}, \tag{4.9}$$

$$-\kappa_j^{DR} P_{j,t}^{L,r} \leq p_{j,t}^{DR} \leq \kappa_j^{DR} P_{j,t}^{L,r},\ \forall j \in \mathcal{N},\ \forall t \in \mathcal{H}. \tag{4.10}$$

In the above formulas, $e_{j,t}^{DR}$ is the part of energy available from DRRs that has already been curtailed at time t. The value of the maximum energy capacity of the DRRs is related to the available responsive load $P_{j,t}^{L,r}$ at MG bus j and κ_j^{DR} is the power to energy ratio, which depends on the technology of the DRR [80].

4.1.5 BES scheduling

This section presents two BES scheduling models that have been used in the optimization problems that were defined in the thesis. The first model is the conventional BES model, which has most frequently been used in relevant literature on optimal MG energy management. The other model, is a measurements-based model, which more accurately represents the behavior of a real BES, as it can capture non-ideal BES operation.

Since the BES throughput is calculated in Wh instead of Ah in the proposed optimization model, the term state-of-energy (SoE) is used instead of the SoC [52]. The SoE level is not affected by fluctuations of the BES voltage in contrast with SOC. However, the term SoC is still used, for the experimental BES measurements presented in the thesis. This thesis also defines DoD as the discharged energy from 100% SoE, i.e., $DoD = 1 - SoE$.

Conventional model

The BES model that has been most frequently used in the latest literature on BES scheduling (e.g., [24, 25, 31, 32]) assumes that the SoE of the BES at each time step is linearly dependent on the cumulative BES throughput of the previous time steps. The charging/discharging energy efficiency and the power limits are considered to be constant and independent of the SoE level. This model is described by the following equations:

$$soe_{j,t} = soe_{j,t-1} + \eta_j^{ch}\frac{p_{j,t-1}^{ch}\Delta t}{E_j^{max}} - \frac{p_{j,t-1}^{dis}\Delta t}{\eta_j^{dis} E_j^{max}},\ \forall j \in \mathcal{N},\ \forall t \in \mathcal{H}, \tag{4.11}$$

$$SoE_j^{min} \leq soe_{j,t} \leq SoE_j^{max},\ \forall j \in \mathcal{N},\ \forall t \in \mathcal{H}, \tag{4.12}$$

$$0 \leq p_{j,t}^{ch} \leq \kappa_j E_j^{max},\ \forall j \in \mathcal{N},\ \forall t \in \mathcal{H}, \tag{4.13}$$

$$0 \leq p_{j,t}^{dis} \leq \kappa_j E_j^{max},\ \forall j \in \mathcal{N},\ \forall t \in \mathcal{H}, \tag{4.14}$$

$$p_{j,t}^{ch} \leq z_{j,t} M,\ \forall j \in \mathcal{N},\ \forall t \in \mathcal{H}, \tag{4.15}$$

$$p_{j,t}^{dis} \leq (1 - z_{j,t}) M,\ \forall j \in \mathcal{N},\ \forall t \in \mathcal{H}. \tag{4.16}$$

In the above formulation, κ_j denotes the power to energy ratio, which determines the maximum charging/discharging power according to the specifications of the battery manufacturer. Moreover, η_j^{ch}/η_j^{dis} respectively refer to the charging/discharging efficiency, E_j^{max} is the installed capacity and $soe_{j,t}$ is the state-of-energy (SoE), which must lie between the lower and upper limit (SoE_j^{min} and SoE_j^{max}, respectively). The binary variable $z_{j,t}$ indicates if the BES is charging or discharging and M is a very large number, which is necessary for the linearization of this BES model. The linearization technique used in this case is called the big-M approach [81].

Measurement-based model

The assumptions that simplify the battery operation, i.e., the constant charging/discharging efficiencies and maximum power limits can be seen in (4.11), (4.13)–(4.14). Depending on the application and the BES state-of-health (SoH), these assumptions might lead to mismatches requested power. Therefore, a sampling-based approach, which was first presented in [53], is used to derive a model that captures more accurately the behavior of an actual BES by utilizing underlying patterns that exist in the charging/discharging data.

This measurement-based model uses sample data from charging/discharging curves and satisfies (4.17)–(4.24), where $\mathcal{M}$ ($\mathcal{K}$) denotes the set of discharging (charging) data and $p_{j,t}^-/p_{j,t}^+$ respectively represent power output/input from/to the battery cells, before/after battery losses have been taken into account. The positive variables $p_{j,t}^-/p_{j,t}^+$ are related to the variables $p_{j,t}^{dis}/p_{j,t}^{ch}$ (i.e., the power injected to/absorbed from the grid) through the positive variables $x_{j,m,t}$ and $y_{j,k,t}$, which are associated respectively with the choice of discharging sample data ($SoE_{j,m}^{dis}, P_{j,m}^-, P_{j,m}^{dis}$) or charging sample data ($SoE_{j,k}^{ch}, P_{j,k}^+, P_{j,k}^{ch}$). The sample data form the convex hull of the feasible region for BES operation points. Thus, the variables ($soe_{j,t}, p_{j,t}^+, p_{j,t}^{ch}, p_{j,t}^-, p_{j,t}^{dis}$) can be written as convex combinations of the sample measurements:

$$soe_{j,t} = soe_{j,t-1} + \frac{p_{j,t-1}^+ \Delta t}{E_j^{max}} - \frac{p_{j,t-1}^- \Delta t}{E_j^{max}},\ \forall j \in \mathcal{N},\ \forall t \in \mathcal{H}, \tag{4.17}$$

$$p_{j,t}^{-} = \sum_{m \in \mathcal{M}} P_{j,m}^{-} x_{j,m,t}, \ \forall j \in \mathcal{N}, \ \forall t \in \mathcal{H}, \tag{4.18}$$

$$p_{j,t}^{dis} = \sum_{m \in \mathcal{M}} P_{j,m}^{dis} x_{j,m,t}, \ \forall j \in \mathcal{N}, \ \forall t \in \mathcal{H}, \tag{4.19}$$

$$p_{j,t}^{+} = \sum_{k \in \mathcal{K}} P_{j,k}^{+} y_{j,k,t}, \ \forall j \in \mathcal{N}, \ \forall t \in \mathcal{H}, \tag{4.20}$$

$$p_{j,t}^{ch} = \sum_{k \in \mathcal{K}} P_{j,k}^{ch} y_{j,k,t}, \ \forall j \in \mathcal{N}, \ \forall t \in \mathcal{H}, \tag{4.21}$$

$$soe_{j,t} = \sum_{m \in \mathcal{M}} SoE_{j,m}^{dis} x_{j,m,t} + \sum_{k \in \mathcal{K}} SoE_{j,k}^{ch} y_{j,k,t}, \ \forall j \in \mathcal{N}, \ \forall t \in \mathcal{H}, \tag{4.22}$$

$$\sum_{m}^{M} x_{j,m,t} = 1, \ 0 \leq x_{j,m,t} \leq 1, \ \forall j \in \mathcal{N}, \ \forall t \in \mathcal{H}, \tag{4.23}$$

$$\sum_{k}^{K} y_{j,k,t} = 1, \ 0 \leq y_{j,k,t} \leq 1, \ \forall j \in \mathcal{N}, \ \forall t \in \mathcal{H}. \tag{4.24}$$

Eq. (4.17) calculates the BES's SoE at each time step. Similarly to (4.11), the SoE depends on the cumulative BES throughput and the SoE at the previous time step. Unlike the conventional model, however, the feasibility regions of BES power and SoE in the measurement-based model are not independent from each other. Instead, 3-dimensional feasibility regions are defined to constrain the values of BES operation (i.e., SoE, power input/output from/to the battery cells, and power injected to/absorbed from the grid), which are now dependent with each other. Constraints (4.18)–(4.19) and (4.22)–(4.23) define the feasibility region for BES operation points during discharging, while constraints (4.20)–(4.22) and (4.24) define the feasibility region during charging. No binary variables are required in this model, provided that the sample data include the BES state, where the BES is an open-circuit and fully charged or fully discharged [53].

It can easily be seen that this model also incorporates the variable (with respect to BES power and SoE) charging/discharging efficiencies (both internal BES losses and DC/DC converter losses are considered), which are given by $\eta_{j,t}^{ch} = \frac{p_{j,t}^{+}}{p_{j,t}^{ch}}$ and $\eta_{j,t}^{dis} = \frac{p_{j,t}^{dis}}{p_{j,t}^{-}}$, respectively, $\forall j \in \mathcal{N}, \forall t \in \mathcal{H}$ [53]. As the efficiencies are correlated with the model's decision variables, the efficiency values (at each BES power and SoE level) depend on the feasible combinations of $x_{i,t}$ and $y_{k,t}$, which determine the choice of p_t^{dis} and p_t^{-} (or p_t^{ch} and p_t^{+} during charging periods).

4.1.6 BES degradation

The BES degradation can be expressed as loss of available capacity or increase in the BES resistance and is linked in a non-linear manner to many factors [47, 82]. Degradation is caused when the BES is cycled as well as during resting periods (when the BES is an open-circuit). Different mechanisms are in effect in each case. Degradation is more prominent with high C-rates (C-rate of 1C indicates discharging at nominal discharging current, C-rate of 2C indicates discharging at twice the nominal current, etc. [53]), frequent cycling with high DoD, high operating temperatures, and resting periods at high SOC [82, 83]. The temperature in residential, stationary BES applications can easily be controlled and is therefore considered to be constant for the BES degradation models that are presented below.

Cycle aging (dependency on cumulative throughput)

The degradation model presented in [84] and modified in [29, 85] is used to model the dependency of cycle aging on cumulative throughput:

$$Q_j^l = B_1 e^{B_2 I_c} \sum_{t \in \mathcal{H}} (p_{j,t}^- + p_{j,t}^+) \Delta t \ , \forall j \in \mathcal{N}. \tag{4.25}$$

In (4.25), Q_j^l represents the cycle-based BES capacity loss in %, while the pre-exponential and exponential factors B_1 and B_2 can be obtained from empirical fitting of experimental data. The daily average C-rate I_c is entered as a parameter and thus (4.25) becomes linear.

The battery degradation cost c_j^B is calculated as:

$$c_j^B = \frac{C_j^{B,0} Q_j^l}{1 - \eta}, \forall j \in \mathcal{N}, \tag{4.26}$$

where $C_j^{B,0}$ is the purchase cost of the battery and η is the the end-of-life retained capacity percentage, i.e., the percentage of retained capacity, when the BES is retired (depending on the manufacturer, the end-of-life retained capacity can range from 65% to 80% [50, 51]). The battery degradation cost, if considered, can be added in the objective function for cost minimization (see (4.1)) as a part of the term c^{DER}.

Cycle aging (dependency on DoD)

To define a cost associated with cycle-based degradation, the model presented in [86] can be used, which estimates cycle aging taking into account the maximum DoD of each cycle. The battery degradation cost, if considered, can be added as a part of the term c_i^{DER} in (4.1). Given a function of lifecycle percentage loss for one cycle of a specific DoD, the cycle-based battery degradation cost entered in the objective function is given by

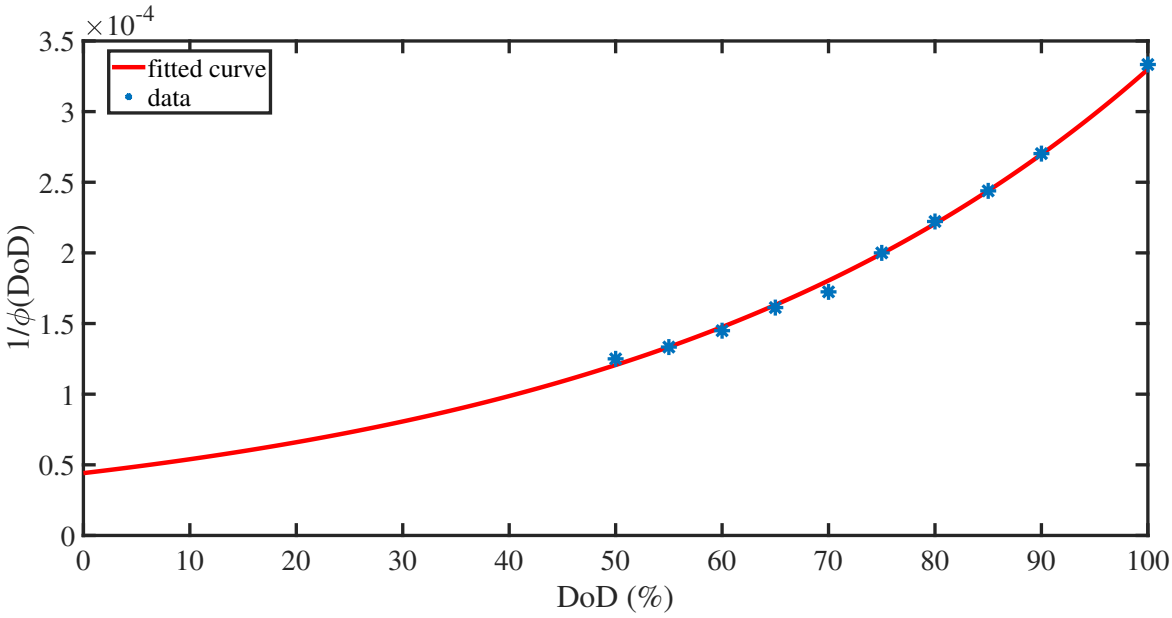

Figure 4.1: The percentage of lifecycle loss as a function of one cycle at a specific DoD.

$$c_j^B = \sum_{t \in \mathcal{H}} c_{j,t}^{DoD}, \ \forall j \in \mathcal{N}, \tag{4.27}$$

where $c_{j,t}^{DoD}$ is the cycle aging cost per time step t, given by

$$c_{j,t}^{DoD_j} = \max\{0, (\rho_{j,t} - \rho_{j,t-1}) C_j^{B,0}\}, \ \forall j \in \mathcal{N}. \tag{4.28}$$

This cost is related to the percentage of lifecycle loss $\rho_{j,t} = 1/\phi(DoD)$ for one cycle at a specific DoD, where $\phi(DoD)$ refers to the lifecycle as a function of DoD. The replacement cost of the BES is denoted by $C_j^{B,0}$. An example of the loss of lifetime as a function of DoD derived from data of a Li-ion BES can be seen in Fig. 4.1 (based on data from [28]).

In (4.28), $\rho_{j,t}$ is greater than $\rho_{j,t-1}$ only when the BES is discharging, since the loss of BES lifetime increases, when the DoD increases. Thus, the aging cost is added for every discharging half-cycle, while it is zero during charging. The degradation model can be piecewise linearized according to (4.29)–(4.34):

$$dod_{j,t} = \sum_{p \in \mathcal{P}} DoD_{j,p} \xi_{j,p,t}, \ \forall j \in \mathcal{N}, \tag{4.29}$$

$$\rho_{j,t} = \sum_{p \in \mathcal{P}} \widehat{\rho}_{j,p} \xi_{j,p,t}, \ \forall j \in \mathcal{N}, \tag{4.30}$$

$$\sum_{p}^{P} \xi_{j,p,t} = 1, \ \forall j \in \mathcal{N}, \tag{4.31}$$

$$0 \leq \xi_{j,p,t} \leq 1, \ \forall j \in \mathcal{N}, \ \forall t \in \mathcal{H}, \tag{4.32}$$

$$\begin{bmatrix} \xi_{j,1,t} \\ \xi_{j,2,t} \\ \vdots \\ \xi_{j,P,t} \end{bmatrix} \leq \begin{bmatrix} \boldsymbol{H} \end{bmatrix} \begin{bmatrix} b_{j,1,t} \\ b_{j,2,t} \\ \vdots \\ b_{j,P-1,t} \end{bmatrix}, \ \forall j \in \mathcal{N}, \tag{4.33}$$

$$\sum_{p=1}^{P-1} b_{j,p,t} = 1, \ \forall j \in \mathcal{N}. \tag{4.34}$$

In (4.29)–(4.30), $\mathcal{P}$ denotes the set of sample points of the lifecycle loss function, while $DoD_{j,p}$ and $\widehat{\rho}_{j,p}$ respectively refer to the sample points of DoD ($dod_{j,t}$) and lifecycle loss percentage ($\rho_{j,t}$), which are used for the piecewise linearization of the lifecycle loss function curve (Fig. 4.1). The positive variable $\xi_{j,p,t}$ is related to the choice of sample point $p \in \mathcal{P}$. Eq. (4.33)–(4.34) are adjacency constraints, where $\boldsymbol{H}$ is the adjacency matrix. The binary variable $b_{j,p,t}$ is used to ensure interpolation of the decision variables $dod_{j,t}$ and $\rho_{j,t}$ between consecutive sample points.

Calendar Aging

A linear model dependent on time-elapsed can be used to evaluate the BES capacity loss due to calendar aging:

$$Q_j^r = Q_j^{r,0} - a_j \Delta t, \ \forall j \in \mathcal{N}. \tag{4.35}$$

In (4.35), Q_j^r is the percentage of retained capacity after the rest period, $Q_j^{r,0}$ is the capacity percentage at the beginning of the rest period, and a_j is a parameter dependent on SoC level.

4.1.7 Network power flow

The network power flow constraints can often be disregarded in the optimal energy scheduling problem of a MG, since the lines within a MG are typically very short. Especially, when the MG-EMS is integrated to the DMS incorporating network constraints of the MG could add unnecessary complexity to an already hard to solve bi-level optimization problem, as the OPF of the large distribution network would be constrained by the OPF of several subnetworks.

If the MG optimal energy scheduling is formulated as an AC OPF problem, the branch flow model (BFM) can be used to describe the network power flow. The BFM

is a relaxed model of the original non-convex OPF problem [87], which applies angle relaxation to eliminate the phase angles of voltages and currents. This relaxation is exact only for radial distribution networks, i.e., the obtained solution for a meshed network might not be globally optimal. The AC power flow of the radial network is described by a set of equations, also known as DistFlow equations, which was first presented in [88].

Below is the derivation of the linearized BFM for a radial distribution network represented by a set of buses $\mathcal{N}$, which was presented in [87].

Branch flow model

The BFM, which is derived after the angle relaxation, is given by [87]:

$$p_j = \sum_{i:j\sim i} p_{ji} - \sum_{i:i\sim j} (p_{ij} - R_{ij}\frac{p_{ij}^2 + q_{ij}^2}{|V_i|^2}) + G_i|V_i|^2,\ \forall j \in \mathcal{N}, \tag{4.36}$$

$$q_j = \sum_{i:j\sim i} q_{ji} - \sum_{i:i\sim j} (q_{ij} - X_{ij}\frac{p_{ij}^2 + q_{ij}^2}{|V_i|^2}) + B_i|V_i|^2,\ \forall j \in \mathcal{N}, \tag{4.37}$$

$$\begin{aligned} |V_j|^2 = |V_i|^2 - 2(R_{ij}p_{ij} + X_{ij}q_{ij}) + (R_{ij}^2 + X_{ij}^2) \\ \frac{p_{ij}^2 + q_{ij}^2}{|V_i|^2}, \forall (i,j) : i \sim j,\ \forall i,j \in \mathcal{N}. \end{aligned} \tag{4.38}$$

where $j \sim i$ represents a line between bus j and bus i. In (4.36)–(4.38), p_j/q_j denote the active/reactive power injection at bus j, p_{ji}/q_{ji} denote the active/reactive power flow from bus j to bus i, and $|V_i|$ refers to the voltage magnitude. Moreover, R_{ij} and X_{ij} respectively denote the resistance and reactance of line $i-j$, while G_i and B_i respectively refer to shunt conductance and shunt susceptance from bus i to ground.

The relaxed model is still non-convex. Neglecting the capacitance of the lines and the quadratic terms that represent the power losses (which are much smaller compared to the power flows), the linearized BFM (also known as LinDistFlow equations) is derived:

$$p_j = \sum_{i:j\sim i} p_{ji} - \sum_{i:i\sim j} p_{ij}, \forall j \in \mathcal{N}, \tag{4.39}$$

$$q_j = \sum_{i:j\sim i} q_{ji} - \sum_{i:i\sim j} q_{ij}, \forall j \in \mathcal{N}, \tag{4.40}$$

$$v_j = v_i - 2(R_{ij}p_{ij} + X_{ij}p_{ij}) \forall (i,j) : i \sim j,\ \forall i,j \in \mathcal{N}, \tag{4.41}$$

where $v_i = |V_i|^2$. The linearized BFM has extensively been used in literature for power flow calculations in radial distribution networks [37, 89]. In fact, the approximations that derive this model only introduce a small relative error of about 1% [90],

while they simplify the network state calculation by reducing it to the following three variables: voltage magnitude, active power and reactive power injections.

MG power flow equations

The MG network AC power flow equations according to the linearized BFM are given by:

$$\sum_{i:j\sim i} p_{ji,t} = P^{L}_{i,t} + p^{ch}_{i,t} - P^{PV}_{i,t} - p^{dis}_{i,t} - p^{DR}_{i,t} - p^{im}_{i,t} + p^{ex}_{i,t},\ \forall i \in \mathcal{N},\ \forall t \in \mathcal{H}, \tag{4.42}$$

$$\sum_{i:j\sim i} q_{ji,t} = -q^{DR}_{i,t} + Q^{L}_{i,t} - q^{im}_{i,t},\ \forall i \in \mathcal{N},\ \forall t \in \mathcal{H}, \tag{4.43}$$

$$v_{j,t} = v_{i,t} - 2(R_{ij}p_{ij,t} + X_{ij}q_{ij,t}),\ \forall (i,j) : i \sim j,\ \forall i,j \in \mathcal{N},\ t \in \mathcal{H}. \tag{4.44}$$

Voltage limits

The magnitude of the voltage must lie within statutory limits:

$$V_{min} \leq |V_i, t| \leq V_{max},\ \forall i,j \in \mathcal{N},\ \forall t \in \mathcal{H}. \tag{4.45}$$

In (4.45), V_{min} is the lower voltage limit and V_{max} is the upper voltage limit.

Feeder capacity limits

The line flow constraints are given given by

$$p^2_{ij,t} + q^2_{ij,t} \leq (S^{max}_{ij})^2,\ \forall i,j \in \mathcal{N},\ \forall t \in \mathcal{H}, \tag{4.46}$$

where S^{max}_{ij} is the rated apparent capacity of line $i - j$.

4.2 Optimization model for the DSO

Generally, the DSOs are not allowed to own or operate DER. The distribution network's DER, which belong to the MGs, can be considered as dispatchable resources only if the DSO is allowed to have full knowledge of the MG constraints and, in addition, is empowered to control the MG resources. Alternatively, the MGs can be considered as dispatchable resources, as they are represented as controllable entities connected at the PCC. For this purpose, there must be proper coordination between the DMS and the MG-EMS.

The case of coordinated energy scheduling of multiple microgrids is formulated as an AC OPF problem for the DSO. The dispatch of MGs and network controllable

devices must satisfy the grid technical constraints, while serving the specific operational targets of the DSO. The DSO may aim to minimize the grid connection charges paid to the transmission system operator (TSO) in order to achieve a more economic operation. Moreover, the DSO can modify the active power exchange between MGs and the connected network to enable flexibility provision after a balancing request from a BRP that operates within the distribution grid (as explained in Section 3.3.

4.2.1 Objective functions

The DSO can achieve economic operation by *minimizing the charges (energy transmission and peak power charges) paid to the TSO*:

$$\min \sum_{t \in \mathcal{H}} p_{i,t}^{SS} C^{SS,tr} + r_i^{SS,p}, \forall i \in \mathcal{D}_s,\ t \in \mathcal{H}. \tag{4.47}$$

In (4.47), $\mathcal{D}_s \subseteq \mathcal{D}$ is the subset of substation buses (connection to the upstream network), which belong to the set of distribution network buses $\mathcal{D}$ (which also includes the MG buses), $p_{i,t}^{SS}$ is the active power at the substation, and $C^{SS,tr}$ is the energy transmission charge. The cost of the peak power measured at the substation is denoted by $r^{SS,p}$, which must satisfy

$$r_i^{SS,p} \geq C^{SS,p} p_{i,t}^{SS},\ \forall i \in \mathcal{D}_s,\ t \in \mathcal{T}, \tag{4.48}$$

where $C^{SS,p}$ is the power-based grid tariff. If the DSO dispatches the connected MGs to enable flexibility provision, then the aim is to *minimize the deviation between aggregated power exchange at the MGs' PCCs from the power amount that was requested by the BRP.* In order to achieve this, the DSO must first receive the MGs' desired schedule for the next time-step, i.e., the active and reactive power exchange at the PCC. The DSO's objective function is then given as:

$$\min \left| P_{req} - \sum_{i \in \mathcal{MG}} (P_i^{MG} - \Delta p_i) \right|. \tag{4.49}$$

In (4.49), P_{req} is the balancing power request, P_i^{MG} is the MGs' desired active power exchange, which is treated as a parameter in the DSO's optimization problem and the variable Δp_i is the optimal flexibility amount that the DSO asks from the MGs.

4.2.2 Network power flow

The AC OPF model described in Section 4.1.7 was also used for the network power flow of the main distribution network. There are slight changes in the formulation of the power flow, depending on whether the DSO has further knowledge of the grid constraints within the microgrids. Normally, the integration of MG-EMS to the DMS should not require the knowledge of any information beyond the PCC

[43], however, the formulation of the power flow equations is given for both cases, as simulations were carried out using both the "full-knowledge" approach and the "privacy-preserving" approach. If the "full-knowledge" approach is considered, then the technical models of the MGs' DER (described in Sections 4.1.3–4.1.5) are also a part of the DSO's optimization problem.

Distribution network power flow equations

The distribution network AC power flow equations according to the linearized BFM are given by:

$$p_{i,t}^{SS} + \sum_{i:j\sim i} p_{ji,t} = P_{i,t}^{L},\ \forall i,j \in \mathcal{D}\setminus\mathcal{N},\ \forall t \in \mathcal{H}, \tag{4.50a}$$

$$\sum_{i:j\sim i} p_{ji,t} = P_{i,t}^{MG} - \Delta p_i,\ \forall i \in \mathcal{MG},\ \forall t \in \mathcal{H}, \tag{4.50b}$$

$$q_{i,t}^{SS} + \sum_{i:j\sim i} q_{ji,t} = Q_{i,t}^{L},\ \forall i,j \in \mathcal{D}\setminus\mathcal{N},\ \forall t \in \mathcal{H}, \tag{4.51a}$$

$$\sum_{i:j\sim i} q_{ji,t} = Q_{i,t}^{MG},\ \forall i \in \mathcal{MG},\ \forall t \in \mathcal{H}, \tag{4.51b}$$

$$\begin{aligned} v_{j,t} &= v_{i,t} - 2(R_{ij}p_{ij,t} + X_{ij}q_{ij,t}),\\ \forall (i,j) : i\sim j,\ \forall i,j &\in (\mathcal{D}\cup\mathcal{MG})\setminus\mathcal{N},\ t\in\mathcal{H}. \end{aligned} \tag{4.52}$$

In (4.50)–(4.52), $q_{i,t}^{SS}$ is the reactive power at the substation and the parameters $P_{j,t}^{MG}/Q_{j,t}^{MG}$ denote the active/reactive power exchange at PCC according to the MGs' schedule. The equations are defined for all the network buses except for the buses that belong to the MGs, i.e., the DSO does not have knowledge of the network structure that belongs to the MGs. The network buses were MGs are connected, i.e., PCCs, which represent the physical interface between the MGs and the main distribution network, are a part of the network power flow model. If it could be assumed that the DSO has full knowledge of the MGs' network and DER technical constraints, then (4.50)–(4.52) could be re-written as:

$$\begin{aligned} p_{j,t}^{SS} + p_{j,t}^{G} + P_{j,t}^{PV} + p_{j,t}^{DR} + p_{j,t}^{dis} - P_{j,t}^{L} - p_{j,t}^{ch}\\ = \sum_{i:j\sim i} p_{ji,t} - \sum_{i:i\sim j} p_{ij,t},\ \forall j\in\mathcal{D},\ t\in\mathcal{H}, \end{aligned} \tag{4.53}$$

$$q_{j,t}^{SS} + q_{j,t}^{G} + q_{j,t}^{DR} - Q_{j,t}^{L} = \sum_{i:j\sim i} q_{ji,t} - \sum_{i:i\sim j} q_{ij,t},\ \forall j\in\mathcal{D},\ t\in\mathcal{H}, \tag{4.54}$$

$$v_{j,t} = v_{i,t} - 2(R_{ij}p_{ij,t} + X_{ij}p_{ij,t})\forall (i,j) : i\sim j,\ \forall i,j\in\mathcal{D},\ t\in\mathcal{H}. \tag{4.55}$$

Voltage limits

The magnitude of the voltage must lie within statutory limits:

$$V_{min} \leq |V_i, t| \leq V_{max}, \ \forall t \in \mathcal{H}. \tag{4.56}$$

The above constraint applies $\forall i \in (\mathcal{D} \cup \mathcal{MG}) \setminus \mathcal{N}$ or $\forall i \in \mathcal{D}$ if the MG buses are included.

Feeder capacity limits

The line flow constraints are given given by

$$p_{ij,t}^2 + q_{ij,t}^2 \leq (S_{ij}^{max})^2, \forall (i,j) : i \sim j, \ \forall i,j \in (\mathcal{D} \cup \mathcal{MG}) \setminus \mathcal{N}, \ \forall t \in \mathcal{H}, \tag{4.57}$$

where S_{ij}^{max} is the rated apparent capacity of line $i - j$. Again, constraint (4.57) applies either $\forall i \in (\mathcal{D} \cup \mathcal{MG}) \setminus \mathcal{N}$ or $\forall i \in \mathcal{D}$ depending on the followed approach.

4.3 Formulation of the optimization problems

Depending on the entity that solved the energy scheduling problem and the solution approach that was followed, different optimization problems were formulated. The optimization models were implemented in GAMS [91], where the interface with the CPLEX optimizer [92] was used to solve the formulated optimization problems. A GAMS to MATLAB [93] interface was also used to prepare the input data and save and process the results.

Energy scheduling strategies

The energy scheduling strategies presented in Section 3.2 solve different MG energy scheduling problems depending on the objectives and the entity that dispatches the MG resources (the MG operator or the DSO). The formulation of the optimal scheduling problem for the MG profit maximization is given by (4.1)–(4.2) and (4.4)–(4.16), where the term c^{DER} in (4.1) is omitted from the PV-BES MG (MG-B) and $c^{DER} = C^{CHP}$ for the CHP-PV-BES MG (MG-A). A description of these MGs and their resources can be found in Section 5.2. The optimal scheduling problem for the minimization of the MG's energy exchange is given by (4.3)–(4.16). Both are MILP problems and since no interaction is considered with the DSO, the MG energy scheduling problem is solved in an uncoordinated way. These problems are used in Strategies 1-3, as were described in Section 3.2. The coordinated MG energy scheduling is formulated as an AC optimal power flow (OPF) problem in Strategy 4, since the purpose is to find the energy scheduling of the MG resources that minimizes the cost for the DSO. The MILP problem is given by (4.47)–(4.48) and (4.53)–(4.56).

Decentralized DMS and MG-EMS coordination

For the coordination procedure presented in Section 3.3, the MG energy scheduling problem is solved by the MG-EMS and is given by (4.1), (4.8)–(4.16), and (4.42)–(4.46), which is a mixed-integer quadratically constrained programming (MIQCP) problem. In Case-3, the DMS solves the problem given by (4.49), (4.50)-(4.52) and (4.56)–(4.57) $\forall i \in (\mathcal{D} \cup \mathcal{MG}) \setminus \mathcal{N}$, which is a quadratically constrained programming (QCP) problem.

Market-based energy management of a building microgrid

Four optimization models were defined based on the choice of cost function and the employed BES scheduling model:

- *Model-1*: The conventional BES scheduling model (Section 4.1.5) is used, while degradation cost is neglected, i.e., c_j^B is omitted from the term c_i^{DER} in (4.1). The formulated MILP problem is given by (4.1)–(4.2), (4.4), and (4.11)–(4.16).

- *Model-2*: A measurement-based BES scheduling model (Section 4.1.5) is used, which was validated with experimental values. As in Model-1, aging is neglected. The formulated LP problem is given by (4.1)–(4.2), (4.4), (4.12), and (4.17)–(4.24).

- *Model-3*: The measurement-based model is combined with the cycle aging model with dependency on throughput, which was presented in Section 4.1.6. The formulated LP problem is given by (4.1)–(4.2), (4.4), (4.12), (4.17)–(4.26).

- *Model-4*: The measurement-based model is combined with the cycle aging model with dependency on DoD, which was presented in Section 4.1.6. The formulated MILP problem is given by (4.1)–(4.2), (4.4), (4.12), (4.17)–(4.24), and (4.27)–(4.34).

These optimization models were developed to simulate the performance of the BMG energy management model and to be integrated to the BMG-EMS, which was designed for the demonstrations. The study approach followed in the simulations and demonstrations of the BMG energy management model was depicted in Fig. 3.7.

Chapter 5

Description of Test Cases: Parameters and Assumptions

This chapter presents the test cases and test systems that have been used in the simulation studies on MG energy scheduling and demonstrations of the solutions implemented by the MG-EMS. Information regarding input data and parameters used in each test case is also given in this chapter. Moreover, this chapter describes the communication and control setup that was developed for the demonstration of the BMG-EMS.

5.1 Input data and parameters

The input data of each test case can be found in the Appendix. The parameters of the test system and the applied study or demonstration are given in the section that describes the test case. The energy and power grid tariffs as well as the reimbursement fee have been taken from the website of the local DSO [94]. For the power-based tariff, the peak power charge applied for companies was used, i.e., the MGs were considered as companies, which is a realistic scenario, when MGs represent network areas and they could consist of multiple buildings. The same peak power charge was also applied for BMGs. In all cases, the peak power cost in (4.1) was scaled down to a cost that suited the simulation (or demonstration) time horizon, as this is in practice a monthly fee paid to the DSO. All the costs are presented in USD, where the average 2018 USD to SEK ratio was used when necessary, which is 1:8.6921. The energy and power grid tariffs that have been used can be seen in Table 5.1 [94].

Table 5.1: Network tariffs and fees.

MG company	
Energy transmission cost (¢/kWh)	0.8
Peak power tariff ($/kW/month)	5.0
Reimbursement fee (¢/kWh)	0.3
10 kV distribution grid	
Energy transmission cost (¢/kWh)	0.4
Peak power tariff ($/kW/month)	4.3

5.2 Case study: Electrical distribution system of Chalmers University of Technology

Aim of the case study

The aim of this case study was to evaluate the cost and performance of the MG operation under different operational objectives. Assessing the effect of MG integration to the cost and operation of the main distribution grid was also an objective of this study. For this purpose, uncoordinated and centrally coordinated MG energy scheduling strategies were tested including MG energy cost minimization, minimization of MG energy exchange with the main grid, minimization of MG imported energy from the main grid, and minimization of the DSO's cost due to grid connection charges. These strategies were presented in Section 3.2. The results are presented in Section 6.1.1.

Parameters of the studied system and assumptions

The 12-kV distribution network of Chalmers (Fig. 5.1) was used in this case study to evaluate the energy scheduling strategies of grid-connected MGs. The electrical load demand, which varies between 2.5 and 6 MW, is supplied by importing energy from the upstream distribution grid and, in addition, by electricity generated through a CHP plant and solar panels. The CHP plant has heating power capacity of 9000 kW, while the electrical capacity of the steam turbine is 0.5-1.0 MW (the heating or electrical operational power output depends on the choice of fuel). The CHP plant is out of operation between April-September, as its boilers are primarily scheduled for heating energy production. The total PV capacity is 831 kWp and the majority of the solar panels have been installed on rooftops of the campus's buildings, with only a few solar panels of 16 kWp total capacity mounted on the wall of a building. The network also hosts two BESs with energy capacity of 200 kWh and 100 kWh and 35 PEV charging points at 32 A/22 kW and 16 A/3.7 kW level, located at two different charging stations. The facilities include an advanced metering infrastructure (AMI) system that consists of an ABB MicroSCADA and smart meters. The buildings of Chalmers campus are also equipped with various energy meters as well as controllable devices that enable the building operator to control the heating, cooling, and ventilation system.

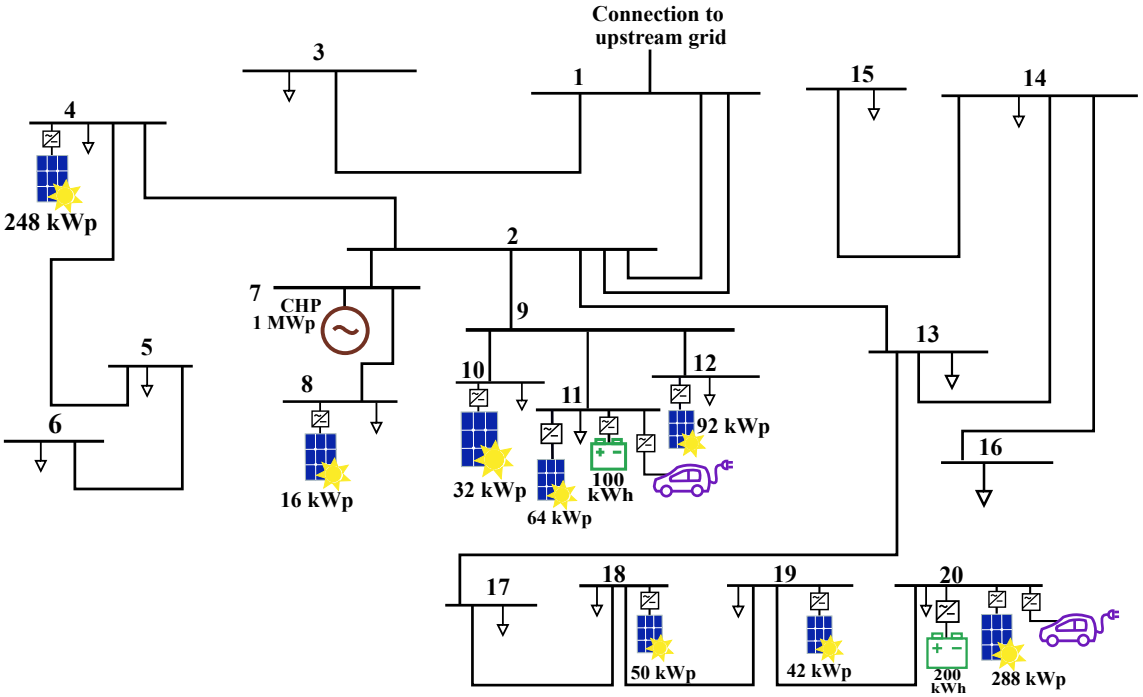

Figure 5.1: The configuration of the distribution network of the Chalmers University of Technology campus.

In this case study, two network areas that have been considered as MGs, as can be seen in Fig. 5.2. Microgrid A (MG-A), shown with blue dotted lines in Fig. 5.2, is a CHP-PV-BES-DRR MG and can produce excess energy, when the CHP is in operation. MG-A has a PV penetration level of 23% (calculated as a percentage of the MG's peak load). Microgrid B (MG-B), shown with the red dashed lines in Fig. 5.2, is a PV-BES-DRR MG. Since MG-B only hosts a small PV capacity (the penetration level is 5%) and has no other local generation sources, it must continuously import power from the main grid. The MGs are the only network areas, where flexible load is available.

Most of the parameters and input data to the MG energy scheduling problems were taken from data obtained from Chalmers campus. The parameters included network configuration, resource topology and resource capacity. Historical data of electricity and heating demand, temperature, and irradiation in 2016 were used as input data. The electricity load data, which were acquired from smart meters at campus' buildings, were aggregated to the corresponding network buses in order to be used as input to the network's power flow. The PV generation was calculated according to [95]. For the electricity prices, the Nord Pool spot market price [96] in 2016 was used assuming that the MGs could purchase or sell electricity from/to the retail electricity provider at wholesale market price. The historical data were treated as "perfect forecasts" by the MG energy scheduling problem.

The parameters that were especially considered for this case study can be seen in Table 5.2. It was assumed that the CHP plant has a fixed electrical power output efficiency ($r^{CHP} = 0.25$) and operates under a constant leading power factor of

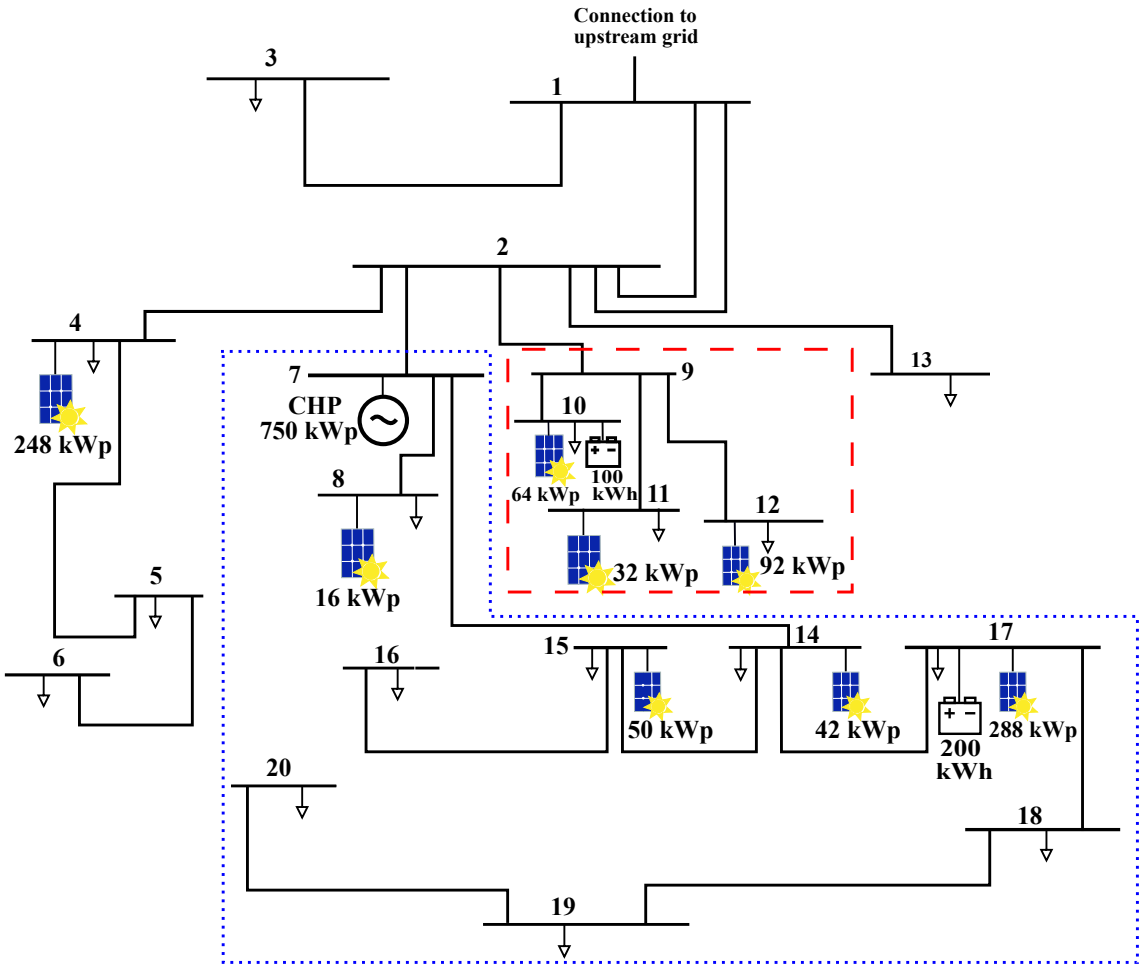

Figure 5.2: The proposed configuration of the distribution network of Chalmers with the interconnection layout of the two MGs (shown with the sections in dashed and dotted lines).

Table 5.2: Parameters of the case study on Chalmers distribution network.

Scheduling horizon	24h
Δt	1h
η^{ch}/η^{dis}	95%/95%
SoE^{min}/SoE^{max}	20%/90%
r^{CHP}	0.25
κ	0.5
κ^{DR}	0.5

0.96, while the load (both flexible and inflexible) has a constant lagging power factor of 0.98. Moreover, $\kappa = 0.5$ and $\kappa^{DR} = 0.5$, while it is assumed that 20% of the load consumption at each MG bus is available for DR at each time step, i.e., $P^{L,r}_{j,t} = 0.2P^{L}_{j,t}$ in (4.9). The SoE ranges between 20% to 90% and $\eta_{ch} = \eta_{dis} = 0.95$, which are typical values used for the BES efficiencies in similar studies [19]. The scheduling horizon was 24h with an hourly time discretization step and the MG energy scheduling problem was solved day-ahead repeatedly for each day with a complete input data set (in total, it was 358 days).

5.3 Case study: 33-bus distribution network

Aim of the case study

The aim of this case study was to depict the effectiveness of implementing decentralized coordination between the DSO and the MG-EMSs for the MG energy management. Below is a brief description of the three different cases of energy scheduling that were tested with the proposed decentralized coordination scheme:

- **Case-1:** Hour-ahead coordinated energy scheduling of MG-EMSs.
- **Case-2:** Coordinated energy scheduling of MG-EMSs with a RH approach.
- **Case-3:** Coordinated energy scheduling of multiple MG-EMS with a RH approach and flexibility dispatch.

An analytic description of the three cases can be found in Section 3.3. The results of this case study are presented in Section 6.1.2.

Parameters of the studied system and assumptions

The MG energy scheduling considering decentralized coordination between the MG-EMSs and the DMS was tested on a 12.6-kV 33-bus network first presented in [88]. The network and the MG configuration layout can be seen in Fig. 5.3. Two 1000 kW PVs are located at buses 18 and 33, two BESs of 1.2 MWh capacity are located at buses 14 and 29, while 200 kW of responsive load is considered for buses 13 and 31, i.e. $P^{L,r}_{13,t} = P^{L,r}_{31,t} = 200kW$ in (4.9).

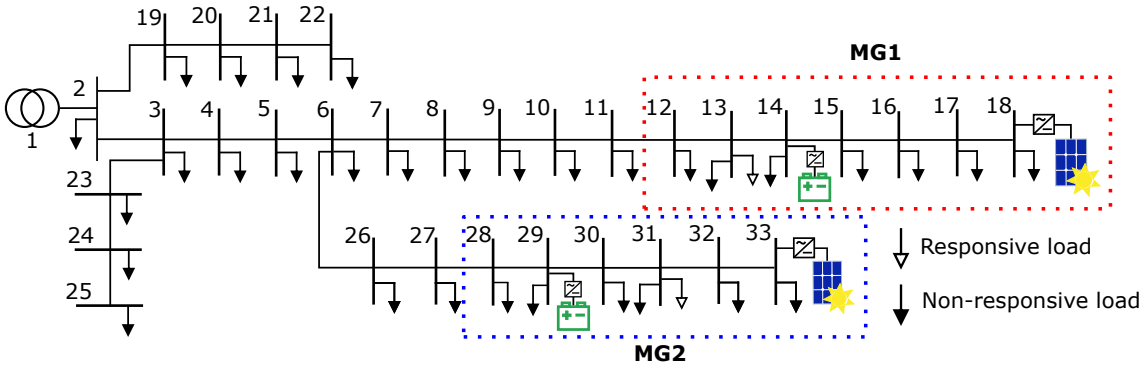

Figure 5.3: The 33-bus 12.6 kV distribution network and the MG configuration layout.

Table 5.3: Parameters of the case study on the 33-bus distribution network.

Scheduling horizon	1h
Δt	5 minutes
η_{ch}/η_{dis}	98%/95%
SoE_{min}/SoE_{max}	30%/80%
κ	0.5
κ^{DR}	0.2

The parameters of the case study are summarized in Table 5.3. The scheduling horizon was 1h, and the time discretization step was Δt = 5 minutes, which means that the solution of the MG energy scheduling problem gave the 5-minute set-points of the BES charging/discharging power and the DRRs' power curtailment/increase for the next hour. In Case-1, only one hour-ahead simulation was required to obtain the set-points for the next hour. In Case-2, twelve energy scheduling simulations were required instead, as the MG energy scheduling followed a RH approach. The input data to the MG-EMS included the load, PV generation, and electricity prices for the scheduling horizon as well as the initial state of the DERs. The load consumption and PV generation profiles of the MGs and the electricity prices that were used in the simulations can be found in the Appendix. At the beginning of the simulations for each case both BESs had a SoE level of 70%, and it was assumed that no load had been curtailed from the DRRs.

The optimization problems that have been formulated for the MG-EMS and the DMS were defined in Section 4.3. The objective function of each MG included the cost of importing energy from the grid and the revenue from selling energy. No peak power cost or any DER operation cost was considered in this case study, i.e., $c_i^{DER} = 0$ and r_i^p in (4.1). A penalty γ was introduced in (4.49), which was used in Case-3, to avoid solutions, where the flexibility requests were unevenly distributed between the two MGs. This was achieved by minimizing the difference between the flexibility amount requested from MG1 (Δp_{MG1}) and the flexibility amount requested from MG2 (Δp_{MG2}). Thus, the objective function for the DSO becomes:

$$\min \left| P_{req} - \sum_{i \in \mathcal{MG}} (P_i^{MG} - \Delta p_i) \right| + \gamma, \tag{5.1}$$

where $\gamma = |\Delta p_{MG1} - \Delta p_{MG2}|$. After the MGs submitted their desired schedule for the next time-step, the DMS treated the PCC active power exchange (P_i^{MG}) as a parameter to solve its individual optimization problem. The solution yielded the flexibility amounts of active power exchange (Δp_{MG1} and Δp_{MG2}), which minimized the deviation from the BRP's imbalance signal.

5.4 Case study: HSB Living Lab

Aim of the case study

The aim of this case study was to validate the proposed BMG energy management model and perform a long-term evaluation of the energy cost and the BES degradation using this model with a market-based approach for the BES dispatch. With this case study, it is attempted to accurately assess the benefits for the BMG operator of using the BES as an energy-flexible resource. This was achieved by investigating the impact of the degradation cost on the BMG energy scheduling solution, by testing different SoE limits of the BES, and by performing a sensitivity analysis of the BES replacement cost. The adopted study approach was described in Section 3.4, while the optimization models and the formulated problems, which are assumed to be solved by the BMG-EMS, were given in Section 4.3. Results are presented in Section 6.1.3.

Parameters of the studied system and assumptions

The HSB Living Lab (HSB LL) building [74,75], which was used in this case study for the market-based energy management model of a BMG, is located at the campus of Chalmers University of Technology. The HSB LL is a multi-family residential building of 29 apartments (Fig. 5.4), which also serves as a testbed for sustainable living solutions.

The study is based on the 7.2 kWh BES with 6 kW charging/discharging power limits, which is installed at the HSB LL building, and the 18 kWp PV system, which consists of the solar panels that are installed on the rooftop and facade of the building. Fig. 5.5 shows the DC/DC converters of the solar strings and the DC/DC converter of the BES, which are connected to the upstream AC grid (400 V) via a converter provided by the Ferroamp company [73]. The grid side converter, which is shown on the top-right side of Fig. 5.5, has bi-directional operation, since the solar energy and the BES stored energy can be exported to the upstream AC grid and, in addition, the BES can be charged through both the upstream AC grid and the PV system (see Fig. 5.6). The converter-embedded controller, which is called EnergyHub, is coupled with sensors that monitor the DC/DC converters of the solar strings and the BES as well as the building consumption and power exchange

Figure 5.4: The facade of the HSB LL building.

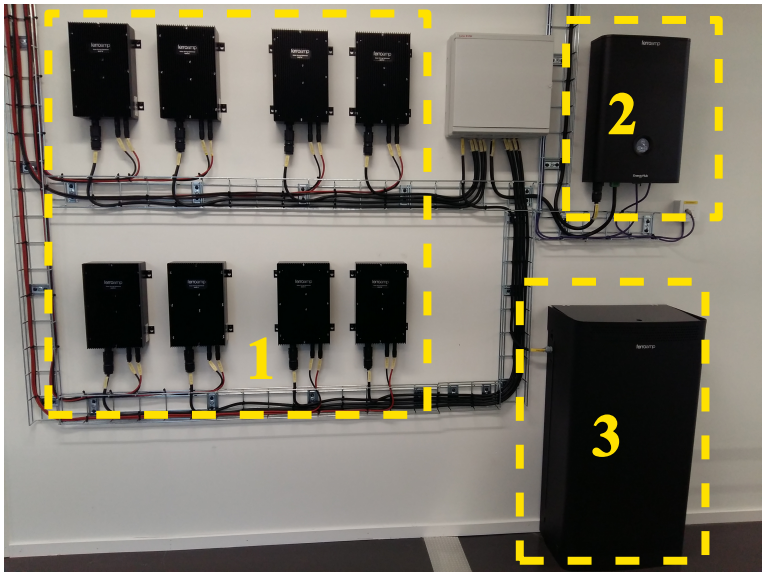

Figure 5.5: The basic components of the HSB LL building microgrid: 1) the DC/DC converters of the solar strings, 2) the bi-directional grid side converter, and 3) the battery energy storage string with the integrated DC/DC converter.

with the grid. The measurements of PV generation, BES power, building load, and power exchange with the grid are collected with a time resolution of 1 sec. In 2019, the building electricity consumption was 84.2 MWh (the daily demand ranged from 162 kWh to 384 kWh), and the local energy production of the solar panels was 12.3 MWh, out of which 0.7 MWh was exported to the grid. The peak building consumption (minute average) was 32 kW, while the peak PV power output that was recorded was 13 kW (minute average).

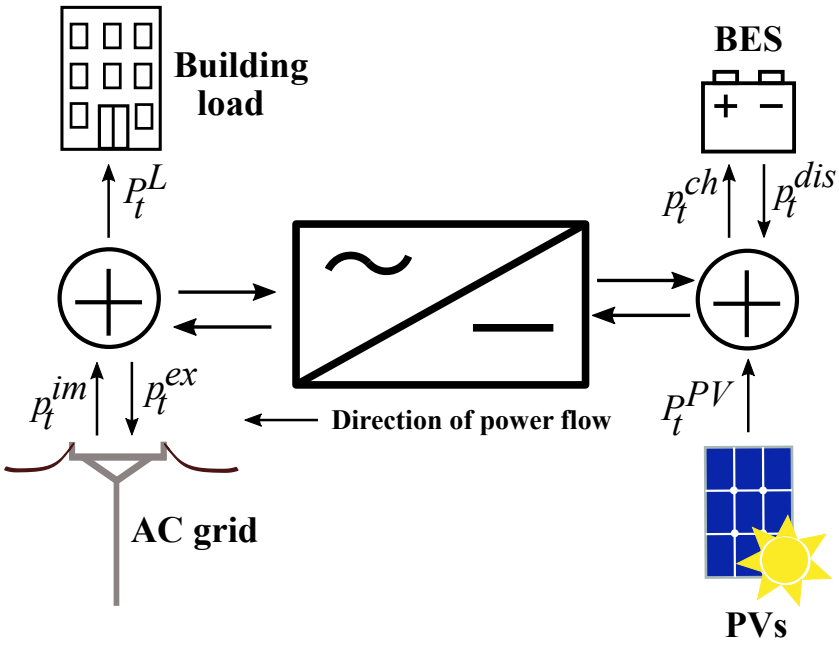

Figure 5.6: Power flow of the building microgrid.

The methodology that was used in the simulations of the BMG-EMS was depicted in Fig. 3.7. In this study, the building load and PV generation as well as the Nordpool [96] spot market prices in 2018 were used to run 365 day-ahead BES scheduling simulations. The input data can be found in the Appendix. The main parameters of the case study are given in Table 5.4. Considering the uncertainty in the future price of residential, stationary BESs [5], a sensitivity analysis was performed with three prices, i.e., \$100, \$290, and \$500 per kWh, for the BES installation cost. These approximately correspond to a best-case, likely, and worst-case scenario. Moreover, two scenarios of SoE limits were investigated: 30%-80% in Scenario-1 and 10%-90% in Scenario-2. The initial and end SoE of each simulation was set to 50%, while the end-of-life retained capacity was assumed to be $\eta = 80\%$. The parameters for the measurement-based model were obtained from sample data of tests on the HSB LL BES, while $\eta_{ch} = 0.91$ and $\eta_{dch} = 0.98$ for Model-1, corresponding to the average values that were recorded during those tests, which were performed in April 2019. Since the measurement-based model is used in Model-2, Model-3, and Model-4 the charging and discharging efficiencies in these models were variable and dependent on SoE and power rate. The Li-ion cycle aging parameters of Model-3 were taken from [84], while the BES lifecycle loss function $\rho_t = 1/\phi(DoD)$, which is used in Model-4, was derived from Li-ion BES data provided in [28]. For the parameter I_c in (4.25), which is included in Model-3, the daily average C-rate was used, which was found to be 0.3 for the charging/discharging profiles of all four models over the 365 day-ahead simulations.

As the flow diagram in Fig. 3.7 showed, the BES capacity was updated after each day-ahead optimization. First, the capacity loss due to cycle aging given by $c^B(1-\eta)/C^{B,0}$ was calculated using one of the models presented in Section 4.1.6 (dependency on throughput or DoD), where the real-time C-rate was used in (4.25).

Table 5.4: Parameters of the case study on the HSB LL building.

Scheduling horizon	24h
Δt	5 minutes
η	80%
η_{ch}/η_{dis} (Model-1)	91%/98%
SoE_{min}/SoE_{max} (Scenario-1)	30%/80%
SoE_{min}/SoE_{max} (Scenario-2)	10%/90%
BES installation prices ($/kWh)	$100, $290, $500
I_c	0.3
B_1	0.0013
B_1	0.3534

Afterwards, this loss was subtracted from the capacity that the BES had at the beginning of the day. Finally, the loss due to calendar aging was calculated according to (4.35) and subtracted from the remaining capacity for every t that was an open-circuit period for the BES. The temperature in stationary BESs can easily be controlled and was therefore considered to be constant ($T = 298K$). The values for a_c were derived from linear interpolation of the calendar aging data given in [83].

5.5 Case study: Brf Viva

Aim of the case study

Similarly to the HSB LL case study, this case study was used to validate the BMG energy management model. Simulation results considering energy scheduling for one day are presented in Section 6.1.4. The adopted study approach was described in Section 3.4. Results are presented in Section 6.1.4.

Parameters of the studied system and assumptions

The Brf Viva, which was used in this case study for the market-based energy management model of a BMG, is a housing association of six buildings (shown in Fig. 5.7), which are in Guldheden, an area close to the campus of Chalmers University of Technology. The buildings consist of 132 residences inhabited since 2018 [76].

The study is based on the 170.8 kWp PV system, which has been installed for local electrical energy production and the 14 second-life Li-ion BESs (Fig. 5.8), each with a rated capacity of about 14 kWh and a maximum charge/discharge power of 6 kW, which have been installed to increase the PV self-consumption and reduce the peak demand. The BESs have been taken from old electric buses (provided by Volvo Buses). Only 5 out of 14 BESs were considered in this case study corresponding to the number of BESs that were available during the demonstrations of the BMG energy scheduling solutions in Brf Viva. The DC/DC converters of the solar strings and the DC/DC converter of the BESs are connected to the upstream AC grid via a 168 kVA multi-level converter provided by Ferroamp [73]. Similarly to the

Figure 5.7: The Brf Viva buildings in Guldheden, Gothenburg (photo courtesy of Ulf Celander and Riksbyggen).

Figure 5.8: The second-life Li-ion batteries of Brf Viva.

HSB LL building, the grid side converter has bi-directional operation and the BESs can be charged through both the upstream AC grid and the PV system. The converter controller, i.e., the EnergyHub system, is coupled with sensors and provides measurements of PV generation, power of the 14 BES system, building load, and power exchange with the grid. In 2019, the building electricity consumption was 162 MWh, and the local energy production of the solar panels was 72 MWh, out of which 11 MWh was exported to the grid. The peak building consumption (minute average) was 198 kW, while the peak PV power output that was recorded was 129 kW (minute average).

Model- 1, Model-2, and Model-4 (presented in Section 4.3) were assumed to be integrated in the BMG-EMS, and the energy scheduling problem was solved for one day in a RH approach. The building electricity consumption and PV generation measured in February 19-20, 2020 were used as inputs to the BMG model. These values were slightly modified to represent the effect of forecast error. Nordpool spot market prices [96] were also used as inputs to the BMG model. The input data can be found in the Appendix. The main parameters of the case study are given in

Table 5.5: Parameters of the case study on Brf Viva.

Scheduling horizon	24h
Δt	5 minutes
η_{ch}/η_{dis}	97%/97%
SoE_{min}/SoE_{max}	30%/80%

Table 5.5. The parameters for the measurement-based model were obtained from sample data of tests on the BESs, while $\eta_{ch} = 0.97$ and $\eta_{dch} = 0.97$ for Model-1, corresponding to the average values that were recorded during those tests, which were performed in December 2019. Since the measurement-based model is used in Model-2 and Model-4, the charging and discharging efficiencies in these models were variable and dependent on SoE and power rate. Same as in HSB LL case study, the BES lifecycle loss function ρ_t, which is used in Model-4, was derived from Li-ion BES data provided in [28].

5.6 Demonstration cases

Aim of the demonstration cases

The HSB LL and Brf Viva buildings, which were used in the case studies described in Section 5.4 and Section 5.5, respectively, have also been used in demonstrations of the energy scheduling solutions obtained from the BMG energy management model. The purpose of the demonstrations was to validate this model integrating online control of the buildings' BESs as well as to validate the accuracy of the BES scheduling models (conventional BES model, measurement-based BES model). A testbed for BMG-EMS was developed for each demonstration site, i.e., HSB LL and Brf Viva. The BMG-EMS testbeds were designed to apply remote control of the on-site BESs utilizing the in-built measurement and control systems of the grid side converters. Demonstration results are presented in Section 6.2.

Parameters and assumptions of the demonstration cases

The BES dispatch could be determined by any of the four optimization models (see Section 4.3), which could be integrated to the BMG-EMS. The BES scheduling was performed in RH, as depicted in Fig. 3.7. The optimization problem was solved before each time interval (Δt). The set-point for the first time step was dispatched after each simulation, while the time horizon was shifted forward by Δt for the next simulation, as shown in the flow diagram (Fig. 3.7). Since the RH approach was used and the set-points were continuously adjusted, Eq. (4.1) did not refer to the actual cost during the scheduling horizon. The SoE limits were set to 30%-80%. During the demonstrations, the system SoC was read online and the real-time measurement was used as an input to the BMG-EMS, whereas for the simulation studies, the initial SoE of each simulation was obtained from the solution of the previous simulation. The development of forecasting models was out of the scope of this thesis. Therefore, historical data or pseudo measurements (generated from

historical data with the addition of noise) were used as input values for the load, PV generation, and electricity prices. These input data for the Brf Viva and HSB LL demonstrations can be found in the Appendix.

Rule-based BES dispatch

The BMG-EMS could also dispatch the BES using a rule-based algorithm (BAU), which can be used to reduce the peak load consumption as well as to even out the aggregated power profile as seen by the DSO at the PCC. The BES dispatch under the rule-based algorithm was demonstrated for comparison with the BES scheduling solutions obtained from the optimization models.

This rule-based algorithm tries to constrain the power exchange with the grid between a peak and a low load threshold (P_{peak} and P_{low}, respectively), which can be externally set by the BMG operator. The algorithm updates the BES charging/discharging power output set-point per iteration n (p_n^{ch}/p_n^{dis}) based on the SoC (soc_n) and the average PCC power exchange (p_n^{PCC}) of the previous iteration loop, which are the input values to the rule-based algorithm. The duration of each iteration loop depends on the choice of Δt. The number of iterations N depends on the scheduling period. To avoid deep discharges/charges of the BES, the SoE (soe) limits are considered (SoE_{min}, SoE_{max}).

Algorithm 1 describes the rule-based algorithm and the interaction between the BMG-EMS and the controlled system via the Message Queue Telemetry Transport (MQTT) protocol. As can be seen, the conventional BES model (see Section 4.1.5) with constant charging/discharging power limits P_{max}^{+}/P_{max}^{-} is used for the calculation of the charging/discharging BES power requests p_n^{ch}/p_n^{dis}. The rule-based algorithm can easily be adjusted to incorporate dependency of power limits to the SoE by utilizing BES measurements. It cannot be expected that the applied BES scheduling will be as accurate as when the measurement-based model is used, however, the BES control can become more effective, which can be useful, if BES requests calculated with the conventional BES model are not fully met.

Communication and control set-up

A schematic diagram of the communication and control set-up, which was the same for both demonstration sites, can be seen in Fig. 5.9. The MQTT protocol, which runs on top of Transmission Control Protocol/Internet Protocol (TCP/IP), was used for real-time data sharing between the server, where the BMG-EMSs were implemented, and the grid side converter at each demo site. The MQTT protocol is a "machine-to-machine (M2M)/"Internet of Things" connectivity protocol [97], which was designed for lightweight and low power message transport and is therefore very useful for remote control applications. With the MQTT protocol the BMG-EMS could interact with the EnergyHub system and receive real-time measurements as input for the energy scheduling problem, as well as send commands (BES power set-points).

The server interfaced MATLAB [93] to set up the communication and control inter-

Algorithm 1: Rule-based BES dispatch algorithm

Connect to the MQTT broker.
Subscribe to the available topics.
while $n \leq N$ **do**
    Read p_n^{PCC} and soc_n;
    Calculate p_n^{ch}/p_n^{dis} so that $P_{low} \leq p_n^{PCC} \leq P_{peak}$;
    if $p_n^{ch}/p_n^{dis} > P_{max}^{+}/P_{max}^{-}$ **then**
        $p_n^{ch}/p_n^{dis} = P_{max}^{+}/P_{max}^{-}$;
    end if
    if $(soe_{n+1} > SoE_{max}) \vee (soe_{n+1} < SoE_{min})$ **then**
        Reduce p_n^{ch}/p_n^{dis} so that $SoE_{min} \leq soe_{n+1} \leq SoE_{max}$;
    end if
    Publish p_n^{ch}/p_n^{dis};
end while

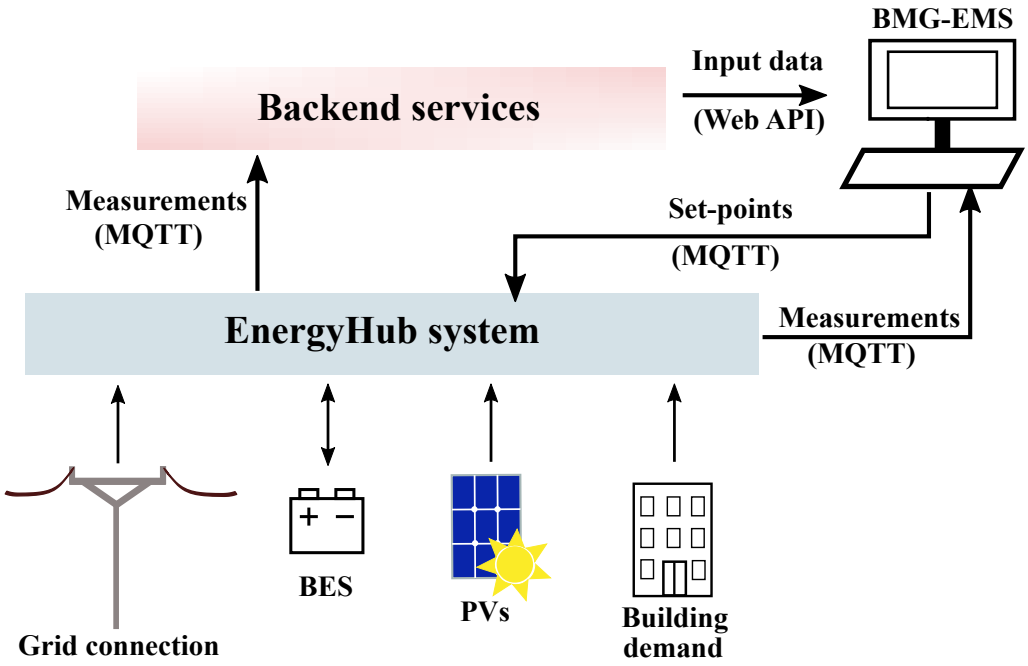

Figure 5.9: Communication and control interface set-up of the BMG-EMS.

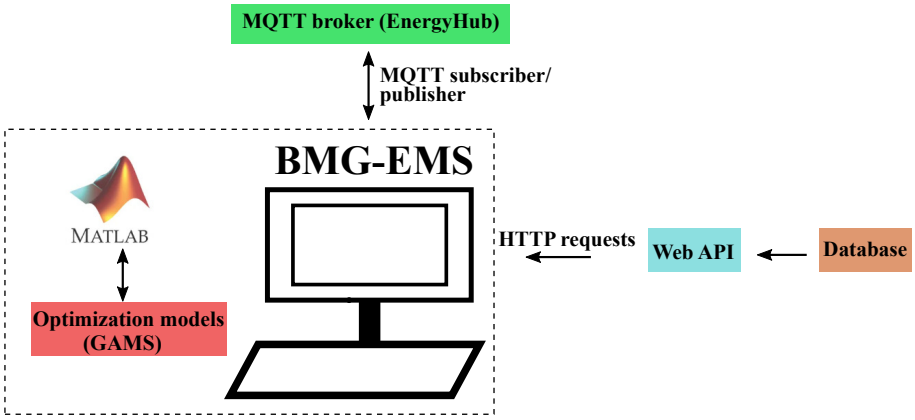

Figure 5.10: The server interfaces that enabled interaction of the BMG-EMS with the grid side converter and the database.

face with the test site. An MQTT publisher/subscriber (also called MQTT client) was built in MATLAB to interact with the MQTT broker run at the controller of each grid side converter. The MATLAB subscriber read real-time measurements that the MQTT broker transmitted in different topics. The MATLAB publisher sent control commands (BES power requests) to the MQTT broker, which would then send these requests to the DC/DC converters of the BESs. The data that the MQTT client and the MQTT broker exchanged were encoded in JSON format. In addition to the MQTT protocol, HTTP requests could be used to retrieve historical data, which were stored in an SQL-database. A MATLAB to GAMS [91] interface was used for data exchange with the optimization models and to retrieve the BES scheduling solution (power set-points), which was dispatched in an online manner. The server interfaces that were employed for the demonstrations can be seen in Fig. 5.10.

The data exchange with MQTT is very fast, and the control set-points were received by the broker in about 50-200 msec (from measurements with the HSB LL BMG-EMS the average response was 130 msec). The process of the command by the converter-embedded controller took about 10 sec. After that, the control signal was transmitted to the BES DC/DC converter through power line communication (PLC), which also added a delay to the dispatch of the set-point. Once the battery management system (BMS) was actuated, the desired value was reached in about 10 sec depending on the BES status and the amount of requested power. The results showed a total delay of 30-40 sec to the dispatch of the BES set-point. This delay is acceptable for close to real-time energy management applications, where the time scale is usually 5-15 minutes.

Chapter 6

Results and Discussions

The following chapter presents results of the performed studies on grid-connected MG energy scheduling. The first part of this chapter presents results from the simulation studies with each section corresponding to results from a different case study. The second part of this chapter presents results from demonstrations of the BMG energy scheduling solutions at two demo sites.

6.1 Simulation results

This section presents results from simulations with the following test systems which were described in Chapter 5: electrical distribution system of Chalmers University of Technology, 33-bus radial distribution network, the HSB LL BMG, and the Brf Viva BMG. Annual cost and performance metrics are given to evaluate energy scheduling strategies of grid-connected MGs in the Chalmers electrical distribution system. Annual building energy and BES degradation cost as well as cycle and calendar aging are given to evaluate the market-based BMG energy management model for the HSB LL building. Results from short-term energy scheduling simulations with the 33-bus radial distribution network are presented to demonstrate the effectiveness of the proposed decentralized coordination between the MG-EMSs and the DMS. The Brf Viva simulation results are presented for comparison with the demonstration of the BMG energy scheduling solutions, which are given later in this chapter.

6.1.1 Electrical distribution system of Chalmers University of Technology

The metrics associated with the MGs and the main grid operation and cost from the case study on Chalmers campus are presented in Table 6.1. The generation cost of the CHP is not included in the results of MG-A because it was entered as a parameter to the optimal energy scheduling problem. The test system was described in Section 5.2 and the energy scheduling strategies (BAU, S1-S4) were presented in Section 3.2.

Cost of energy scheduling strategies

As can be seen in Table 6.1, S1 reduced the cost of all three entities (MG-A, MG-B, DSO) compared to BAU, which means that all interconnected systems benefited from the deployment of two MG-EMSs that seek to locally optimize the MG costs. The cost reduction was 2% for MG-B and DSO and 4% for MG-A. When S2 was applied, the cost of MG-A was increased by 7% compared to BAU; however, the self-supply level of MG-A was significantly improved. Specifically, MG-A could operate as a virtual island and supply its customers with its own resources for 3211 hours (about 4.5 months) throughout the year.

The centrally coordinated energy scheduling (S4), yielded the most economic operation for the DSO resulting in a 2.5% reduction compared to the BAU case. However, this solution was not optimal for the MGs, as their costs were similar to the cost of their BAU solution. This shows a conflict between the solutions of local and global optimization.

As an example, Fig. 6.1 shows the variation in the scheduling pattern of the BES and DRRs of MG-A (positive values indicate discharging and load curtailment), when S1 and S4 were applied during an autumn day (the CHP was out of operation). In S4, the BES is only scheduled to contribute to the system's peak reduction (in Fig. 6.1 the BES was not used for this day). Unlike S4, the scheduling in S1 is affected by the spot price and follows its fluctuation. Therefore, in this example, the BES was discharged and load was curtailed from 13:00-14:00 at high PV production because the spot price had a high value at that hour.

The peak load consumption of the whole distribution system was kept at its lowest points with S1 and S4, whereas S2 and S3 resulted in an increase of 3-5% compared to S4 because with these strategies MG-A interacted less with the upstream network.

Table 6.1: Annual cost and performance metrics (electrical distribution network of Chalmers University of Technology)

	BAU	S1	S2	S3	S4
MG-A					
Annual cost (k$)	104	99	110	105	104
Imported energy (GWh)	2.99	2.95	2.95	2.95	2.99
Exported energy (MWh)	337	296	0	295	329
Zero energy exchange hours	0	601	3 211	725	0
MG-B					
Annual cost (k$)	243	239	239	246	243
Imported energy (GWh)	6.95	6.95	6.95	6.95	6.95
DSO					
Annual cost (k$)	312	306	311	314	304
Imported energy (GWh)	28.72	28.72	29.02	28.72	28.72
Peak power (MW)	5.66	5.47	5.61	5.70	5.44

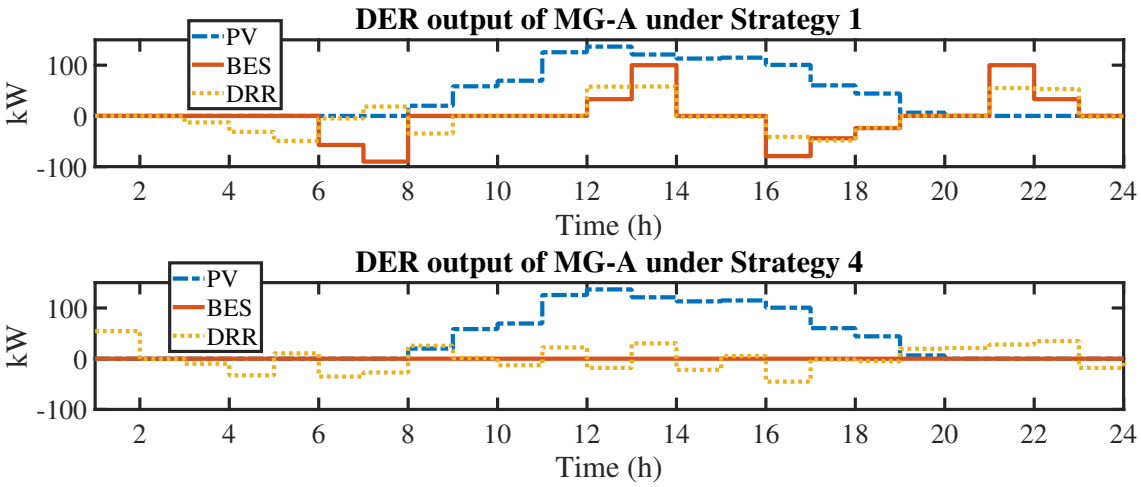

Figure 6.1: The DER output of MG-A for the day-ahead simulation of September 17, 2016 (comparison between S1 and S4).

Therefore, MG-A did not contribute to reduce the peak consumption of neighboring areas in the grid. Considering the low peak as well as the reduced cost for the DSO it is clear that S1, which was optimal for both MGs, is the best option out of all the simulated strategies. However, with additional MGs it is possible that the need for coordinated MG operation will increase.

Distribution system operation

After the day-ahead simulations power flow calculations were performed to validate that the uncoordinated energy scheduling solutions satisfied the network constraints (voltage limits, feeder constraints). All the simulations resulted in operation within technical limits. It should be noted, though, that the modeled network has sufficient feeder capacity and relatively low PV penetration level (14%). A minimum interaction between the MGs and the DSO could be applied (e.g., the DSO could approve or reject a MG schedule) to ensure that the MG operation does not undermine the operation of a distribution system.

Cycle-based BES degradation

The link between the BES scheduling of each strategy and the expected BES lifetime was investigated using manufacturers' data of the lifecycle loss function in relation to the DoD, which can be found in [28]. The rainflow algorithm [45] was used to calculate the number of half cycles and full cycles of the BESs along with the cycle range and an average SoE. From this information, the number of full cycles was calculated and an average DoD was estimated.

The results showed that the proposed strategies were unsuitable for BESs with low lifecycle (e.g., lead acid BESs), since the BES performance could not be guaranteed for more than 5 years. They also showed that energy arbitrage and cost minimization, whether performed locally (S1) or for the whole system (S4), increased the number of cycles resulting in faster BES degradation. Therefore, these strategies

Table 6.2: BES utilization and expected lifetime for Li-ion BESs

	BAU	S1	S2	S3	S4
MG-A					
BES cycles	67	403	153	144	317
Average DoD (%)	78.5	80	80	80	80
Lifetime in years	>15	11	>15	>15	14
MG-B					
BES cycles	200	400	400	0	317
Average DoD (%)	79	80	80	–	80
Lifetime in years	>15	11	11	–	14

should only be considered for BESs with high lifecycle (e.g., Li-ion or NaS BESs). Table 6.2 summarizes the results and presents the estimated expected lifetime for Li-ion BESs.

6.1.2 33-bus distribution network

The case study was described in Section 5.3. The solution methodology that was used to obtain the solution of the MG energy scheduling problem is depicted in Fig. 3.6. This section presents results from this methodology.

Case-1

The dispatch of the MGs' DERs according to the hour-ahead energy scheduling can be seen in Fig. 6.2–6.3. Both MGs were able to implement their desired schedule, as the set-points of their hour-ahead energy scheduling solutions did not violate the network's constraints. MG1 estimated a profit of \$5.2 from selling the energy (which was exported to the main grid), while MG2 estimated a profit of \$16.4. The imported active power at the substation is given in Fig. 6.4. The peak imported power was 2.33 MW at time step 3 of the simulation (10-15 minutes).

The dispatched set-points were assumed to be transmitted only once at the beginning of the hourly control horizon and therefore, rapid changes in PV generation and load affected the realized cost/income of the MGs within this hour. Therefore, both MGs had a decreased profit than their initial estimation, i.e., \$2.7 and \$8 for MG1 and MG2, respectively. At the end of the scheduling horizon, the BESs in both MGs had reached their lower SoE limit, i.e., 30%. The MG-EMSs utilized the maximum potential of their resources to achieve the hourly optimal scheduling solution limiting their scheduling options for the next hour, which could result in increased costs for the MGs.

Case-2

The dispatch of the MGs' DERs in Case-2 can be seen in Fig. 6.5–6.6. Both MGs were able to implement their desired schedule at each time step. It can be

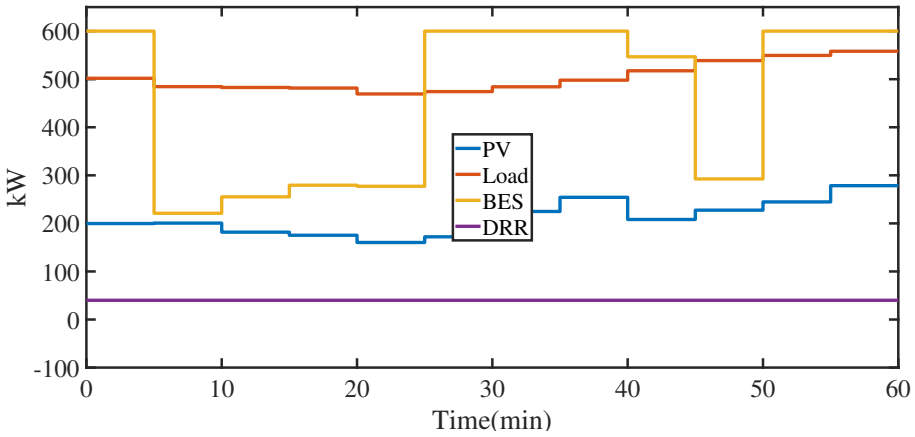

Figure 6.2: The DER output of MG1, when they are dispatched according to hour-ahead energy scheduling.

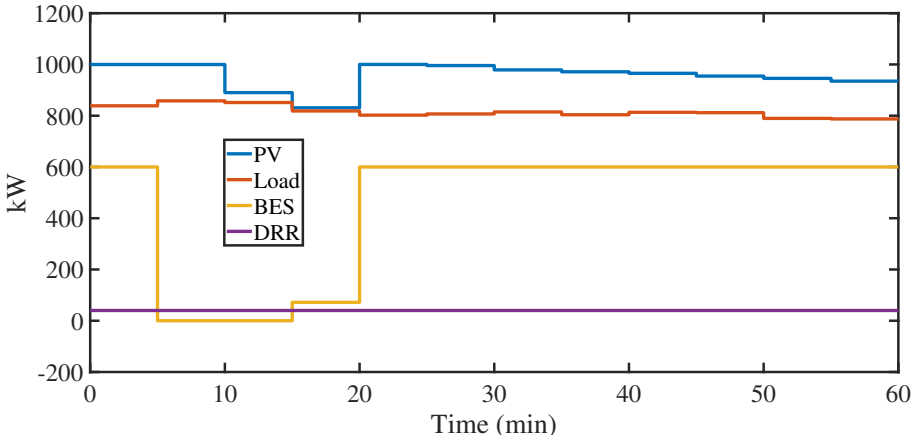

Figure 6.3: The DER output of MG2, when they are dispatched according to hour-ahead energy scheduling.

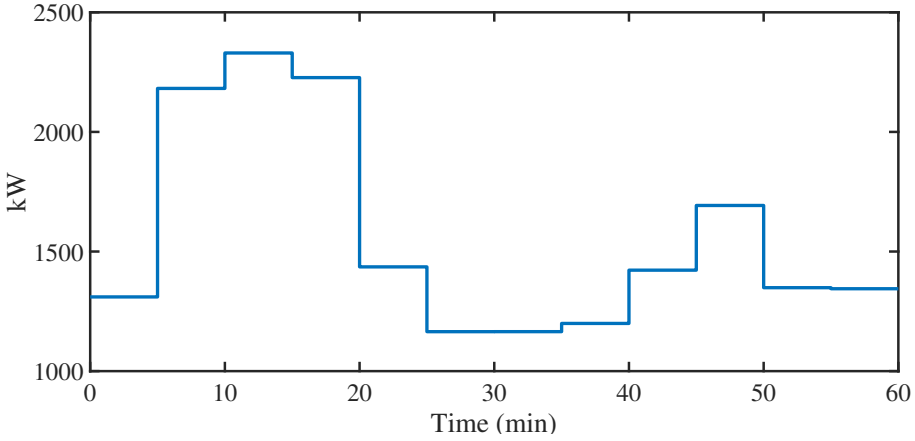

Figure 6.4: Imported active power at the substation, when the MG-EMSs dispatch their optimal set-points after performing an hour-ahead energy scheduling.

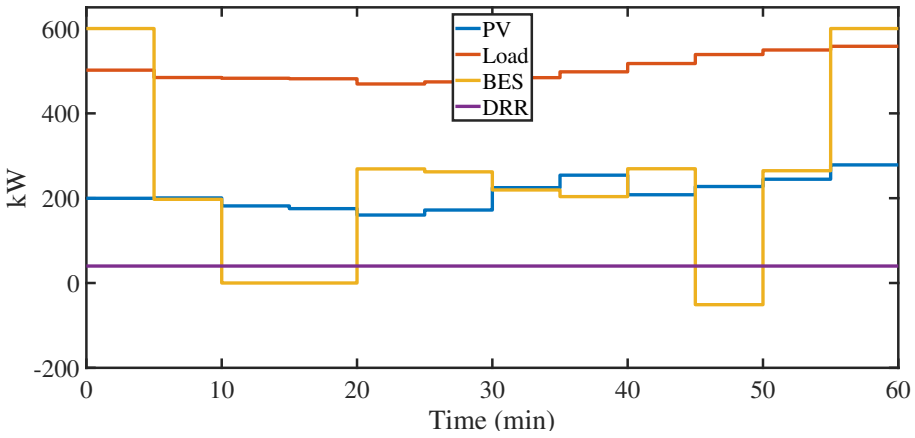

Figure 6.5: The DER output of MG1, when they are dispatched according to the RH approach.

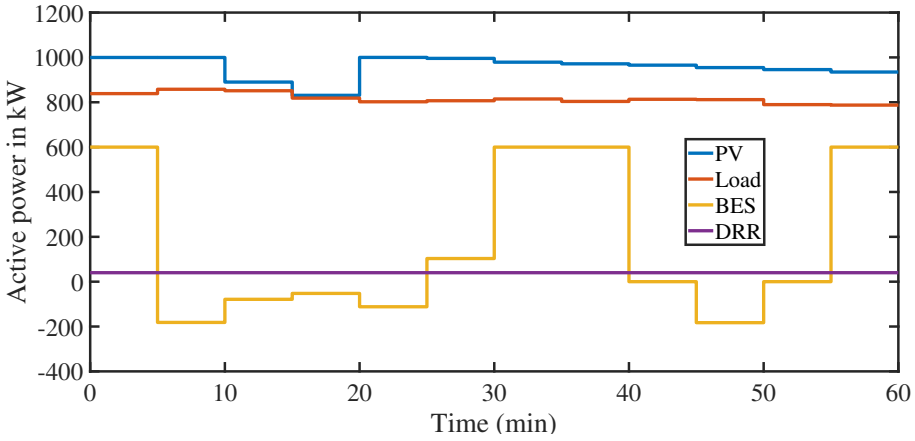

Figure 6.6: The DER output of MG2, when they are dispatched according to the RH approach.

observed that there were fewer deep discharges in the BES dispatch compared to the hour-ahead energy scheduling of Case-1. As the MGs exported less power to the grid in the RH approach, higher peaks were observed in the imported power at the distribution system's substation, as can be seen in Fig. 6.7. The peak imported power was 2.82 MW at time step 10 (45-50 minutes). MG1 had a cost of ¢15, while MG2 had a profit of $9.1.

In contrast with Case-1, where the lowest SoE limits had been reached by the end of the scheduling horizon, the SoE of the BES in MG1 was 49% and in MG2 it was 55%. In reality, when the RH is not implemented, end SoE conditions are defined, which specify a certain (or a minimum) SoE level that should be maintained. This ensures that the MG has the ability to use a part of its own resources in the next scheduling period. However, some solutions, which could also result in a better response to electricity price volatility or other fluctuations in the inputs to the MG-EMS (demand, local generation), are being excluded. When the RH approach is applied, no SoE conditions are required.

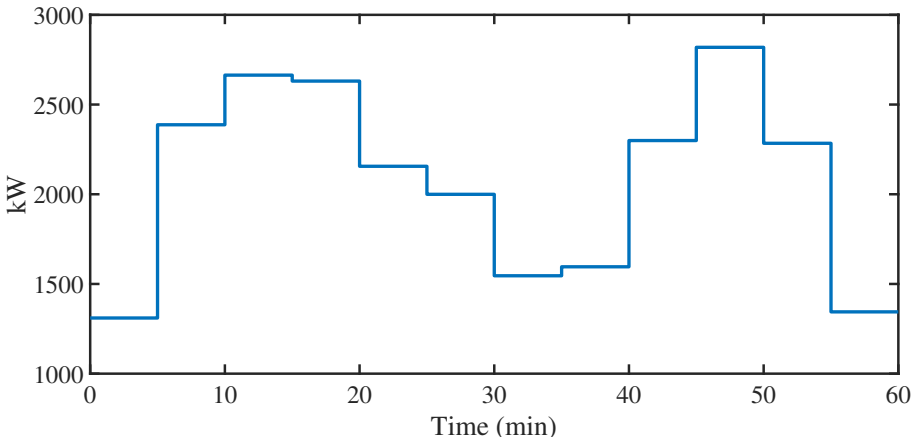

Figure 6.7: Imported active power at the substation, when the MG-EMSs dispatch their optimal set-points after performing energy scheduling with a RH approach.

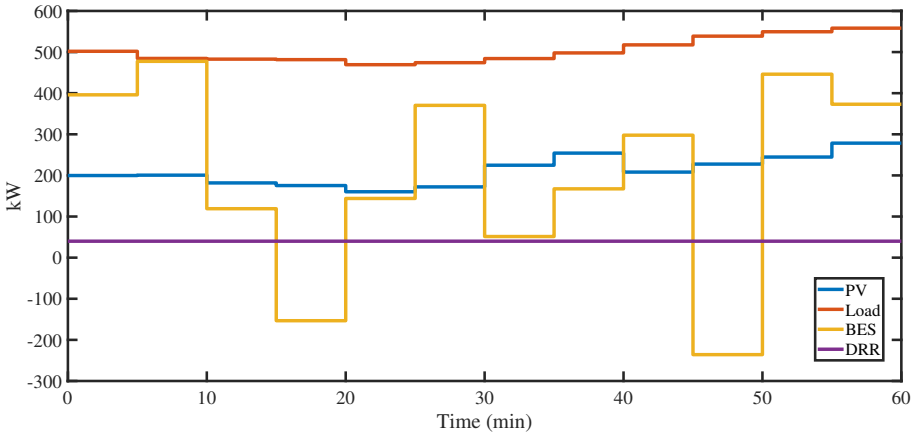

Figure 6.8: The DER output of MG1, when they are dispatched after the MG responds to the DSO's flexibility request.

Case-3

The dispatch of the MGs' DERs in Case-3 can be seen in Fig. 6.8–6.9, which show the results of applying coordinated MG energy scheduling with response to DSO flexibility requests. All flexibility requests could be met by the proposed coordination by re-scheduling the MG resources (modifying the solution that was obtained by the RH approach) in every time step. The MG-EMSs responded positively to all DMS requests at the first iteration, as no MG gave a negative response or responded with a smaller flexibility amount than the requested. The initially scheduled active power exchange between the MGs and the main grid as well as the exchange after the re-scheduling to satisfy the PCC set-points sent by the DMS is presented in Fig. 6.10, where positive values show an aggregated (for both MGs) export towards the upstream network.

The comparison with the optimal MG energy scheduling of Case-1 and Case-2 demonstrates the difference between applying locally optimal solutions and applying coordinated scheduling with the aim to fully satisfy the DSO's objectives. In

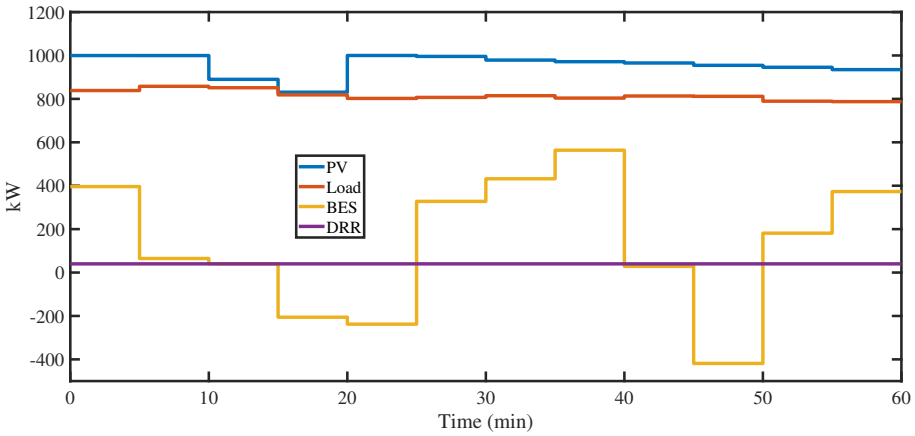

Figure 6.9: The DER output of MG2, when they are dispatched after the MG responds to the DSO's flexibility request.

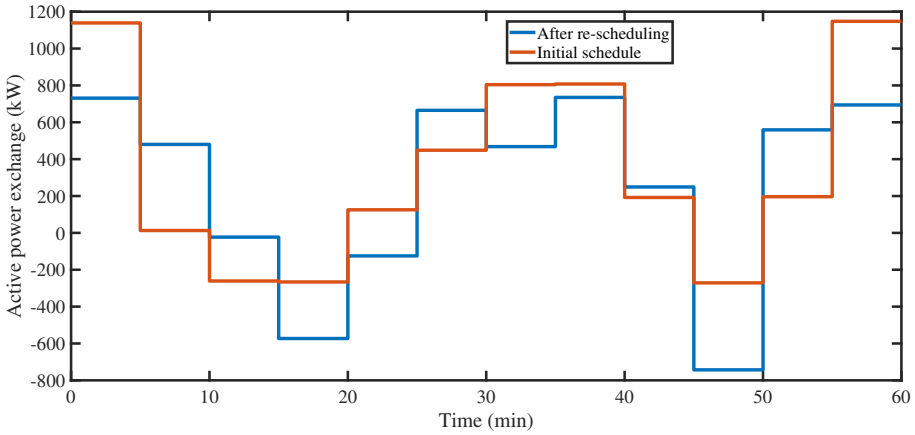

Figure 6.10: Active power exchange at the MGs' PCC (according to initial schedule and after the re-scheduling and the coordination with the DMS).

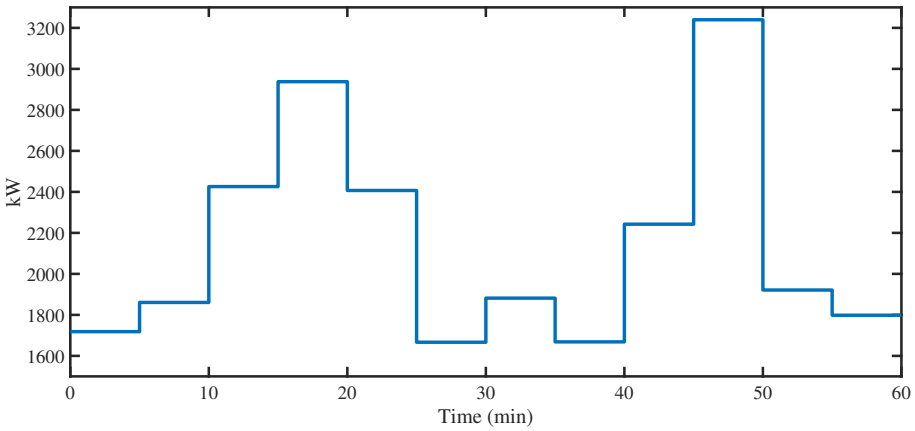

Figure 6.11: Imported active power at the substation, when the MG-EMSs dispatch their optimal set-points after performing energy scheduling with a RH approach.

Case-3, MG1 had a cost of \$1.4, while MG2 had a profit of \$8, which means that the MG energy scheduling of Case-3 yielded a higher cost for MG1 and a lower or at most equal profit for MG2. In order to utilize the MGs the DSO should pay for the difference between the realized MG cost and the MG cost according to the initial schedule. The peak imported power in this case, which was 3.24 MW at time step (45-50 minutes) as can be seen in Fig. 6.11, was increased compared to both Case-1 and Case-2. However, this is due to the TSO's balancing request, which the DSO seeks to fully satisfy by re-scheduling the MGs. Therefore, the MGs import more power from the upstream grid after the re-scheduling.

The primary aim of Case-3 was to show the effectiveness of utilizing the MGs as energy flexible resources. The coordinated MG-EMS was formulated as a bilevel optimization problem, where the upper level was represented by the DMS and the lower level by the MG-EMSs. It was assumed, however, that the MGs would always respond to the DSO's request, if it was feasible. This decreases the feasibility region of the bilevel problem and simplifies the solution, although there might still be areas of the feasibility region that are not searched. These areas could contain an improved solution for one or more entities. In other heuristic approaches, there can be negotiation between the DMS and the MG-EMSs to obtain a compromised solution that satisfies both the constraints and the objectives of the connected entities.

6.1.3 HSB Living Lab

Below are the annual assessment metrics of the BES dispatch according to the four models presented in Section 4.3 in Scenario-1 and Scenario-2. These scenarios correspond to two different SoE limits, as was described in Section 5.4. The assessment of the models was performed according to the measurement-based BES model. Thus, the maximum feasible charging/discharging power was chosen, when the BES power set-points of Model-1 were infeasible with respect to the measurement-based model. Fig. 6.12 shows an example of one day-ahead simulation, where the measurement-based model gives a different estimation of the SoE profile, when the set-points of

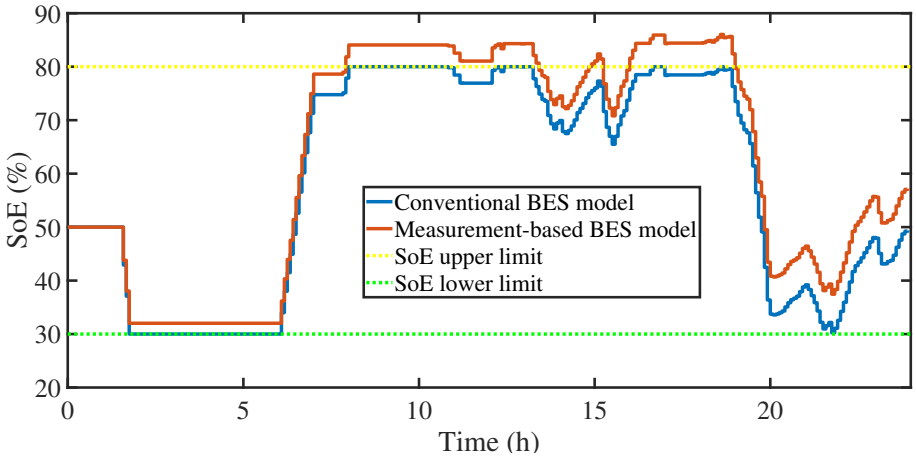

Figure 6.12: The difference in the SoE estimation, when the solution (BES power set-points) of Model-1 (conventional BES model) is used as an input to the measurement-based model.

Model-1 are used as an input. The assessment metrics for Scenario-1 and Scenario-2 are given in Fig. 6.13 and Fig. 6.14, respectively.

Scenario-1

As Fig. 6.13 shows, Model-3 and Model-4 yielded the most economic operation for the prices of \$290 and \$500, as the total cost for either model was not higher than \$4610 at \$290 and \$4830 at \$500. Even though the energy cost was increased in these models, the total capacity loss was lower than in Model-1 and Model-2, which did not include the cycle aging cost in their objective functions and gave a total cost of at least \$4620 at \$290 and \$4851 at \$500. For the lowest BES price there are indications that Model-4 could potentially give a higher (up to 0.4%) cost than Model-1 or Model-2. That can be explained by the fact that Model-4 causes higher calendar aging, as it tries to avoid high DoD values, without substantially reducing the energy cost by the BES dispatch. Comparing with the highest cost of either Model-1 or Model-2, a reduction of up to 0.5%, 0.7%, and 1% could be observed for Model-3 at the price of \$100, \$290, and \$500, respectively. Similarly, a reduction of up to 0.8%, and 1.8% could be observed for Model-4 at the price of \$290, and \$500, respectively.

As the BES prices increase, the cycle aging decreases for Model-3 and Model-4. At the same time, calendar aging increases, as the BES is cycled less. Model-4 caused the lowest capacity loss among all models, which was not higher than 2.7% (at \$100). Interestingly, Model-2 caused the highest capacity loss due to cycle aging (at least 1.5%), which was even higher than in Model-1. Apparently, the less accurate SoE estimation of Model-1 led to slower cycle aging. However, Model-2 could yield a lower total cost than Model-1, especially at lower BES prices, because it caused the lowest calendar aging (1.7%) and, more importantly, yielded the lowest energy cost (\$4290) out of all models. Model-4 gave the highest energy cost at all BES prices (at least \$4328).

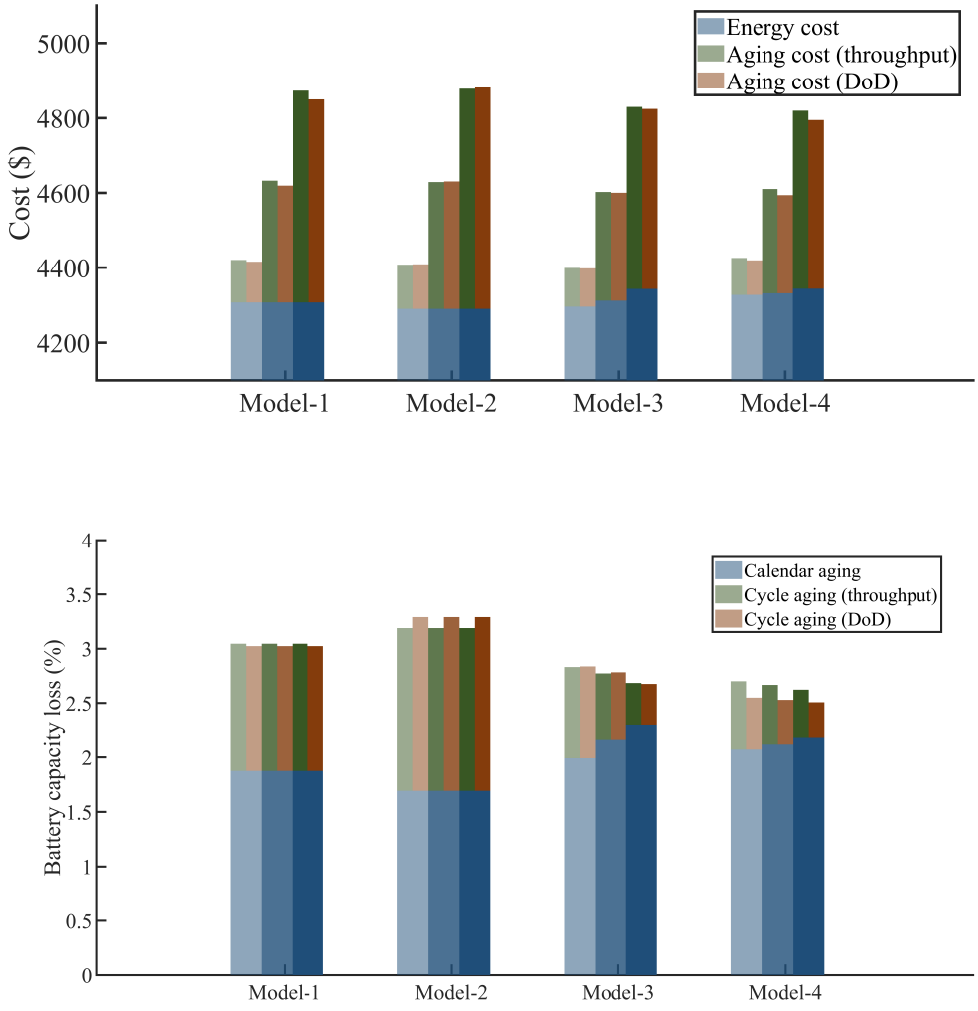

Figure 6.13: The assessment metrics of Scenario-1 (SoE limits of 30%-80%), where light shade of the same color corresponds to BES installation price of $100/kWh, medium shade to the price of $290/kWh and dark shade to the price of $500/kWh

.

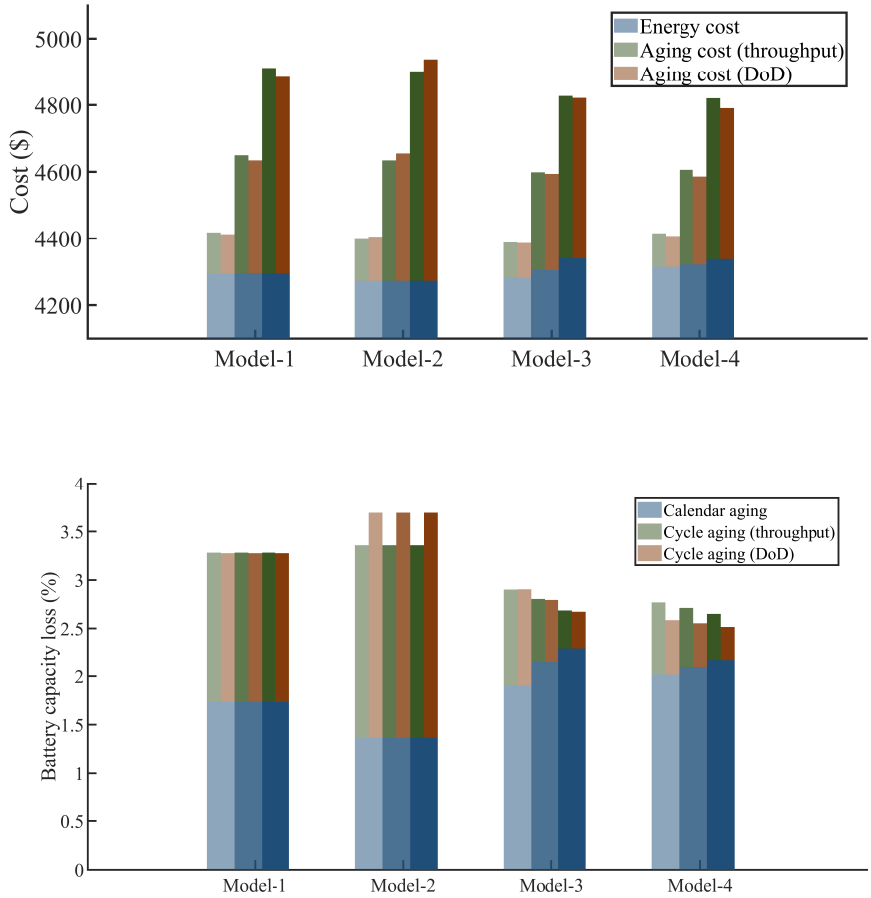

Figure 6.14: The assessment metrics of Scenario-2 (SoE limits of 10%-90%), light shade of the same color corresponds to BES installation price of $100/kWh, medium shade to the price of $290/kWh and dark shade to the price of $500/kWh

.

Scenario-2

Similar trends with Scenario-1 can be observed among the models and across the three BES prices in Scenario-2, Fig. 6.14. The economic performance of Model-3 and Model-4 was enhanced in Scenario-2, where the total cost of either model was not higher than $4606 at $290 and $4828 at $500. These costs are lower than the respective costs in Scenario-1. Apart from the lower energy cost in Scenario-2, the calendar aging also decreased, as lower values of SoE helped the BES retain more capacity during rest periods.

In contrast, Model-1 and Model-2 gave higher total costs in Scenario-2, which were at least $4634 at $290 and $4885 at $500. Again, comparing with the highest cost of either Model-1 or Model-2, a reduction of up to 0.7%, 1.1%, and 1.7% could be observed for Model-3 at the price of $100, $290, and $500, respectively, Similarly, a reduction of up to 1.5%, and 3% could be observed for Model-4 at the price of $290, and $500, respectively. Model-2 gave the lowest energy cost ($4273) and the

lowest capacity loss due to calendar aging (1.4%) out of all models. At the same time, however, it caused the highest cycle-based capacity loss (at least 2%) leading to the largest BES degradation, while Model-4 gave the lowest capacity loss in total, which was not higher than 2.8% at $100.

Discussion on energy and degradation cost

The evaluation of Model-3 and Model-4 highlighted the importance of including both energy and degradation cost in the objective functions that determine the BES dispatch. These models, which combined the measurement-based model with cycle aging models dependent on throughput (Model-3) or DoD (Model-4), could reduce the annual energy and degradation cost by up to 3% under the considered pricing scheme compared to when cycle aging cost was neglected in the BES scheduling. Ideally, the cost of calendar aging should also be included in the optimization model to obtain the most economic BES schedule and it will be considered in future work. As shown by the results, there is a trade-off between cycle and calendar aging and thus, a BES schedule that induces lower cycle aging causes higher calendar aging and vice versa. Nevertheless, Model-3 and Model-4 always yielded the lowest degradation (Model-4 gave the lowest total capacity loss out of all models).

In both scenarios, Model-3 gave the lowest total cost at $100 and Model-4 gave the lowest total cost at $500, irrespective of the deviation between the two different assessments of the cycle-based degradation. Model-4 caused a lower calendar aging (despite directly forcing the BES to higher SoE values), which contributed to a reduced degradation cost, when this was a larger part of the total cost. On the other hand, Model-3 gave a much lower energy cost at $100, which contributed to the reduction of its total cost, when the degradation cost was a less significant part of it. When cycle aging was omitted from the cost function, there was no clear advantage of using the more accurate measurement-based BES model (Model-2) instead of the conventional one (Model-1).

Discussion on SoE limits

Model-3 and Model-4 could be used with either conservative SoE limits or with less strict SoE limits, as both scenarios resulted in almost equal economic benefits for the building owner and the resident. On the other hand, if degradation is neglected in the BES scheduling, it is suggested that conservative limits should be applied to prolong the BES lifetime and reduce the degradation cost. The building operator could apply the appropriate SoE limits depending on whether the implemented BES scheduling seeks to avoid degradation.

Discussion on battery retirement

The degradation cost in this study is related with η, which is used to evaluate the remaining useful lifetime of the BES and serves as a termination (retirement) criterion [98]. It is assumed that, when the BES capacity is reduced to η% of its initial value, the BES is replaced. However, storing electricity generated from RES is a less demanding function than powering EVs. This is also the motivation

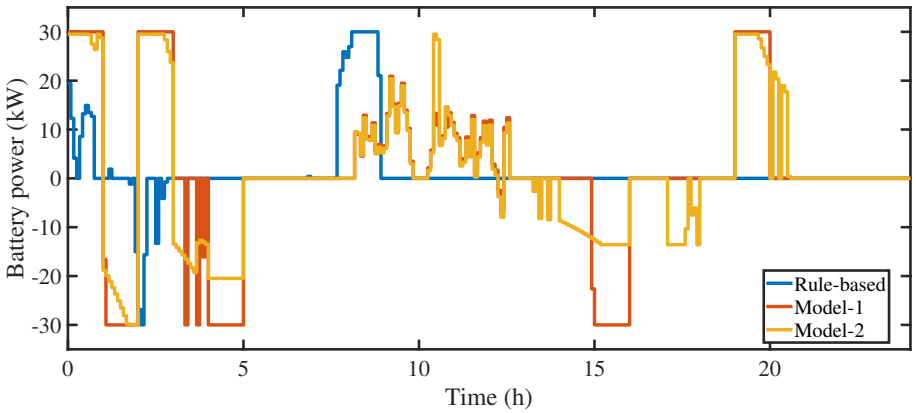

Figure 6.15: The BES dispatch according to the rule-based algorithm, Model-1, and Model-2.

behind using retired EV BESs as second-life BESs in load shifting applications [99]. BESs with reduced capacity could still be used in energy management, which could potentially lead to an overestimation of the degradation cost, if the BES is ultimately replaced at a capacity, which is lower than η. In practice, the BES needs to be replaced after a certain part of its initial capacity is lost, as the benefit of using the BES for load shifting is reduced and the overall BES performance deteriorates. The choice of η, however, is still an open question, as there are relatively few research studies and applications of residential, stationary BES.

6.1.4 Brf Viva

A daily energy scheduling of the Brf Viva BMG was simulated considering the same input data (load, PV generation, and electricity prices) that were used in the demonstrations (see the Appendix). A comparison of the daily BES scheduling and SoE profile obtained from Model-1, Model-2, Model-4, and the rule-based algorithm was can be seen in Fig. 6.15–6.18.

The BES power dispatch in Fig. 6.15 and the SoE profile in Fig. 6.16 show that the BES was cycled more, when the BES was used to minimize energy cost (Model-1 and Model-2), as the BES power followed the fluctuations of the spot price. Small variations in the BES power (e.g., between hour 8 and hour 13) can be attributed to the fact that in each simulation the forecast of the load and the PV generation was updated, which made the BMG-EMS re-adjust the charging or discharging rate. Bigger variations in BES power were a result of the spot price difference, since the BMG-EMS tried to maximize the profit through energy arbitrage. This can be observed, e.g., in the first four hours of the simulation, where there were big changes in the electricity price of each hour. Between the BES scheduling according to Model-1 and the BES scheduling according to Model-2 there were only small differences, as can be seen from their SoE profiles.

When BES degradation was considered, however, there was a trade-off between the minimization of energy cost through load shifting and the minimization of BES

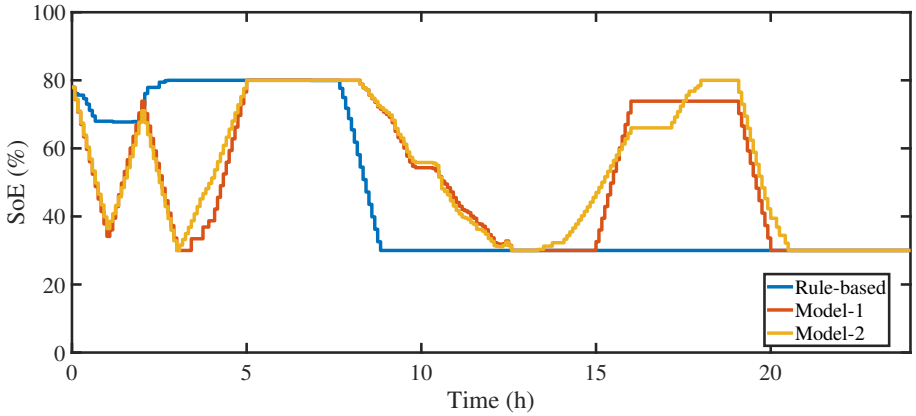

Figure 6.16: The estimation of SoE according to the rule-based algorithm, Model-1, and Model-2.

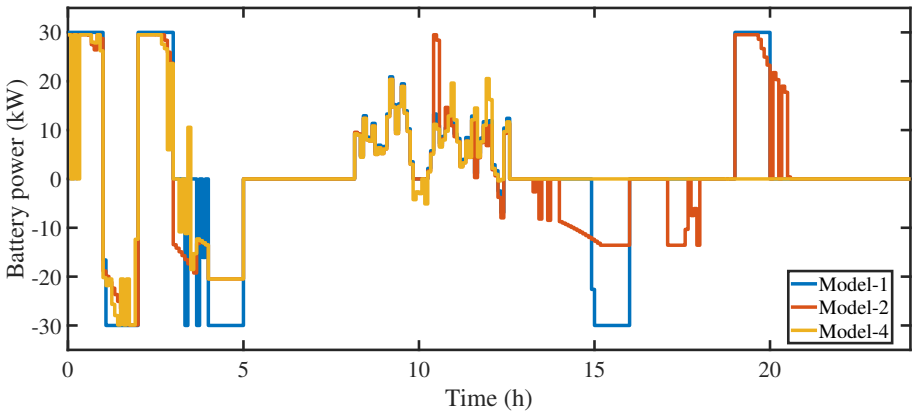

Figure 6.17: The BES dispatch according to Model-1, Model-2, and Model-4.

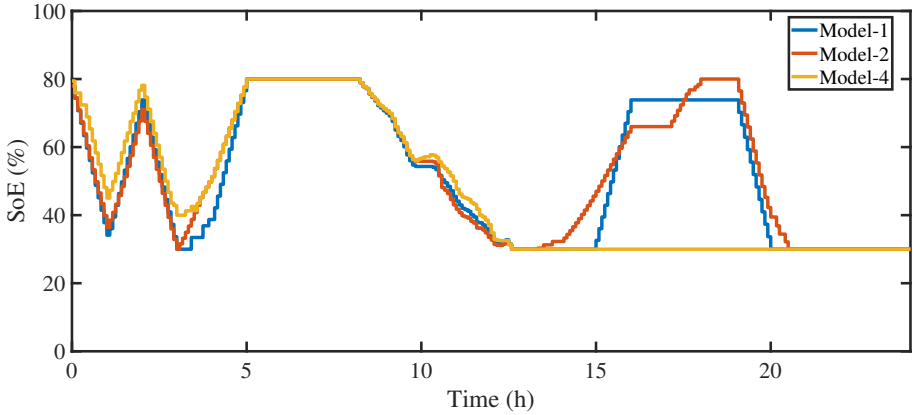

Figure 6.18: The estimation of SoE according to Model-1, Model-2, and Model-4.

degradation cost. The cost of cycle aging, which is considered in Model-4, penalizes both the number of cycles and deep discharges resulting in the BES dispatch and SoE profile seen in Fig. 6.17–6.18. As can be seen, even when the BES was cycled in the first hours (Fig. 6.17), it did not reach the low SoE value that Model-1 and Model-2 yielded (Fig. 6.18). In addition to this, the BES was not cycled during the second half of the scheduling period (as it happened with Model-1 and Model-2) because the profit from energy arbitrage was very small and did not compensate for the cost of lifecycle loss of the BES. This profit was in fact that small, that the daily BMG energy cost (including peak power cost) was practically similar among the optimization models (about $70).

When the rule-base algorithm was applied, the daily BMG energy cost was higher (about $72), although that could be different depending on the choice of the peak and low load threshold. The rule-based algorithm, however, uses the BES in a non-optimal way and it is hard to capture and reduce the peak power. Since the future load and PV generation profiles are not considered, the energy storage levels might be depleted, when the daily peak power occurs. This problem can be observed in Fig. 6.15–6.16, where there is big discharge power rate applied by the rule-based algorithm starting around hour 8, whereas the optimization models (Model-1, Model-2, and Model-4) apply a more conservative BES scheduling, saving energy for the expected peak power. Therefore, the rule-based algorithm results in a peak load of 152.2 kW, while the peak power according to the optimization models ranges from 131.9 to 132.9 kW.

6.2 Demonstration results

The demonstrations validated the BES scheduling models and thus the performance of the BMG-EMS, as the actual behavior of the BESs was captured very well by the developed BMG energy management model under specific operation conditions. Challenges, limitations, and lessons learnt from the demonstrations are discussed at the end of this section. Below is a detailed presentation of the demonstration results.

6.2.1 Brf Viva

The results from the demonstration of the BES dispatch with the designed BMG-EMS showed that both the conventional and the measurement-based BES scheduling model had acceptable accuracy and the BES dispatch followed the schedule. Moreover, the demonstration results matched the simulation results, which were presented in Section 6.1.4. The same input data (including initial SoC measured at $t = 0$) were used both for demonstrations and simulations to allow for comparison of their results. As an example, Fig. 6.19–6.21 present the results from the demonstration of BES scheduling with Model-2.

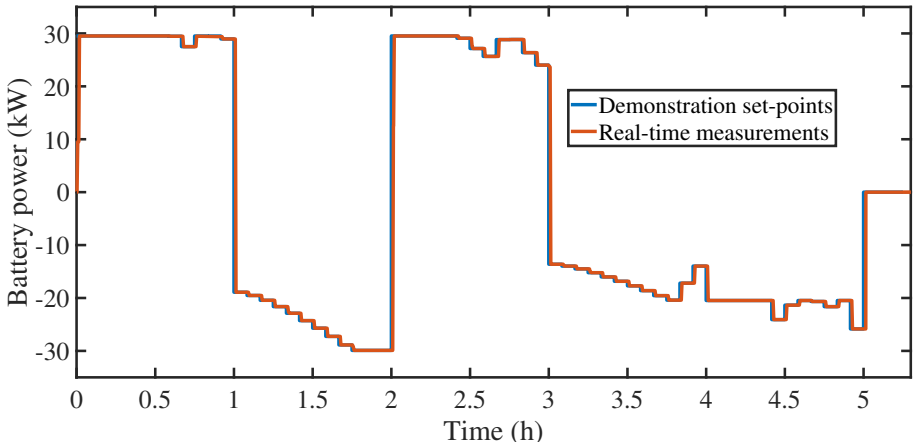

Figure 6.19: The dispatched set-points of Model-2 and the real-time power measurements (demonstration with the system of BESs at Brf Viva).

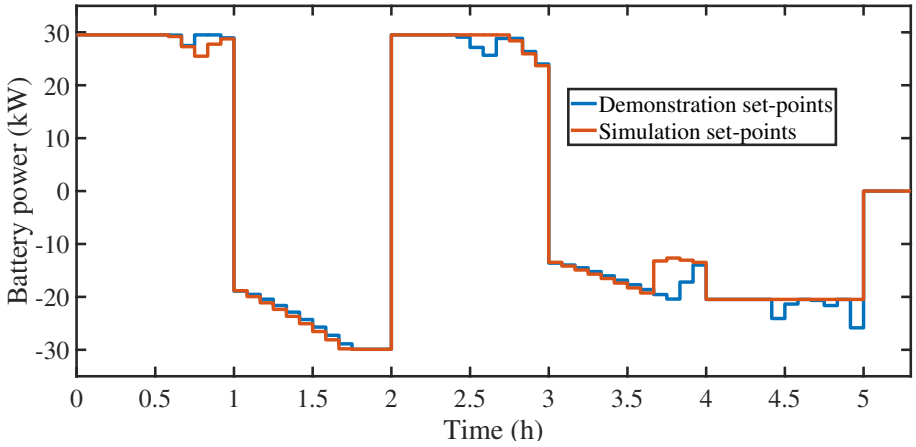

Figure 6.20: The BES power set-points of simulated and demonstrated BES scheduling of the system of BESs at Brf Viva under Model-2.

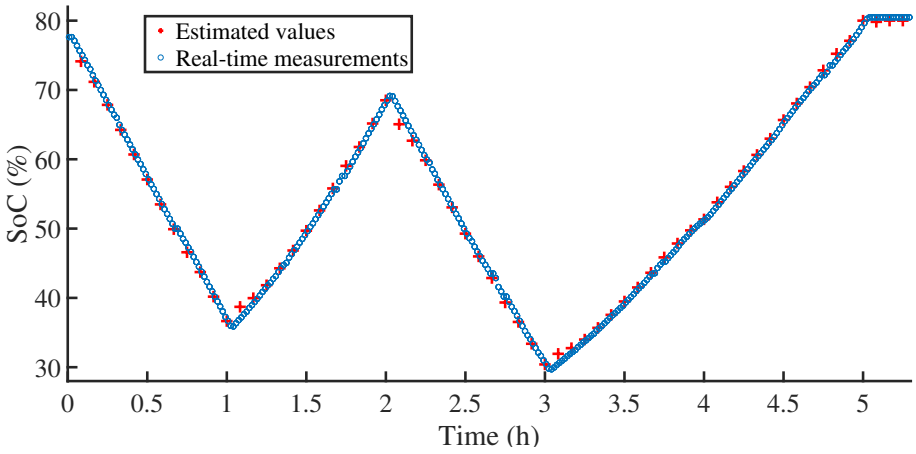

Figure 6.21: The estimated SoC during the demonstration of BES scheduling under Model-2 and the real-time value of SoC (updated per minute) of the system of BESs at Brf Viva.

BES dispatch

As can be seen in Fig. 6.19, the response of the system of BESs matches the requests from the BMG-EMS, which proves that the proposed model can be used for close to real-time energy management. Small deviations in the power dispatch compared to the simulated BES scheduling (see Fig. 6.20) are attributed to the fact that in the demonstration, the measured SoC was entered as an input to the algorithm, whereas simulations used estimated SoE levels as inputs.

SoE estimation

Fig. 6.21 also validates the accuracy of Model-2, as the estimated on a 5-minutes time scale SoE according to Model-2 is compared to the SoC measurements (updated per minute) provided by the converter controller. The accuracy of the SoE estimation proved that the BES scheduling solution of the BMG energy management model could be implemented on a 5-minutes time scale. To evaluate the accuracy of the SoE quality the following index was defined:

$$q^{idx} = \frac{||soe_t - soc_t||}{soe_t}. \tag{6.1}$$

The quality index q^{idx} gives the percentage value of the difference between the estimated SoE and the measured SoC of one time step. The average quality index for Model-1 and Model-2 was 1.5% and 1%, respectively, suggesting a slightly improved performance of the BMG energy management model, when the measurement-based BES scheduling model was used.

6.2.2 HSB Living Lab

The demonstrations with the HSB LL BES showed that the BES dispatch could not follow the schedule obtained with Model-1 as well as the schedule obtained with Model-2. The same input data (including initial SoC measured at $t = 0$) were used for both demonstrations to allow for comparison of their results.

BES dispatch

Fig. 6.22 and Fig. 6.23 respectively show the BES response during a 24-hour demonstration of Model-1 and Model-2 at HSB LL building. In Fig. 6.22, it can clearly be observed that the dispatched power did not match the big charging request. The BES response was significantly improved in the demonstration of Model-2, as can be seen in Fig 6.23. The total mismatch in delivered charging and discharging BES energy over the requested BES energy was 3.7% and 13.3% in the demonstration of Model-2 and Model-1, respectively. This validates the enhanced accuracy of the measurement-based model and, by extent, the simulation results in Section 6.1.3.

The comparison of Model-1 and Model-2 showed that the BES was cycled more, when the accuracy of the BES model was improved. This confirms what was indicated by the simulation results, as Model-2 gave a higher cycle aging, which means

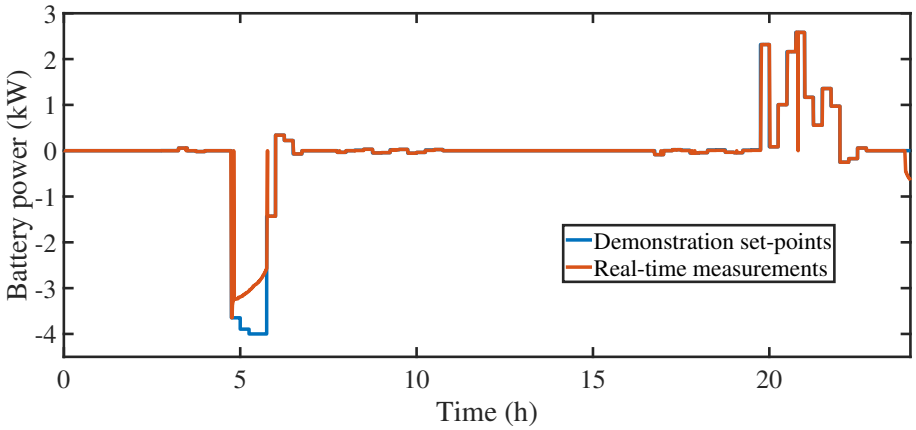

Figure 6.22: The set-points and the real-time measurements of the battery power (demonstration of Model-1 at HSB LL building).

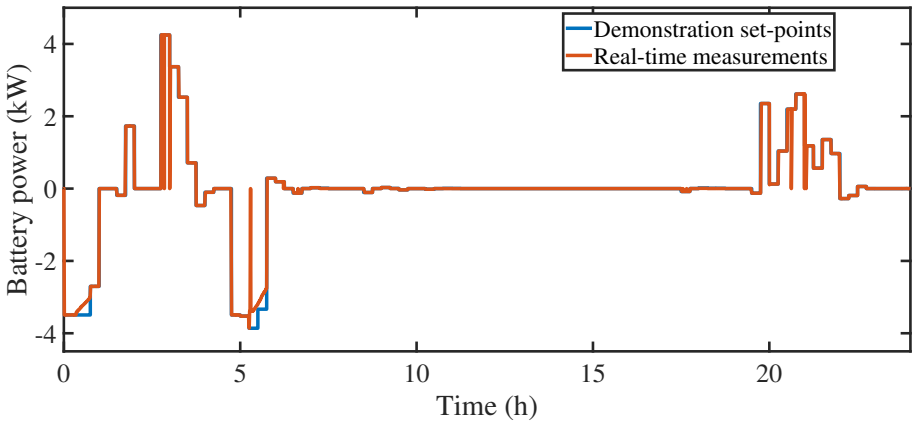

Figure 6.23: The set-points and the real-time measurements of the battery power (demonstration of Model-2 at HSB LL building).

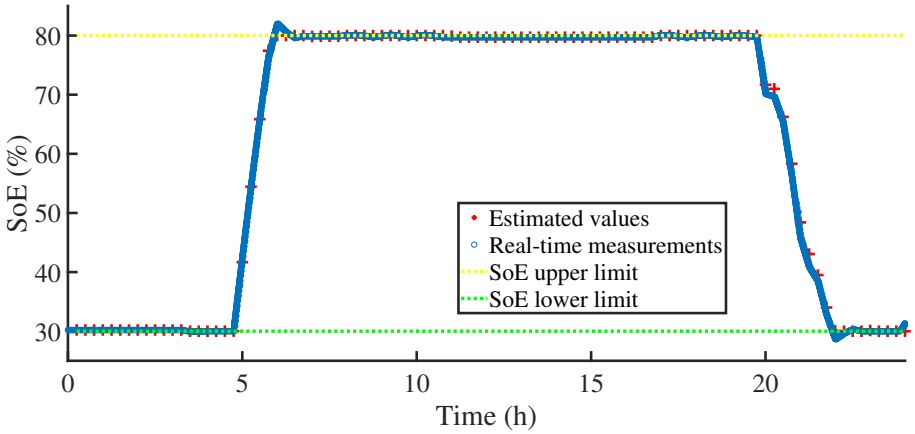

Figure 6.24: The estimated SoE of the BES dispatch model during the demonstration of Model-1 at HSB LL building and the real-time value of SoC as measured by the converter (updated per 5 seconds).

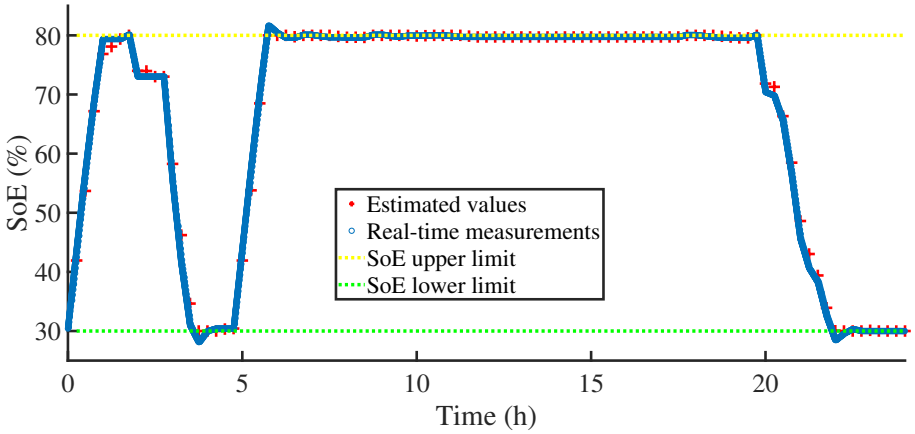

Figure 6.25: The estimated SoE of the BES dispatch model during the demonstration of Model-2 at HSB LL building and the real-time value of SoC as measured by the converter (updated per 5 seconds).

that for certain days the BES performed more cycles, when it followed the schedule obtained with Model-2.

SoE estimation

Fig. 6.24–6.25 show the estimated on a 15-minutes time scale SoE according to Model-1 and Model-2, respectively. These values are compared with the SoC measurements (updated per 5 seconds) provided by the converter controller and the SoE limits (as were defined by the BMG operator). Both models provided an accurate SoE estimation on a 15-minutes time scale, while the violations of the SoE limits were negligible. The average quality index for Model-1 and Model-2 was 0.5% and 1.2%, respectively. Model-1 had a better performance in terms of SoE estimation, however, the two models gave a different BES scheduling and SoE profile, as the BES performed more cycles with Model-2.

6.2.3 Discussion of results, challenges, and lessons learnt

The demonstrations at the two demo sites showed that the BESs could follow the requests that were transmitted from the BMG-EMS, if certain operation conditions were satisfied. It was important that the SoE limits of the BMG-EMS would be stricter than the SoC limits of the current limiter function of the BES DC/DC converter. Furthermore, there were additional challenges at each demo site that affected the BES response to the power request commands.

The results in Brf Viva revealed that the system of BESs could follow the power requests with a negligible deviation. This was observed both for the BES dispatch according to the conventional BES scheduling model (Model-1) and for the BES dispatch according to the measurement-based model (Model-2). In either case, it was not an easy task to implement the BES scheduling models with the designed BMG-EMS, which dispatched the BESs as a system and the power request was equally divided to all BESs. Each BES could end in a different SoC level and this problem was intensified by a maintenance function implemented by each BMS. Therefore, the demonstration at the Brf Viva buildings was only possible after deactivating the maintenance mode of the BESs. Otherwise, the system of BESs would only reliably deliver the rated power within a much stricter SoE region, i.e., 40%-70%, than that implemented by the current limiter function, which was 27%-80%.

The results in HSB LL also showed very good response of the BES, when additional limitations in delivered charging power were considered. Larger charging requests were not always met, probably due to the SoH of some battery cells. This is why the value of using the measurement-based model was more evident for this demo site. The measurement-based model was validated with the real tests at HSB LL building showing a considerable improvement in the BES responses, as compared to those of the conventional BES model. As the results showed, the daily undelivered BES energy over the total request was reduced from 13.3% to 3.7% at the same time as the BES usage was increased. This indicates a more reliable implementation of the BES dispatch following the targets of the building operator without the necessity of imposing additional charging power limits, which would limit the BES in the whole operational SoE region, as was the case with the conventional BES model.

Apart from the accuracy of the BES scheduling models, there are several other factors that may influence the results and the expected costs of the applied BES operation strategy. One of these factors is the forecast models that are integrated in the BMG-EMS. These models should forecast the load, the PV generation, and the energy price with small errors to ensure an accurate cost estimation as the result of implementing the energy scheduling solution. Another factor is the BES degradation model and the considered BES stress factors and degradation parameters. This model and stress factors may vary for each specific BES type. Morevoer, degradation impacts the performance of the BES, which means that the parameters of the BES scheduling model might have to be re-adjusted.

The demonstrations validated the BES scheduling models under the operation conditions that have been described. The measurement-based model that was developed

for each site was found to be suitable for close to real-time BMG energy management. This model was incorporated in the proposed Model-3, which was assessed in the HSB LL simulation study that was performed for a year of the BMG operation. The developed BMG energy management model can therefore be utilized by the BMG operator both for close to real-time energy management and long-term assessment studies. Using this model for close to real-time energy scheduling can reduce the expected energy cost in short-term. Long-term studies with the proposed model can more accurately estimate the benefit of BES's flexibilities in reducing the building total costs and help the BMG operator choose which operation strategy is more economic.

Chapter 7

Conclusions and Future Work

This chapter summarizes the work of the thesis and the key implications of the simulation and demonstration results. Suggestions for future research are also provided at the end of the chapter.

7.1 Conclusions

This thesis has dealt with energy management of grid-connected MGs that use BES as the main energy flexible resource. The developed energy management model can be integrated in a MG-EMS and utilized for optimal energy scheduling of the MG resources either in an uncoordinated way (only considering local constraints/targets) or in coordination with the DSO.

Regarding the first research question that was formulated in Section 1.1, the MG energy scheduling model was tested with different schemes of coordination with the DSO in two distribution grid test systems. The simulation results, which were presented in Section 6.1.1, showed that, **even without coordination, the distribution system can benefit from the implementation of multiple MG-EMSs that locally optimize their day-ahead resource scheduling**. The MG energy scheduling solution that would most benefit the DSO did not benefit the MGs, as their cost would be the same compared to the base case. In answering the first question, the cost difference between the optimal solution for the MGs and the optimal solution for the DSO could be used to define the cost that the DSO would pay to the MG owners, if the MGs were used to optimize the operation of the main grid. The same applies for the simulation results, which were presented in Section 6.1.2, which proved **the effectiveness of the decentralized coordination in re-scheduling the MG resources to satisfy the DSO's requested flexibility**.

The MG energy management model was also applied for a BMG that uses BES as a flexible resource considering the energy market-based participation of the buildings. In answering the second research question that was formulated in Section 1.1, the developed mathematical model incorporated the measurement-based BES model, which can capture realistic performance characteristics, with cycle aging models,

which can assess the impact of the energy scheduling solution to the capacity of the BES. The calendar aging was also calculated after the final dispatch decisions for a comprehensive evaluation of the degradation. The validation of the BMG energy management model with simulations and demonstrations at real residential buildings proved the **feasibility of integrating a more detailed mathematical BES model to the LP optimization problem for the energy scheduling of MGs.**

In answering the third research question that was formulated in Section 1.1, the simulation studies of the BMG energy management model were used to evaluate the cost and degradation of the implemented BES dispatch that followed the schedule obtained from the model. The proposed Model-3 and Model-4, which combined the measurement-based BES model with cycle aging models dependent on throughput and DoD, respectively, **could reduce the annual energy and degradation cost by up to 3%** compared to when degradation cost was omitted from the objective function, as the study at HSB LL in Section 6.1.3 showed. Moreover, it was shown that it is possible to have **more flexible limits on the SoE levels** of the BES and allow more BES capacity to be used, if these models are employed. On the other hand, if degradation is neglected in the BES dispatch, conservative limits should be applied to prolong the BES lifetime.

The demonstrations validated the BMG energy management model integrating the BESs at each demonstration site, which was one of the objectives of this thesis. In Brf Viva, both the measurement-based and the conventional BES model gave reliable solutions, as the real test showed that the system of BESs could follow the schedule of the BMG-EMS. It should be noted, however, that a maintenance function of these BESs had to temporarily be removed otherwise the reliability of the solution was severely compromised. In the HSB LL demonstrations, there was a considerable improvement in the BES responses, when the measurement-based model was used, as compared to the BES responses, when the conventional BES model was used, which was shown in Fig. 6.22–6.23. As a result, the daily undelivered BES energy over the total request was reduced from 13.3% to 3.7% at the same time as the BES usage was increased. This indicated **a more reliable implementation of the BES dispatch** according to the measurement-based model, as the BES could more accurately follow the schedule that reflected the targets of the building operator. The demonstration results also validated the reliability of the solution of the proposed Model-3 and Model-4, which coupled cycle-based degradation models with the measurement-based model.

The results from the simulation and demonstrations proved that the developed MG energy management model can be employed both for close to real-time energy management and for long-term assessment studies. Thus, the proposed model contributes to a more accurate estimation of the benefits associated with BES's flexibility for the MG operator and the DSO.

7.2 Future research

In this thesis, the MG energy management was studied with an emphasis on BES flexibility. Although the BES modeling and degradation was studied in greater detail than the majority of the literature on MG energy management, there are still areas that require further research. Apart from the accuracy of the mathematical model of the BES, the forecasting error associated with the input data to the MG-EMS (such as load consumption, PV generation, electricity price) could also influence the results. These two factors and their effect in the optimal MG energy scheduling solution should be further examined. Moreover, the accuracy of the estimated aging can vary depending on the BES chemistry. The aging models used in this thesis might not be applicable to all Li-ion BESs and it is therefore advised that tests with different aging models are conducted to further guarantee the benefits in terms of cost reduction for the BMG.

Moreover, the thesis introduced the first steps on interaction between grid-connected MGs and the DSO. Coordination of multiple BES-based MGs or BESs with the control devices of the main grid is a very interesting research area, as existing approaches have so far been using the conventional BES model and neglecting the impact of degradation. It would also be useful to study other types of MGs (e.g., MGs that are based on different resources) and also different configurations of distribution systems with multiple interconnected MGs. If the research gaps that were identified during the work of this thesis are further explored, there will be a deeper understanding of the benefit of BES flexibility both for the MG owner and for the DSO.

Following are some topics, which are suggested for future research:

- The use of the measurement-based model both results in reliable implementation of the BES scheduling model and simplifies the optimization problem. Thus, advanced AC OPF with fewer relaxations can be used for the distribution network operation. Then, the coordination between DSO and MGs can further be developed to consider MG re-scheduling for network loss minimization.

- In regard to the above suggestion, the advanced OPF with the measurement-based BES model could be used to coordinate the operation of on-load tap changer operation and BESs utilizing the DMS and MG-EMS interface.

- The parameters of the measurement-based model are not constant throughout the BES's lifetime. Instead they depend on the aging-induced changes of the BES performance. The development of a measurement-based BES scheduling model with adjustable parameters is suggested for future work. Future research could use ANNs for the estimation of these parameters.

- Future research should expand the MG energy management model to include the cost of calendar aging. This can be a challenging task, especially if calendar aging cost is to be incorporated in Model-4 of this thesis, as more integrality constraints will have to be added to the MILP problem. Model-3 or other

MG energy management models that consider degradation cost can also be tested, however, it is expected that integrality constraints cannot be avoided altogether, if the optimization problem is to account for the impact of DoD of each BES cycle.

- The optimal MG energy scheduling should also be applied for the island operation mode, where the MG's cost minimization should consider seamless transition between modes. The trade-off between MG resiliency and cost minimization is a very interesting subject, as these two objectives are expected to result in different BES utilization.

- The MG energy scheduling problem could use forecasting models to obtain the input values of load, PV, and electricity price. It would be valuable if future research could quantify the effect of the forecasting error to the cost of the energy scheduling solution. It would also be interesting to investigate which scheduling horizon and time scale of the energy scheduling are suitable to minimize the effect of the forecasting error.

- It would be valuable to compare revenue streams and assess the economic benefits of both portable and stationary BESs as flexible energy resources for a building owner. For this purpose, the BES degradation induced by each BES service should be quantified. Second-life applications of BESs should also be considered.

References

[1] S. Klaus, "Nordic energy technology perspectives," https://backend.orbit.dtu.dk/ws/portalfiles/portal/110808060/ETP2015_ENS_june2015_Klaus_Skytte.pdf, June 2015, Accessed: June 2020.

[2] https://www.government.se/press-releases/2017/09/government-making-broad-investments-in-energy/, Accessed: April 2020.

[3] Statement of government policy, Government of Sweden, Sep. 2019.

[4] IRENA, "Off-grid renewable energy solutions to expand electricity access: An opportunity not to be missed," *Int. Renewable Energy Agency*, Abu Dhabi, 2019.

[5] ——, "Electricity storage and renewables: Costs and markets to 2030," *Int. Renewable Energy Agency*, Abu Dhabi, 2017.

[6] A. Eller and D. Gauntlett, "Energy storage trends and opportunities in emerging markets," *Navigant Consulting Inc.: Boulder, CO, USA*, 2017.

[7] I. S. F. Gomes, Y. Perez, and E. Suomalainen, "Coupling small batteries and PV generation: A review," vol. 126, p. 109835, July 2020.

[8] N. Hatziargyriou, "The microgrids concept," in *Microgrids: Architectures and control*. Wiley—IEEE press, 2014, ch. 1, pp. 1–24.

[9] A. Hirsch, Y. Parag, and J. Guerrero, "Microgrids: A review of technologies, key drivers, and outstanding issues," *Renewable and Sust. Energy Rev.*, vol. 90, pp. 402–411, July 2018.

[10] CIGRÉ Working Group C.22 Microgrids Evolution Roadmap, "Microgrids 1: Engineering, Economics, Experience," http://www.e-cigre.org/publication/635-microgrids-1-engineering--economics--experience, Oct. 2015.

[11] D. Y. Yamashita, I. Vechiu, and J.-P. Gaubert, "A review of hierarchical control for building microgrids," *Renewable and Sust. Energy Rev.*, vol. 118, p. 109523, Feb. 2020.

[12] H. Fontenot and B. Dong, "Modeling and control of building-integrated microgrids for optimal energy management–A review," *Appl. Energy*, vol. 254, p.

113689, Nov. 2019.

[13] S. Dorahaki, R. Dashti, and H. R. Shaker, "Optimal energy management in the smart microgrid considering the electrical energy storage system and the demand-side energy efficiency program," *J. Energy Storage*, vol. 28, p. 101229, Apr. 2020.

[14] W. Hu, P. Wang, and H. B. Gooi, "Toward optimal energy management of microgrids via robust two-stage optimization," *IEEE Trans. Smart Grid*, vol. 9, no. 2, pp. 1161–1174, Mar. 2018.

[15] S. Suthar, N. Kumar, and N. M. Pindoriya, "Cost-effective energy management of grid-connected PV and BESS: A case study," in *Proc. IEEE Innovative Smart Grid Technologies-Asia (ISGT Asia)*, Chengdu, China, Oct. 2019, pp. 4122–4127.

[16] W. Shi, N. Li, C.-C. Chu, and R. Gadh, "Real-time energy management in microgrids," *IEEE Trans. Smart Grid*, vol. 8, no. 1, pp. 228–238, Jan. 2017.

[17] W. Su, J. Wang, and J. Roh, "Stochastic energy scheduling in microgrids with intermittent renewable energy resources," *IEEE Trans. Smart Grid*, vol. 5, no. 4, pp. 1876–1883, July 2014.

[18] M. El-Hendawi, H. Gabbar, G. El-Saady, and E.-N. Ibrahim, "Control and EMS of a grid-connected microgrid with economical analysis," *Energies*, vol. 11, no. 1, p. 129, Jan. 2018.

[19] B. Zhao, X. Wang, D. Lin, M. M. Calvin, J. C. Morgan, R. Qin, and C. Wang, "Energy management of multiple microgrids based on a system of systems architecture," *IEEE Trans. Power Syst.*, vol. 33, no. 6, pp. 6410–6421, Nov. 2018.

[20] F. Khavari, A. Badri, and A. Zangeneh, "Energy management in multi-microgrids via an aggregator to override point of common coupling congestion," *IET Gener., Transmiss. & Distribution*, vol. 13, no. 5, pp. 634–642, Mar. 2019.

[21] P. Tian, X. Xiao, K. Wang, and R. Ding, "A hierarchical energy management system based on hierarchical optimization for microgrid community economic operation," *IEEE Trans. Smart Grid*, vol. 7, no. 5, pp. 2230–2241, Sep. 2016.

[22] S. Wang, H. Gangammanavar, S. D. Ekşioğlu, and S. J. Mason, "Stochastic optimization for energy management in power systems with multiple microgrids," *IEEE Trans. Smart Grid*, vol. 10, no. 1, pp. 1068–1079, Jan. 2019.

[23] L. Zhang, N. Gari, and L. V. Hmurcik, "Energy management in a microgrid with distributed energy resources," *Energy Convers. and Manage.*, vol. 78, pp. 297–305, Feb. 2014.

[24] J. A. Pinzon, P. P. Vergara, L. C. Da Silva, and M. J. Rider, "Optimal management of energy consumption and comfort for smart buildings operating in a microgrid," *IEEE Trans. Smart Grid*, vol. 10, no. 3, pp. 3236–3247, May 2019.

[25] C. Ju, P. Wang, L. Goel, and Y. Xu, "A two-layer energy management system for microgrids with hybrid energy storage considering degradation costs," *IEEE Trans. Smart Grid*, vol. 9, no. 6, pp. 6047–6057, May 2017.

[26] C. Liu, X. Wang, X. Wu, and J. Guo, "Economic scheduling model of microgrid considering the lifetime of batteries," *IET Gener., Transmiss. & Distribution*, vol. 11, no. 3, pp. 759–767, Feb. 2017.

[27] Y. Shang, W. Wu, J. Guo, Z. Ma, W. Sheng, Z. Lv, and C. Fu, "Stochastic dispatch of energy storage in microgrids: An augmented reinforcement learning approach," *Appl. Energy*, vol. 261, p. 114423, Mar. 2020.

[28] I. Alsaidan, A. Khodaei, and W. Gao, "A comprehensive battery energy storage optimal sizing model for microgrid applications," *IEEE Trans. Power Syst.*, vol. 33, no. 4, pp. 3968–3980, July 2018.

[29] G. Cardoso, T. Brouhard, N. DeForest, D. Wang, M. Heleno, and L. Kotzur, "Battery aging in multi-energy microgrid design using mixed integer linear programming," *Appl. energy*, vol. 231, pp. 1059–1069, Dec. 2018.

[30] P. Zhuang and H. Liang, "Hierarchical and decentralized stochastic energy management for smart distribution systems with high BESS penetration," *IEEE Trans. Smart Grid*, vol. 10, no. 6, pp. 6516–6527, Nov. 2019.

[31] H. Farzin, M. Fotuhi-Firuzabad, and M. Moeini-Aghtaie, "A stochastic multi-objective framework for optimal scheduling of energy storage systems in microgrids," *IEEE Trans. Smart Grid*, vol. 8, no. 1, pp. 117–127, Jan. 2017.

[32] M. Sedighizadeh, M. Esmaili, A. Jamshidi, and M.-H. Ghaderi, "Stochastic multi-objective economic-environmental energy and reserve scheduling of microgrids considering battery energy storage system," *Int. J. Elect. Power & Energy Syst.*, vol. 106, pp. 1–16, Mar. 2019.

[33] V.-H. Bui, A. Hussain, and H.-M. Kim, "Double deep Q-learning-based distributed operation of battery energy storage system considering uncertainties," *IEEE Trans. Smart Grid*, vol. 11, no. 1, pp. 457–469, Jan. 2020.

[34] D. E. Olivares, A. Mehrizi-Sani, A. H. Etemadi, C. A. Cañizares, R. Iravani, M. Kazerani, A. H. Hajimiragha, O. Gomis-Bellmunt, M. Saeedifard, R. Palma-Behnke *et al.*, "Trends in microgrid control," *IEEE Trans. Smart Grid*, vol. 5, no. 4, pp. 1905–1919, July 2014.

[35] "IEC 61970, Energy management system application program interface (EMS-API)—Part 1: Guidelines and general requirements," IEC, 2005.

[36] M. F. Zia, E. Elbouchikhi, and M. Benbouzid, "Microgrids energy management systems: A critical review on methods, solutions, and prospects," *Appl. energy*, vol. 222, pp. 1033–1055, July 2018.

[37] Z. Wang, B. Chen, J. Wang, M. M. Begovic, and C. Chen, "Coordinated energy

management of networked microgrids in distribution systems," *IEEE Trans. Smart Grid*, vol. 6, no. 1, pp. 45–53, 2015.

[38] Z. Wang, B. Chen, J. Wang, and J. Kim, "Decentralized energy management system for networked microgrids in grid-connected and islanded modes," *IEEE Trans. Smart Grid*, vol. 7, no. 2, pp. 1097–1105, Mar. 2015.

[39] R. Minciardi and M. Robba, "A bilevel approach for the stochastic optimal operation of interconnected microgrids," *IEEE Trans. Autom. Science and Eng.*, vol. 14, no. 2, pp. 482–493, Apr. 2017.

[40] M. Jalali, K. Zare, and H. Seyedi, "Strategic decision-making of distribution network operator with multi-microgrids considering demand response program," *Energy*, vol. 141, pp. 1059–1071, Dec. 2017.

[41] Y. Du and F. Li, "Integrating a multi-microgrid system into real-time balancing market: Problem formulation and solution technique," in *Proc. IEEE Power & Energy Soc. General Meeting (PESGM)*, Portland, OR, USA, Aug. 2018.

[42] M. P. Moghaddam, S. Bahramara, M. Damavandi, and M. Haghifam, "Distribution company and microgrids behaviour in energy and reserve equilibirum," in *Proc. IEEE PES Asia-Pacific Power and Energy Eng. Conf. (APPEEC)*, Brisbane, QLD, Australia, Nov. 2015.

[43] J. Wang, C. Chen, and X. Lu, "Requirements for DMS integration with DERMS and microgrids," in *Guidelines for implementing advanced distribution management systems.* Argonne National Lab. (ANL), U.S. DOE, Argonne, IL, Aug. 2015.

[44] M. C. Argyrou, P. Christodoulides, and S. A. Kalogirou, "Energy storage for electricity generation and related processes: Technologies appraisal and grid scale applications," *Renewable and Sust. Energy Rev.*, vol. 94, pp. 804–821, Oct. 2018.

[45] Y. Shi, B. Xu, Y. Tan, and B. Zhang, "A convex cycle-based degradation model for battery energy storage planning and operation," in *Proc. Annual American Control Conf. (ACC)*, Wisconsin, US, Aug. 2018, pp. 4590–4596.

[46] J. E. Contreras-Ocana, M. A. Ortega-Vazquez, and B. Zhang, "Participation of an energy storage aggregator in electricity markets," *IEEE Trans. Smart Grid*, vol. 10, no. 2, pp. 1171–1183, Mar. 2019.

[47] M. Koller, T. Borsche, A. Ulbig, and G. Andersson, "Defining a degradation cost function for optimal control of a battery energy storage system," in *Proc. IEEE Grenoble Conf.*, Grenoble, France, Nov. 2013.

[48] C. Bordin, H. O. Anuta, A. Crossland, I. L. Gutierrez, C. J. Dent, and D. Vigo, "A linear programming approach for battery degradation analysis and optimization in offgrid power systems with solar energy integration," *Renewable Energy*, vol. 101, pp. 417–430, Feb. 2017.

[49] A. Perez, R. Moreno, R. Moreira, M. Orchard, and G. Strbac, "Effect of battery degradation on multi-service portfolios of energy storage," *IEEE Trans. Sust. Energy*, vol. 7, no. 4, pp. 1718–1729, Oct. 2016.

[50] https://www.tesla.com/sv_SE/powerwall, Accessed: June 2020.

[51] https://www.samsungsdi.com/ess/energy-storage-system-application.html, Accessed: June 2020.

[52] H. Pandžić and V. Bobanac, "An accurate charging model of battery energy storage," *IEEE Trans. Power Syst.*, vol. 34, no. 2, pp. 1416–1426, Mar. 2019.

[53] A. J. Gonzalez-Castellanos, D. Pozo, and A. Bischi, "Non-ideal linear operation model for li-ion batteries," *IEEE Trans. Power Syst.*, vol. 35, no. 1, pp. 672–682, Jan. 2020.

[54] S. Boulmrharj, R. Ouladsine, Y. NaitMalek, M. Bakhouya, K. Zine-dine, M. Khaidar, and M. Siniti, "Online battery state-of-charge estimation methods in micro-grid systems," *J. Energy Storage*, vol. 30, p. 101518, Aug. 2020.

[55] Y. Naitmalek, M. Najib, M. Bakhouya, and M. Essaaidi, "Forecasting the state-of-charge of batteries in micro-grid systems," in *Proc. 2019 4th World Conf. on Complex Systems (WCCS)*. Ouarzazate, Morocco: IEEE, Apr. 2019.

[56] https://new.abb.com/distributed-energy-microgrids/our-offering/e-mesh/ems, Accessed: April 2020.

[57] https://new.siemens.com/global/en/products/energy/energy-automation-and-smart-grid/microgrid/spectrum-power-mgms.html, Accessed: April 2020.

[58] https://gegridsolutions.com/multilin/catalog/mcs.htm, Accessed: April 2020.

[59] A. Ali, W. Li, R. Hussain, X. He, B. Williams, and A. Memon, "Overview of current microgrid policies, incentives and barriers in the European Union, United States and China," *Sustainability*, vol. 9, no. 7, June 2017.

[60] S. Willette and P. Asmus, "Microgrid Deployment Tracker 2Q19," Navigant Research, https://guidehouseinsights.com/reports/microgrid-deployment-tracker-2q19, 2019, Accessed: June 2020.

[61] R. Husblad, G. Morén, J. Nordström, C. V. Nylander, L. Tedebrand and S. Wahlberg, "Ren energi inom EU–Ett genomförande av fem rättsakter," Energimarknadsinspektionen, www.ei.se, Feb. 2020.

[62] P. C. Kotsampopoulos, V. A. Kleftakis, and N. D. Hatziargyriou, "Laboratory education of modern power systems using phil simulation," *IEEE Trans. Power Systems*, vol. 32, no. 5, pp. 3992–4001, Sep. 2017.

[63] G. Agundis-Tinajero, N. L. D. Aldana, A. C. Luna, J. Segundo-Ramirez, N. Visairo-Cruz, J. M. Guerrero, and J. C. Vazquez, "Extended-optimal-power-

flow-based hierarchical control for islanded AC microgrids," *IEEE Trans. on Power Electron.*, vol. 34, no. 1, pp. 840–848, Jan. 2019.

[64] A. Charalambous, L. Hadjidemetriou, L. Zacharia, A. D. Bintoudi, A. C. Tsolakis, D. Tzovaras, and E. Kyriakides, "Phase balancing and reactive power support services for microgrids," *Appl. Sciences*, vol. 9, no. 23, p. 5067, Nov. 2019.

[65] B. Aluisio, A. Cagnano, E. De Tuglie, M. Dicorato, G. Forte, and M. Trovato, "PrInCE lab microgrid: early experimental results," in *Proc. Int. Annual Conf. (AEIT)*, Capri, Italy, Oct. 2016.

[66] L. L. Jansen, N. Andreadou, I. Papaioannou, and A. Marinopoulos, "Smart grid lab research in Europe and beyond," *Int. J. Energy Res.*, vol. 44, no. 3, pp. 1307–1336, Dec. 2019.

[67] A. Dimeas, S. Hatzivasiliadis, and N. Hatziargyriou, "Control agents for enabling customer-driven microgrids," in *Proc. IEEE Power & Energy Soc. General Meeting*, Calgary, AB, Canada, July 2009.

[68] J. Østergaard and J. E. Nielsen, "The Bornholm power system An overview," *Kgs. Lyngby, Denmark*, May 2010.

[69] A. Zecchino, A. M. Prostejovsky, C. Ziras, and M. Marinelli, "Large-scale provision of frequency control via V2G: The Bornholm power system case," *Electric Power Syst. Res.*, vol. 170, pp. 25–34, May 2019.

[70] B. Washom, J. Dilliot, D. Weil, J. Kleissl, N. Balac, W. Torre, and C. Richter, "Ivory tower of power: Microgrid implementation at the university of California, San Diego," *IEEE Power Energy Mag.*, vol. 11, no. 4, pp. 28–32, July/Aug. 2013.

[71] W. Feng, M. Jin, X. Liu, Y. Bao, C. Marnay, C. Yao, and J. Yu, "A review of microgrid development in the United States–A decade of progress on policies, demonstrations, controls, and software tools," *Appl. Energy*, vol. 228, pp. 1656–1668, Oct. 2018.

[72] N. Akhtar, "Analysis of Simris hybrid energy system design and working and checking the effects of using high capacity factor wind turbine," in Halmstad University Dissertations, 2019.

[73] Ferroamp, EnergyHub System, https://ferroamp.com/en/energyhub-system/, Accessed: May 2020.

[74] K. Antoniadou-Plytaria, A. Srivastava, M. A. F. Ghazvini, D. Steen, L. A. Tuan, and O. Carlson, "Chalmers campus as a testbed for intelligent grids and local energy systems," in *2019 Int. Conf. on Smart Energy Systems and Technologies (SEST)*, Porto, Portugal, Sep. 2019.

[75] HSB, "HSB living lab." [Online]. Available: https://www.hsb.se/hsblivinglab/

[76] https://www.riksbyggen.se/ny-bostad/aktuella-projekt/vastra-gotaland/brf-viva/, Accessed: April 2020.

[77] A. Papageorgiou, A. Ashok, T. H. Farzad, and C. Sundberg, "Climate change impact of integrating a solar microgrid system into the Swedish electricity grid," *Appl. Energy*, vol. 268, p. 114981, June 2020.

[78] S. Kim, M. Pollitt, Y. Jin, J. Kim, and Y. Yoon, "Contractual framework for the devolution of system balancing responsibility from the transmission system operator to distribution system operators," [Online] Available: https://doi.org/10.17863/CAM.15493, 2017.

[79] M. Bozorg, F. Sossan, J.-Y. Le Boudec, and M. Paolone, "Influencing the bulk power system reserve by dispatching power distribution networks using local energy storage," *Electric Power Systems Research*, vol. 163, pp. 270–279, Oct. 2018.

[80] M. Quashie, F. Bouffard, C. Marnay, R. Jassim, and G. Joós, "On bilevel planning of advanced microgrids," *Int. J. Elect. Power & Energy Syst*, vol. 96, pp. 422–431, Mar. 2018.

[81] I. E. Grossmann, "Review of nonlinear mixed-integer and disjunctive programming techniques," *Optim. and Eng.*, vol. 3, no. 3, pp. 227–252, Sep. 2002.

[82] J. Schmalstieg, S. Käbitz, M. Ecker, and D. U. Sauer, "From accelerated aging tests to a lifetime prediction model: Analyzing lithium-ion batteries," in *Proc. IEEE World Electric Vehicle Symp. and Exhib. (EVS27)*, Barcelona, Spain, Nov. 2013.

[83] E. Wikner and T. Thiringer, "Extending battery lifetime by avoiding high SOC," *Appl. Sciences*, vol. 8, no. 10, p. 1825, Oct. 2018.

[84] J. Wang, J. Purewal, P. Liu, J. Hicks-Garner, S. Soukazian, E. Sherman, A. Sorenson, L. Vu, H. Tataria, and M. W. Verbrugge, "Degradation of lithium ion batteries employing graphite negatives and nickel–cobalt–manganese oxide+ spinel manganese oxide positives: Part 1, aging mechanisms and life estimation," *J. Power Sources*, vol. 269, pp. 937–948, Dec. 2014.

[85] D. Wang, J. Coignard, T. Zeng, C. Zhang, and S. Saxena, "Quantifying electric vehicle battery degradation from driving vs. vehicle-to-grid services," *J. Power Sources*, vol. 332, pp. 193–203, Nov. 2016.

[86] M. A. Ortega-Vazquez, "Optimal scheduling of electric vehicle charging and vehicle-to-grid services at household level including battery degradation and price uncertainty," *IET Gener., Transmiss. & Distribution*, vol. 8, no. 6, pp. 1007–1016, June 2014.

[87] M. Farivar and S. H. Low, "Branch flow model: Relaxations and convexification——Part I," *IEEE Trans. Power Syst.*, vol. 28, no. 3, pp. 2554–2564, Apr. 2013.

[88] M. E. Baran and F. F. Wu, "Network reconfiguration in distribution systems for loss reduction and load balancing," *IEEE Trans. Power Del.*, vol. 4, no. 2, pp. 1401–1407, Apr. 1989.

[89] K. Zhang, S. Hanif, S. Troitzsch, and T. Hamacher, "Day-ahead energy trade scheduling for multiple microgrids with network constraints," in *Proc. IEEE Power & Energy Soc. General Meeting (PESGM)*. Atlanta, GA, USA: IEEE, Aug. 2019.

[90] M. Farivar, X. Zho, and L. Che, "Local voltage control in distribution systems: An incremental control algorithm," in *Proc. IEEE Int. Conf. Smart Grid Commun. (SmartGridComm)*, Miami, FL, USA, Nov. 2015, pp. 732–737.

[91] GAMS. [Online]. Available: https://www.gams.com/

[92] CPLEX Optimizer. [Online]. Available: https://www.ibm.com/analytics/cplex-optimizer

[93] MATLAB 2018b, The MathWorks, Inc., Natick, Massachusetts, United States. [Online]. Available: https://www.mathworks.com/

[94] Göteborg Energi. [Online]. Available: https://www.goteborgenergi.se/

[95] Z. Norwood, E. Nyholm, T. Otanicar, and F. Johnsson, "A geospatial comparison of distributed solar heat and power in Europe and the US," *PLoS ONE*, vol. 9, no. 12, p. e112442, Dec. 2014.

[96] Nord Pool. [Online]. Available: https://www.nordpoolgroup.com/

[97] MQTT, http://mqtt.org/, Accessed: May 2020.

[98] X. Li, C. Yuan, and Z. Wang, "Multi-time-scale framework for prognostic health condition of lithium battery using modified Gaussian process regression and nonlinear regression," *J. Power Sources*, vol. 467, p. 228358, Aug. 2020.

[99] C. Heymans, S. B. Walker, S. B. Young, and M. Fowler, "Economic analysis of second use electric vehicle batteries for residential energy storage and load-levelling," *Energy Policy*, vol. 71, pp. 22–30, Aug. 2014.

Appendix A

Input Data for the Test Cases

This appendix presents the input data that were used in each test case. These include load consumption, PV generation, and electricity prices. The electricity prices are presented in USD, where the average 2018 USD to SEK ratio was used, which is 1:8.6921.

A.1 Electrical distribution system of Chalmers University of Technology

Fig. A.1–A.3 show the load consumption and PV generation profiles of the Chalmers distribution network, MG-A, and MG-B, respectively. The electricity prices that were used in the case study are shown in Fig. A.4.

A.2 33-bus distribution network

Fig. A.5–A.8 show the load consumption and PV generation profiles of the two grid-connected MGs. An error was introduced in these values to create a set of pseudo measurements that represented a non-perfect forecast profile of the actual values.

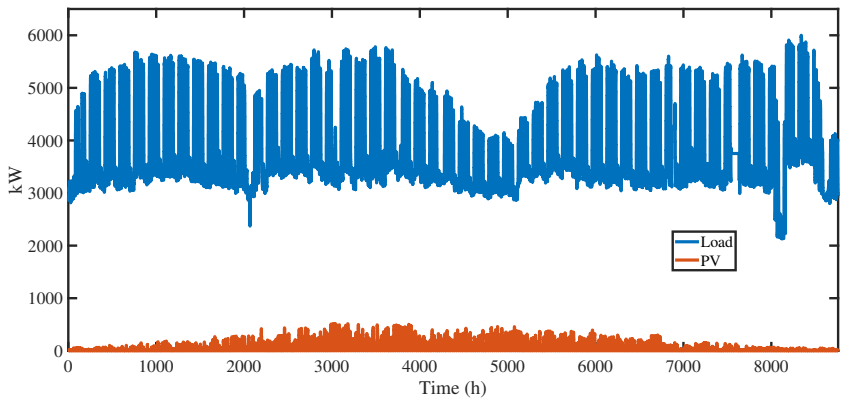

Figure A.1: Load consumption and PV generation in 2016 of the electrical distribution system of Chalmers University of Technology.

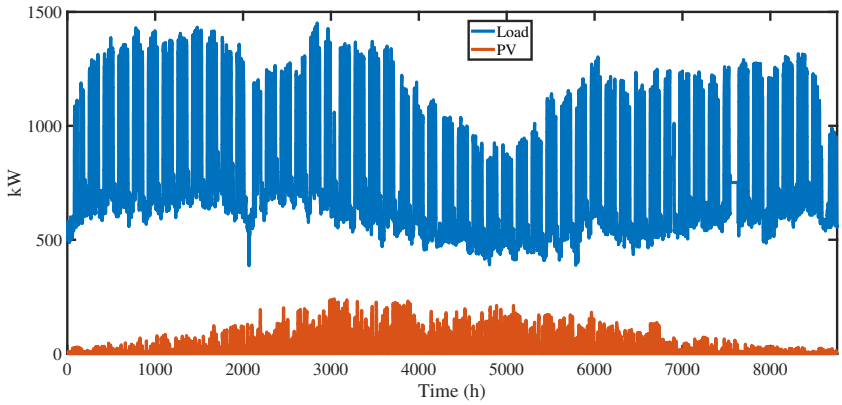

Figure A.2: Load consumption and PV generation of MG-A.

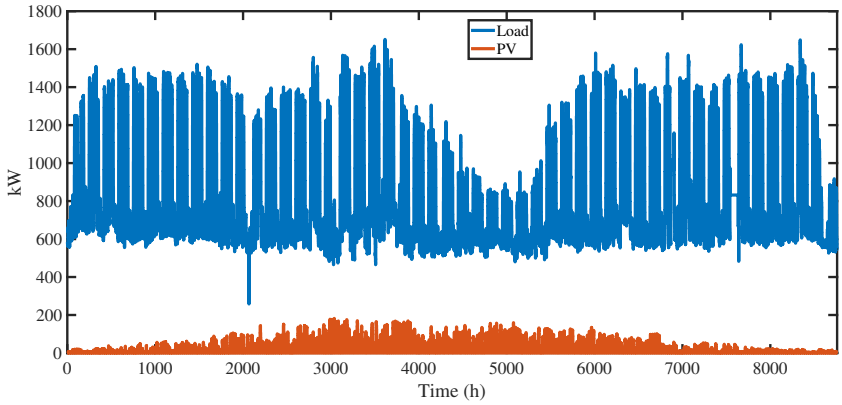

Figure A.3: Load consumption and PV generation of MG-B.

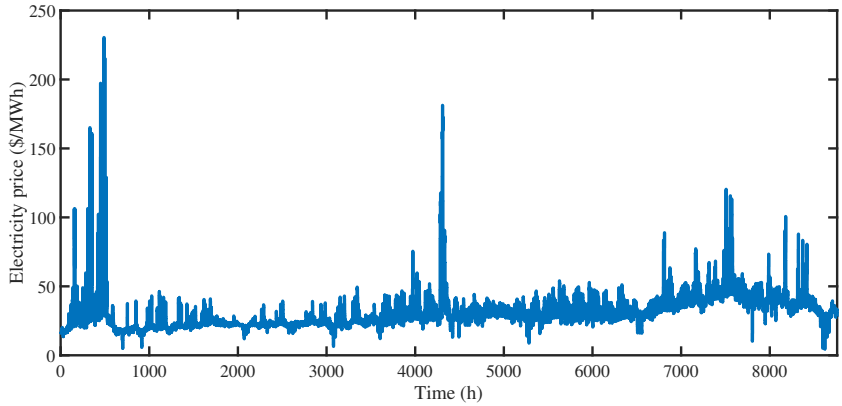

Figure A.4: Electricity prices of the case study on the electrical distribution system of Chalmers University of Technology (Nordpool spot market prices in 2016).

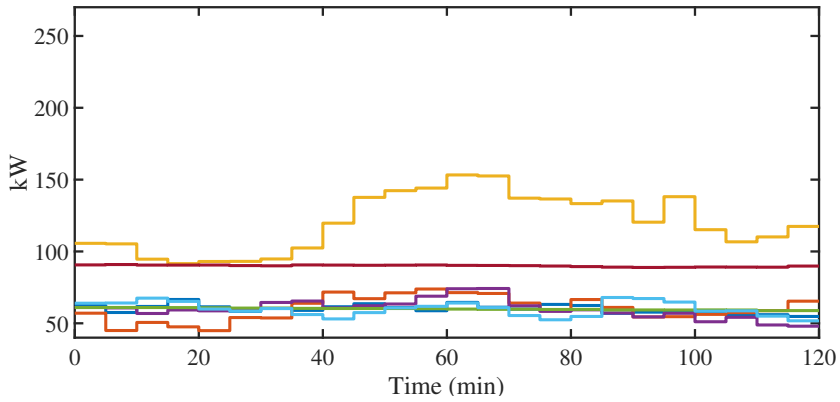

Figure A.5: Load consumption of the buses that belong to MG1.

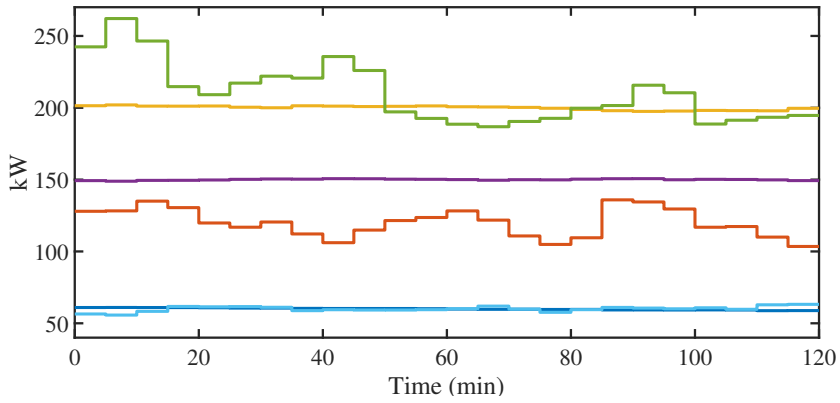

Figure A.6: Load consumption of the buses that belong to MG2.

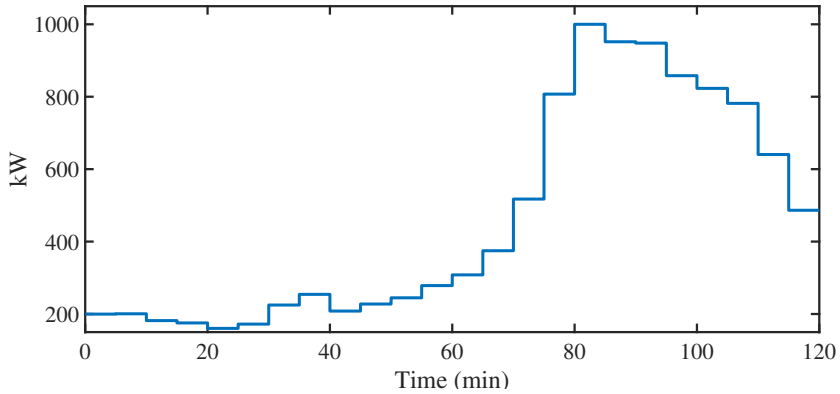

Figure A.7: PV generation of the PV system installed at MG1.

The electricity prices that were used in the simulations are given in Fig. A.9.

A.3 HSB Living Lab

Fig. A.10 shows the HSB LL building load consumption and PV generation in 2018 (where that the profiles are interrupted, it means that data was unavailable), which were used as input to the simulation studies. The input data to the simulation

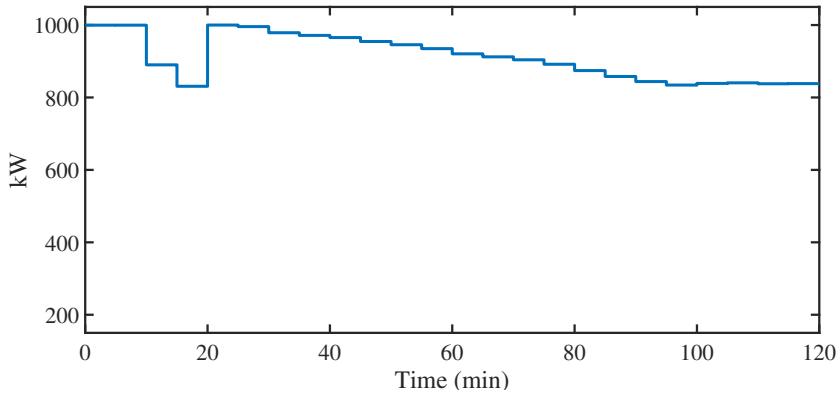

Figure A.8: PV generation of the PV system installed at MG2.

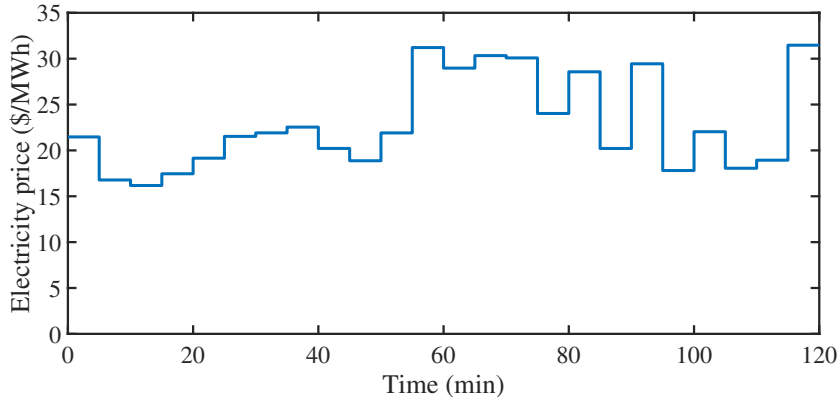

Figure A.9: Electricity prices of the case study on the 33-bus distribution network.

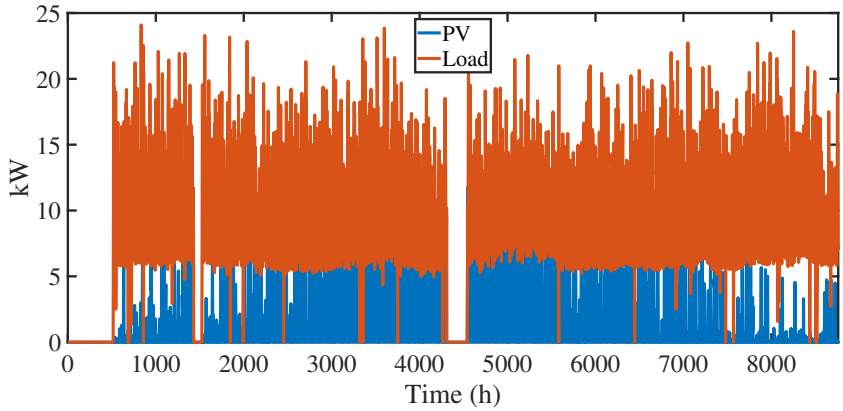

Figure A.10: Building load consumption and PV generation at HSB LL (2018).

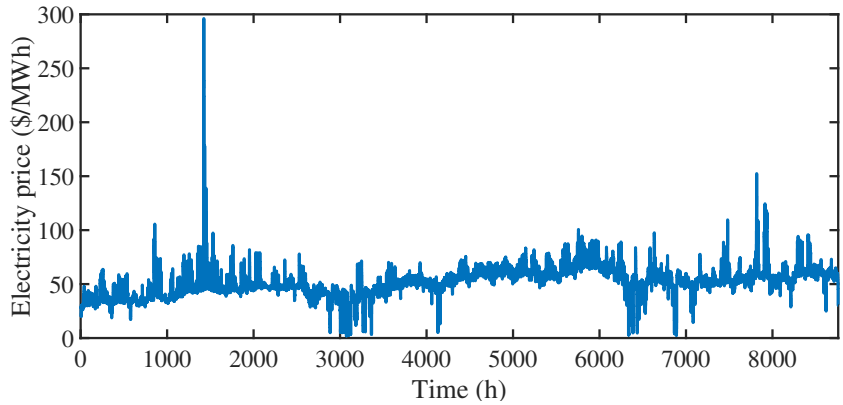

Figure A.11: Electricity prices used as input in the simulation studies of HSB LL (2018).

studies also include the 2018 Nordpool spot market prices, which are shown in Fig. A.11.

Fig. A.12 shows the building load consumption and PV generation that was used as input to the BMG-EMS of HSB LL in the demonstrations. The load and PV generation profile corresponds to the first scheduling horizon, when the demonstration started. As the RH approach was used, the input changed every Δt minutes. For the HSB LL demonstration it was $\Delta t = 15$ minutes. The electricity prices that were used in the demonstrations are given in Fig. A.13.

A.4 Brf Viva

Fig. A.14 shows the building load consumption and PV generation that was used as an input to the Brf Viva test case (both in simulations and demonstrations). An error was introduced in these input data to account of the effect of forecast error. The load and PV generation profiles correspond to the inputs used for the first 24-hour scheduling horizon, when the demonstration started (at time 09:30). As the RH approach was used, the input changed every Δt minutes. For the Brf Viva simulations and demonstrations it was $\Delta t = 5$ minutes. The electricity prices that

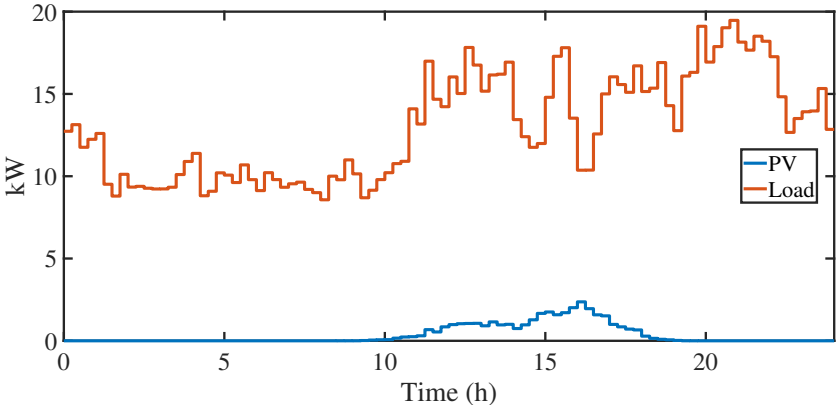

Figure A.12: Daily building load consumption and PV generation at HSB LL (February, 2020).

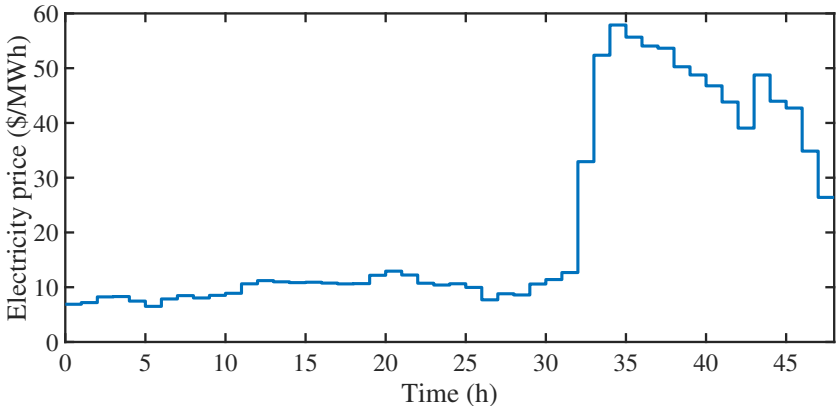

Figure A.13: Electricity prices used as input in the demonstrations at HSB LL (February, 2020).

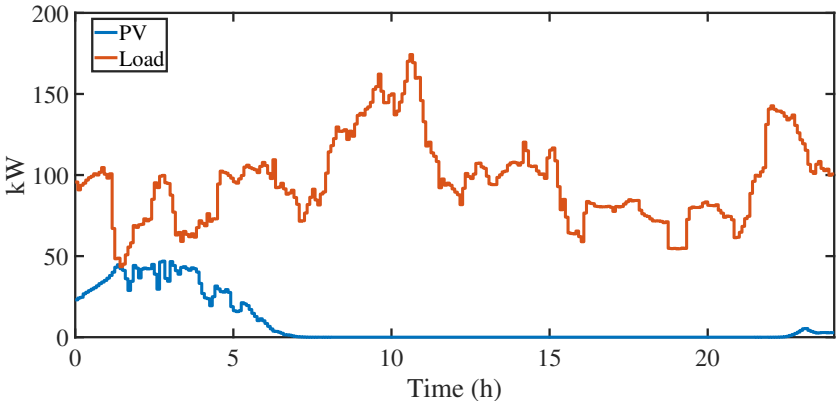

Figure A.14: Building load consumption and PV generation at Brf Viva (February, 2020).

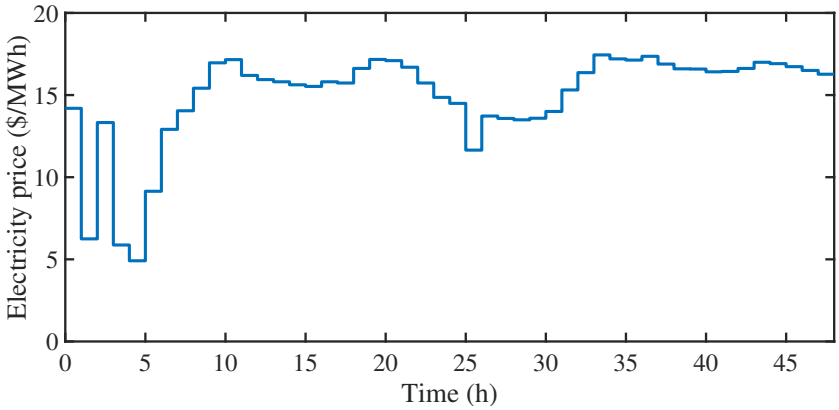

Figure A.15: Electricity prices used as input the simulation studies and demonstrations at Brf Viva (February, 2020)

were used are given in Fig. A.15.